Scuola Internazionale Superiore di Studi Avanzati - Trieste

Scuola Internazionale Superiore di Studi Avanzati - SISSA
International School for Advanced Studies - ISAS

Trieste, Italy

Scuola Internazionale Superiore di Studi Avanzati

Expression of calcium-activated chloride channels TMEM16A and TMEM16B in adult mouse vomeronasal epithelium and during embryonic development of the olfactory epithelium

Thesis submitted for the degree of "*Doctor Philosophiae*"

Academic Year 2013/2014

Candidate

Devendra Kumar Maurya

Supervisor

Prof. Anna Menini

SISSA - Via Bonomea 265 - 34136 TRIESTE - ITALY

Scuola Internazionale Superiore di Studi Avanzati - SISSA
International School for Advanced Studies - ISAS

Trieste, Italy

Scuola Internazionale Superiore di Studi Avanzati

Expression of calcium-activated chloride channels TMEM16A and TMEM16B in adult mouse vomeronasal epithelium and during embryonic development of the olfactory epithelium

Thesis submitted for the degree of "*Doctor Philosophiae*"

Academic Year 2013/2014

Candidate

Devendra Kumar Maurya

Supervisor

Prof. Anna Menini

Declaration

The work described in this thesis was carried out at International School for Advanced Studies (SISSA), Trieste, Italy between November-2010 and October-2014.

Experiments performed during these four years are included in:

1. Dibattista M, Amjad A, **Maurya DK**, Sagheddu C, Montani G, Tirindelli R, Menini A. 2012. Calcium-activated chloride channels in the apical region of mouse vomeronasal sensory neurons. J Gen Physiol, 3-15. PMID: 22732308. (*journal's cover page article*)

2. **Maurya DK**, Menini A. 2014. Developmental expression of the calcium-activated chloride channels TMEM16A and TMEM16B in the mouse olfactory epithelium. Dev Neurobiol, 657-675. PMID: 24318978. (*journal's cover page article*)

3. **Maurya DK**, Marini M, Pedemente N, Galietta L, Rock JR, Harfe BD, Menini A. Development of the olfactory epithelium and nasal glands in TMEM16A$^{-/-}$ and TMEM16$^{+/+}$ mice. *Manuscript is submitted.*

The immuno-histochemical data reported in above articles were performed by me. I have also been actively involved in experimental design, analysis of data and drafting of manuscripts.

I have also been involved in the data analysis and drafting of manuscript mentioned below:

1. Dibattista M, Massimino ML, **Maurya DK**, Menini A, Bertoli A, Sorgato MC. 2011. The cellular prion protein is expressed in olfactory sensory neurons of adult mice but does not affect the early events of the olfactory transduction pathway. Chem senses, 791-797. PMID: 21680753.

To my parents and wife

Abstract

Olfaction enables animals to be familiar with the surrounding environmental changes. Exchange of odor molecules between animals is a way to communicate with each other and is necessary for various physiological processes, like reproduction, food preferences, prey detection, etc. The olfactory epithelium is always in contact with the inhaled air that is accompanied by odor molecules. Olfactory sensory neurons are the primary neurons of the olfactory epithelium. These neurons follow the “one receptor one neuron” rule, i.e. each individual olfactory sensory neuron expresses only one type of olfactory receptor out of ~1300 types in mouse. These neurons are specialized to convert chemical interaction, between odor molecules and olfactory receptor, into electrical signals by specific transduction mechanisms, which occur in the cilia of these neurons. The ciliary membrane contains cyclic nucleotide-gated channels and calcium-activated chloride channels. It is well documented that calcium-activated chloride channels are used to enhance signal to noise ratio in olfactory sensory neurons but we do not know about their involvement in the development of olfactory epithelium. TMEM16A and TMEM16B, the members of transmembrane proteins 16 (TMEM16) family, are responsible for the calcium-activated chloride current in various cells. In present work, I studied expression of TMEM16A and TMEM16B proteins during embryonic development of mouse and tried to find their role in olfactory epithelium development.

I found expression of TMEM16A and TMEM16B in the developing olfactory epithelium at different embryonic ages. At embryonic day 12.5 (E12.5), TMEM16A immunoreactivity was present at the apical surface of the entire olfactory epithelium, but from E16.5 became restricted to a region near the transition zone with the respiratory epithelium. Olfactory sensory neurons are devoid of TMEM16A but this channel is expressed in the apical organelle free region and microvilli of supporting cells. Nasal septal glands and lateral nasal glands also express TMEM16A at the luminal surface of glands. In contrast, TMEM16B immunoreactivity was observed at E14.5 at the apical surface of the olfactory epithelium. Its expression was observed only in mature olfactory sensory neurons. With the maturation of olfactory sensory neurons and elongation of cilia TMEM16B expression is increased along with ACIII, CNGA2 and acetylated-tubulin. Interestingly, olfactory sensory neurons express only TMEM16B, but I found expression of TMEM16A as well as of TMEM16B in microvilli of vomeronasal sensory neurons. These findings indicate different physiological roles for TMEM16A and TMEM16B in the developing as well as in the postnatal olfactory and vomeronasal epithelia.

Taking into account the previous evidences, I hypothesized that the presence of TMEM16A at the apical part and in microvilli of the supporting cells as well as in nasal glands is involved (1) in the regulation of the chloride ionic composition of the mucus covering the apical surface of the olfactory epithelium and/or (2) in proliferation and development during embryonic development. By comparing immunohistochemistry experiments on TMEM16A$^{-/-}$ and TMEM16A$^{+/+}$ littermate mice I excluded the hypothesis that TMEM16A is involved in proliferation or development of the olfactory epithelium. So, either TMEM16A does not play a central role in the development of the olfactory epithelium or its genetic ablation does not affect olfactory development. Supporting cells, Bowman's and nasal glands morphology remained unchanged in TMEM16A$^{-/-}$ mice, but at present we do not know whether the mucus composition is same as in TMEM16A$^{+/+}$ littermate mice. Localization of TMEM16B to the cilia of mature olfactory sensory neurons and in microvilli of vomeronasal sensory neurons is consistent with a role in sensory signal transduction mechanism.

In conclusion, the present work explored the dynamic expression pattern of TMEM16A and TMEM16B. It might be possible that different physiological roles of these proteins depend on the intracellular and extracellular factors expressed in the corresponding cells.

Acknowledgments

It was a wonderful stay at SISSA and in a beautiful coastal city Trieste. I am grateful to many people who have, intentionally or unintentionally, helped me to complete this work. First and foremost, I thank my advisor, Prof Anna Menini for her constant encouragement and support throughout my time in her lab. She is a creative and enthusiastic scientist with a good personality and it was a privilege to be her PhD student. Throughout my work she has nurtured my ideas and has continuously guided me with concern for what was best for my project and my future career. She also encouraged me to be a better speaker, a better writer and a better scientist.

I would like to acknowledge Prof Sid Simon, Duke University, USA for his critical comments on the published manuscript presented in the section 4.2 of this thesis. Writing experience with him has really improved my scientific writing skill. I thank faculty members at SISSA Prof Andrea Nistri, Prof Vincent Torre and Prof Enrico Cheribuni for their critical and valuable comments during the annual progress reports. It was my pleasure to work with efficient technical staff at SISSA. I would like to thank Micaela for her advice related to microscopy and sectioning; Tullio for our safety; Alessandra, Andrea and Valeria for making bureaucratic procedures easy. Many thanks to animal house staff for their assistance in breeding mice. I also thank my collaborators and unknown reviewers of my manuscripts, whose critical comments made my work more comprehensive and informative.

It was my good luck that in last four years, I worked with lab-mates of good nature. I started working with Michele, Fulvio, Valentina, Giulia, Asma, Lijo, Simone and now new members Gianluca, Andres, Stefano and Tiago are in lab. In a way, a whole generation has changed but all the past and present member of lab were good persons by heart. Many thank to my batch-mate Ayisha, for coffee time, and being my friend in these years. Many thanks to SISSA students and post-docs, for making an intellectual and good environment to work.

I also want to acknowledge my family. I am lucky to have parents that have always encouraged me to follow my dreams and I am indebted for their constant love and support throughout this and other endeavors. I thank my brothers, Dharmendra and Jitendra for their love and support. Finally, I thank my beloved wife Anita, for her patience in the hope that some time in the future I will spend plenty of time with her. I hope I will make her feel as loved and supported as she makes me feel every day.

Finally, I would like to thank MIUR, Rome and SISSA, Trieste for the uninterrupted financial support.

Table of Contents

1. Introduction

Chemosensation is an ability of living beings that enables them to discriminate various molecules among those they come in contact in their everyday life. Olfaction is a type of chemosensory process which makes animal aware about the airborne changes in the surrounding environment. Lower mammals including rodents in general rely on the olfactory systems for the detection of changes in the surrounding environment. In rodents olfaction is necessary to assess quality of food, dam-pups interaction, identification of conspecific mate partner, detection of prey and all together is necessary for their survival (Dulac and Torello 2003; Munger et al. 2009; Patris et al. 2013). In this thesis mouse is used as animal model, so in general I will discuss about the mouse olfactory systems. Olfactory systems can be categorized in two parts: (1) *peripheral part* - this is in contact with external environment and resides in the nose of mice and (2) *central part* - this is involved in the processing of peripheral information and resides in the forebrain.

Peripheral part is comprised of Grüneberg's ganglion, septal organ, main olfactory epithelium and vomeronasal organ. Grüneberg's ganglion is located in the most anterior part of the nasal cavity (Fig. 1). It is involved in perception of cool ambient temperatures, dam-pups interaction and detection of alarm pheromones (Fuss et al. 2005; Brechbühl et al. 2008; Mamasuew et al. 2008). Septal organ is located at the base of the nasal septum (Fig. 1A, B). Septal organ is susceptible to odor molecules and it is comprised of olfactory sensory neurons. However a group of researcher suggests that it is involved also in the mechanosensation (Grosmaitre et al. 2007; Ma 2010). Main olfactory epithelium and vomeronasal organ are the most studied and well documented part of peripheral olfactory system. In this thesis most of work is done on main olfactory epithelium and vomeronasal organ. I will discuss them in more elaborative way.

1.1 Organization of olfactory epithelium and vomeronasal organ

1.1.a Olfactory epithelium

Main olfactory epithelium is a pseudostratified epithelium normally referred as *olfactory epithelium*. In mouse it is located in the dorsal-posterior part of nasal cavity (Fig. 1). It always remains in contact with the inhaled air passing through the nasal cavity which occasionally carries various odor molecules. Olfactory epithelium is mainly comprised of olfactory sensory neurons, supporting or sustentacular cells, basal cells and a small population of microvillous cells. The duct of Bowman's glands traverses the thickness of olfactory epithelium, while glands reside in lamina propria of olfactory mucosa.

In the olfactory epithelium, olfactory sensory neurons are the primary neurons. They are bipolar neurons and their basal side projects an axon towards the olfactory bulb. In the olfactory bulb, axon terminals expressing the same olfactory receptors coalesce and form olfactory glomeruli. Towards the apical side each olfactory sensory neuron projects a dendrite which forms a dendritic knob at the luminal surface (apical surface) of the olfactory epithelium (Fig. 1C). Several cilia protrude from the dendritic knob in the nasal lumen and are always immersed in mucus secreted by Bowman's glands. Cilia can attain length up to 60 µm and intermingle to form a meshwork at the top of the olfactory epithelium. In some species (for example amphibians) the length of cilia can be up to 200 µm (McEwen et al. 2008). Interestingly in mouse, cilia align parallel to each other and have spooned shaped endings (Noda and Harada 1981). Olfactory cilia are non-motile however they have a (9+2) configuration of microtubular organization that is typical for motile cilia (Menco 1984). Olfactory ciliary membrane is enriched with the components of olfactory signal transduction. This is an anatomically and molecular advantage because odor molecules interact with cilia of olfactory sensory neurons (Kleene 2008). At any given time two types of olfactory sensory neurons are always present in olfactory epithelium of rodents; in the upper part mature and in the lower part immature neurons (Fig. 1D). Depending on physiological condition and age the area covered by mature and immature sensory neurons may change (Graziadei and Graziadei 1978; Lee and Pixely 1994).

Supporting or sustentacular cells have oval shape nuclei and they are aligned almost in a single row in the apical part of olfactory epithelium. They are non-ciliated columnar epithelial cell with broad apical cell body and basal narrow, elongated, branched projections towards lamina propria. These cells act like glia and they electrically separate olfactory sensory neurons (Breipohl et al. 1974). From the apical side numerous microvilli emerge and protrude into the nasal lumen (Noda and Harada 1981; Nomura et al. 2004). Microvilli of supporting cells are intermixed with cilia of olfactory sensory neurons and together they make the luminal surface of the olfactory epithelium. The exact function of supporting cells in mammals is not known. However various studies suggest that supporting cells metabolize

the inhaled xenobiotic molecules (Dahl and Hadley 1991; Ling et al. 2004; Yu et al. 2005). Supporting cells can also regulate the ionic composition of mucus covering the luminal surface of the olfactory epithelium (Mendoza1993; Menco et al. 1998; Rochelle 2000).

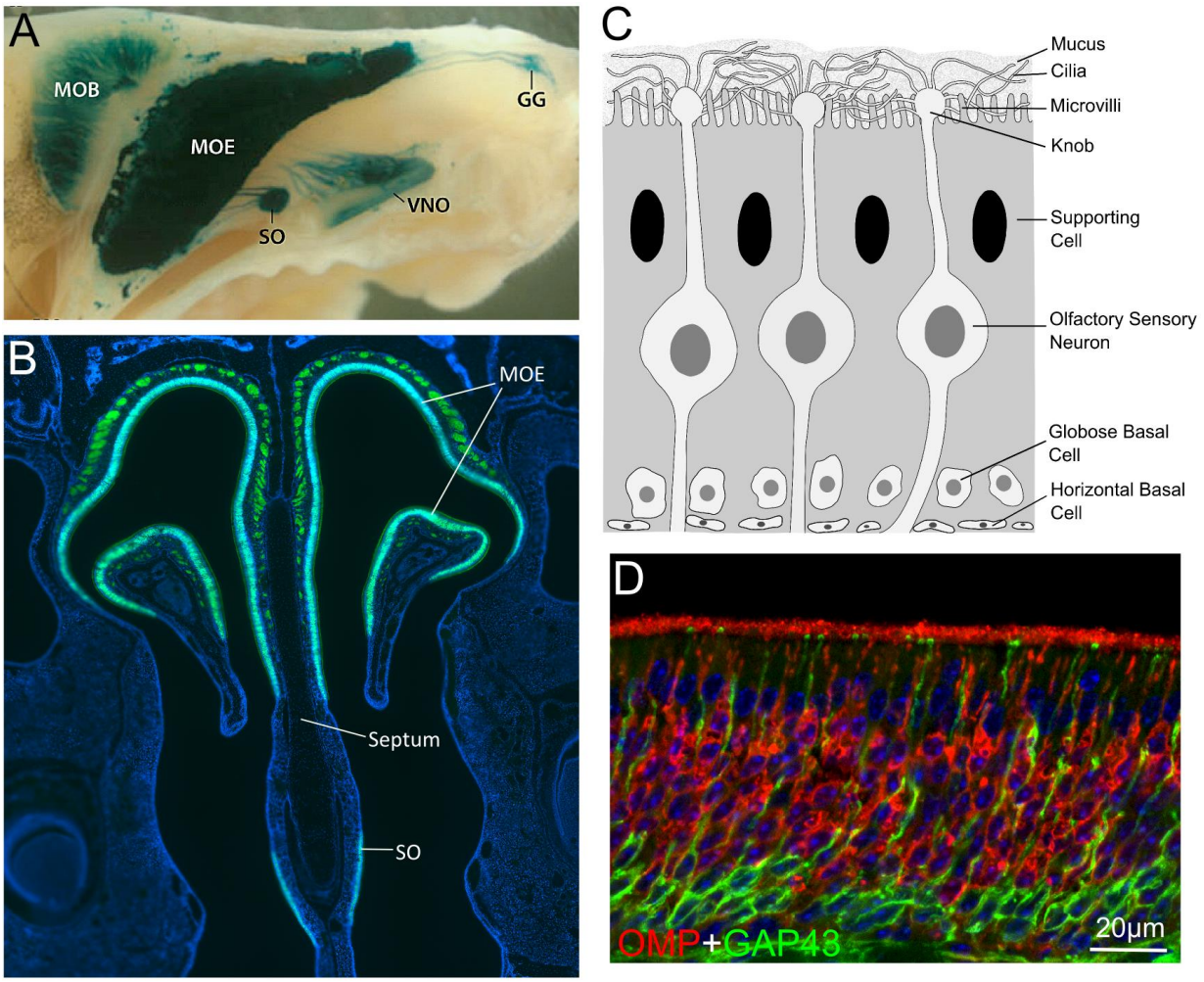

Fig. 1: ***(A)*** Anatomical organization of mouse olfactory systems. X-Gal stained whole mount sagittal section of OMP:tau-LacZ transgenic mouse. In this mouse olfactory marker protein co-expresses with LacZ, so all sensory neurons of the olfactory system are visualized by X-Gal staining (Blue). Grüneberg's ganglion (GG) is located most anteriorly near the tip of nose. Vomeronasal organ (VNO) is in the anterior-ventral part of nasal cavity just above the hard palate of the oral cavity. Septal organ (SO) is seen distinctly separated from main olfactory epithelium (MOE). Neurons that form the olfactory epithelium project axons to the main olfactory bulb (MOB). *Modified from Storan and Key 2006; Munger et al. 2009*. ***(B)*** Coronal section of nasal cavity at the level of septal organ of an OMP-GFP mouse. In this mouse all mature neurons express green fluorescent protein (GFP) instead of olfactory marker protein (OMP). ***(C)*** A schematic diagram showing different cell types present in olfactory epithelium. Olfactory sensory neurons (OSNs) are the bipolar neuron projecting dendrites towards the luminal surface of the olfactory epithelium. The dendritic ending forms knob that protrudes cilia in the nasal lumen. OSNs are surrounded by supporting cells that protrude microvilli in the nasal lumen. Cilia and microvilli are submerged in a mucus layer that covers the luminal surface (apical surface) of olfactory epithelium. Axons emerge from the basal part of OSNs and make synapses in the olfactory bulb. At the basal part of the olfactory epithelium two types of dividing cells are present; flat in shape horizontal basal cells (HBCs) and spherical in shape globose basal cells (GBCs). ***(D)*** Mature and immature OSNs are always present in the olfactory epithelium. Mature OSNs express olfactory marker protein (red, OMP) while immature OSNs express growth associated protein 43 (green, GAP43). OSN bodies make a distinguish layer in olfactory epithelium. Mature and immature neurons cell bodies respectively make upper and lower part of this layer. *B-D: unpublished data from Maurya and Menini*.

Basal cells are the proliferating cells of the olfactory epithelium. They are aligned in the basal part of the epithelium and are self-renewing population of cells. Division of these cells provides a consistent pool of neurons and supporting cells to the olfactory epithelium over the whole life span. They are of two types: horizontal basal cell (HBC) and globose basal cell (GBS). HBCs remain close to the lamina propria and are flat in shape, while GBCs are round in shape and align just above the HBC (Graziadei and Graziadei 1978, 1979; Schwob et al. 1994; Suzuki et al. 2000). It is debatable which basal cell type is the stem cell. Some evidence suggests that HBCs are either stem cell or provide a niche of stem cells (Carter et al. 2004). Other evidences suggest that GBCs can give rise to neurons as well as supporting cells (Caggiano et al. 1994; Huard et al. 1998; Beites et al. 2005).

Microvillous or microvillar cells are a minor cell population in the olfactory epithelium. Microvillous cells are of different types depending on the shape of microvilli they project into nasal cavity (Menco and Morrison 2003). Few of them also project axon (Rowley et al. 1989). However other studies did not find axons in these cells (Carr et al. 1991; Asan and Drenckhalm 2005).

Bowman's glands are the main mucus secreting glands in the olfactory epithelium. Bowman's gland duct cells traverse through the epithelium and form a duct opening at the top of the olfactory epithelium. Bowman's gland acinar cells reside in lamina propria below the olfactory epithelium (Schwob et al. 1994; Nomura et al. 2004).

1.1.b Vomeronasal Organ

Although the olfactory epithelium and vomeronasal organ are two distinct systems, they have common origin, i.e. olfactory placode (Cuschieri and Bannister 1975a). Both systems have synaptic connection with gonadotropin-releasing hormone (GnRH) neurons, thus they remain connected via GnRH neurons (Meredith 1998; Boehm et al. 2005; Hagino-Yamagishi 2008). Most non-volatile molecules including pheromones, major urinary proteins (MUPs) are detected by the vomeronasal organ (Tirindelli et al. 2009; Touhara and Vosshall 2009).

Vomeronasal organ is encapsulated by a protective layer of cartilage and located in the anterior-ventral part of the nasal cavity. The anterior part of the cartilaginous capsule is exposed to the nasal cavity; via it molecules come in contact with the luminal fluid present in the vomeronasal organ's lumen (Døving and Trotier 1998). The luminal cavity of the vomeronasal organ is enclosed by sensory and non-sensory epithelium. Vomeronasal sensory epithelium is a pseudostratified epithelium. Vomeronasal sensory neurons, supporting cells and dividing cells are the main cellular component of the sensory epithelium. Like olfactory sensory neurons, vomeronasal sensory neurons are bipolar neurons and project an axon towards the accessory olfactory bulb where axon terminals form glomeruli.

Towards the luminal side of the organ, vomeronasal sensory neurons project dendrites from which numerous microvilli protrude in the lumen. Microvilli are enriched with different proteins involved in vomeronasal signal transduction. Based on the location in the vomeronasal organ two types of vomeronasal sensory neurons are present in rodents. Apical neurons are located near to luminal surface of epithelium, express G-protein αi2 subunit, PDE4A, and receptors of V1R or formyl peptide receptor family. Basal neurons are located close to the basal lamina, express G-protein αo subunit and receptors of V2R or formyl peptide receptor family (Berghard and Buck 1996; Jia and Halpern 1996; Ryba and Tirindelli 1997; Lau and Cherry 2000; Leinders-Zufall et al. 2004; Liberles et al. 2009).

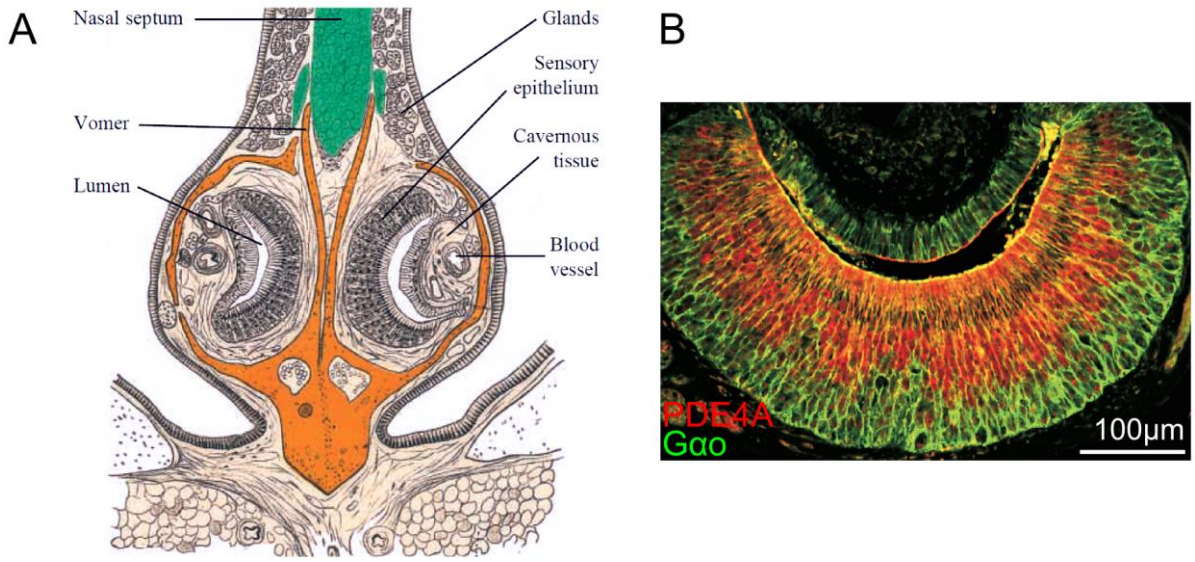

Fig. 2: ***(A)*** A schematic coronal section of the vomeronasal organ (VNO). The tubular shape, bilaterally symmetrical organ resides at the basal part of nasal septum in the anterior-ventral nasal cavity. Both half of the organ are encapsulated by the vomer bone. Sensory epithelium is of crescent shape and its corners is connected with non-sensory epithelium. Lumen is enclosed by apical or luminal surfaces of sensory and non-sensory epithelium. Vomeronasal sensory neurons (VSNs) are the main neurons of this sensory epithelium. VSNs protrude dendrites towards luminal surface of sensory epithelium. Dendritic endings protrude microvilli in lumen, where pheromones interact with them. *Adapted from Døving and Trotier 1998.* ***(B)*** Neurons are segregated anatomically in two different parts of the vomeronasal sensory epithelium. Apical neurons towards luminal surface are immuno-positive for PDE4A while the basal neurons are immuno-positive for Gαo. *Modified from Leinders-Zufall et al. 2004*.

Supporting cells are non-neural cells with oblong cell body which occupy the apical part (towards luminal surface) of epithelium. Supporting cells have thin cytoplasmic projections towards basal side of the vomeronasal organ (Vaccarezza et al. 1981, Ghiaroni et al. 2003). Dividing cells are abundant at the corners of crescent shaped sensory epithelium in between sensory and non-sensory epithelium. However some studies also suggest presence of these cells at the basal part of sensory epithelium (Vaccarezza et al. 1981; Naguro and Breipohl 1982).

1.2 Prenatal development of olfactory systems

1.2.a Olfactory epithelium prenatal development

The olfactory epithelium is derived from the olfactory placode which is induced from non-neuronal ectoderm located at rostro-lateral region of the head of a developing mouse embryo. Olfactory placode is seen at around embryonic day 9 (E09) (Cuschieri and Bannister 1975a; Treloar et al. 2010). Although the mechanism that induces non-neuronal ectoderm is elusive, induced-ectoderm in mouse expresses high levels of Six3, Eya1 and Dach1 proteins (Purcell et al. 2005). It seems that transcription factors Sox2, Oct1 and Pax6 mediated mechanisms are vital for the induction of the olfactory placode (Donner et al. 2006; Treolar et al. 2010). Olfactory placode differentiation and development of embryonic olfactory epithelium are governed by various subtypes of retinoic acid (RA), fibroblast growth factor (FGF) and bone morphogenic protein (BMP) secreted by surrounding mesenchyme and epithelial cells (Treolar et al. 2010).

Olfactory placode cells are multipotent in nature and give rise to olfactory sensory neurons, vomeronasal sensory neurons, gonadotropin-releasing hormone (GnRH) neurons and supporting cells (Cuschieri and Bannister 1975a, b; Suárez et al. 2012). At E09, olfactory placode is distinguishable from surrounding mesenchyme and it invaginates to form the olfactory pit at E10. Axons are distinguishable at E10. Dendrites are noticeable at E11 however they are devoid of olfactory vesicles or knobs (Cuschieri and Bannister 1975a, b; Kerjaschki and Hörandner 1976). At E11 the nasal cavity is formed and presumptive olfactory epithelium can be distinguished anatomically (Cuschieri and Bannister 1975a). At E11 an inward thickness is seen at the medial wall of olfactory epithelium, by E12 this medial wall thickens and invaginates to form presumptive vomeronasal organ. At E12, numerous immature olfactory sensory neurons are present in the olfactory epithelium. At this stage few dendritic swellings protrude from the apical surface of the epithelium with one or two small cilia that give the epithelium an irregular appearance (Cuschieri and Bannister 1975b; Graziadei et al. 1980; Noda and Harada 1981). Contrary to neonatal and adults, during early embryonic development (generally till E14) dividing cells can be seen at the apical part of the olfactory epithelium. In later stages and throughout life dividing cells are present at the basal olfactory epithelium (Smart 1971; Cuschieri and Bannister, 1975a; Graziadei and Graziadei 1978; Farbman 1994; Lee and Pixley 1994; Carson et al. 2006). At E14 mature olfactory sensory neurons are observed and numerous dendritic swellings protruding multiple cilia of ~2-3 µm in length are seen in the epithelium (Graziadei et al. 1980; Noda and Harada 1981; Schwarzenbacher et al. 2005; McEwen et al. 2008).

During early phase of development (E10-12), electron dense dark embryonic stem cells with elongate nuclei and pale sensory neurons with round nuclei are randomly

distributed in the epithelium. After E15-16 most of the embryonic stem cells are aligned in the basal part of the epithelium. The oval nuclei in the uppermost part of the epithelium differentiate into supporting cells. Sensory neurons are aligned in between supporting cells and stem cells, with mature sensory neurons in apical part and immature neurons in the lower part (Smart 1971; Cuschieri and Bannister 1975b). At E16 dendritic swellings have numerous cilia and attain morphology of dendritic knobs. From the apical free surface of supporting cells microvilli protrude into the nasal lumen. In mouse at E15 various small size microvilli are present at epithelial surface (Noda and Harada 1981). Microvilli in rat can attain an average length of ~3-4 µm before birth (Menco and Frabman 1985).

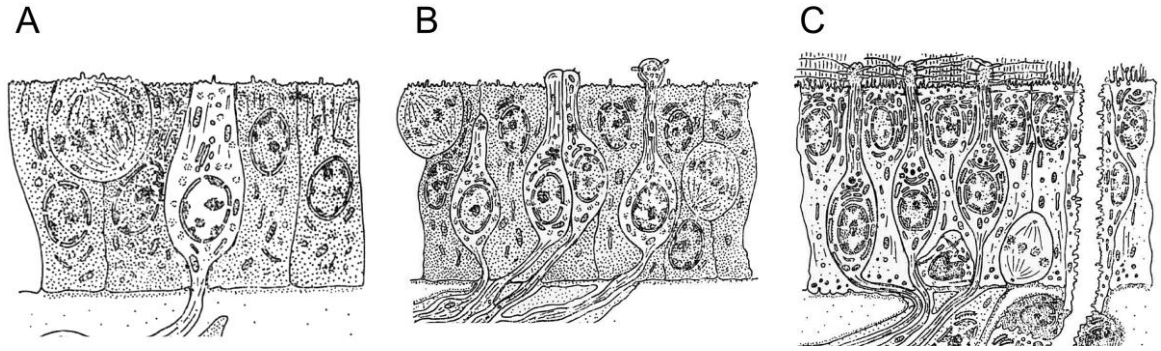

Fig. 3: A schematic diagram summaring the major changes during mouse olfactory epithelium development. ***(A)*** At E10-E11 dark embryonic stem cells and pale neurons are seen. Dividing cells are seen in the apical part of the epithelium. Epithelium surface is irregular and lacks dendritic knobs. ***(B)*** From E12-E14 neurons with prominent axons and dendrites can be distinguished. Dendrite swellings can be seen at the epithelium surface with few sort cilia. ***(C)*** Between E16-E18 olfactory epithelium attains complete cellular morphology like in the neonatal mouse. Cilia emerging from dendrite knobs and microvilli from supporting cells cover the apical surface of olfactory epithelium. Supporting cells are well distinguishable from olfactory sensory neurons. Dividing cells are seen only at the basal part of the epithelium. Bowman's gland duct traverses through the thickness of epithelium is seen at the final stage of development. *Modified from Cuschieri and Bannister 1975b.*

Epithelium thickness increases and multilayer olfactory epithelium is formed by E18 (Smart 1971). Supporting cells are prominent and their cell bodies make the uppermost part of epithelium. Olfactory sensory neurons appear in a prominent layer, in the upper part more mature neurons are present compared to previous stages while the lower part is occupied by immature neurons. The dividing cells are in the basal part of the epithelium. Thus before birth olfactory epithelium is well organized and it remains the same in neonates. In postnatal mice mature neurons are abundant and most part of the sensory neuron layer is taken over by mature neurons and remaining by immature neurons (Fig. 1D).

1.2.b Vomeronasal organ prenatal development

Vomeronasal organ originates from the olfactory pit but its development lags behind olfactory epithelium development. Vomeronasal organ development could be categorized in six phases, three of them are prenatal; (*1*) anlage, (*2*) early morphogenesis and (*3*) late morphogenesis. Development of vomeronasal organ continues after birth with remaining

three stages; (*4*) initiation of secretory activity, (*5*) cytoarchitectural maturity and (*6*) complete histogenesis (Garrosa et al. 1992).

Development of vomeronasal organ differs from species to species (Garrosa et al. 1998). For example; in rat vomeronasal duct is open during embryonic development but in mouse remains closed even after birth. Thus vomeronasal organ remains non-functional in mouse throughout embryonic development (Coppola and O'Connell 1989; Coppola et al. 1993; Garrosa et al. 1998). Here I will discuss mainly prenatal development stages of mouse vomeronasal organ.

Anlage: at E11 the medial wall of presumptive olfactory epithelium thickens which forms the vomeronasal primordium. Soon vomeronasal primordium starts to invaginate and forms the vomeronasal organ. Most of the cells are immature with prominent nucleolus. Sensory and non-sensory epitheliums are not distinguishable at this stage (Cuschieri and Bannister 1975a; Garrosa et al. 1998).

Early morphogenesis: vomeronasal organ attains tube like structure between E12 to E14. The crescent shaped vomeronasal lumen is formed surrounded by sensory and non-sensory epithelium. Sensory epithelium becomes thicker and aligns medially. Immature neurons with axons and dendrites, supporting cell precursors and basal cells are recognizable at this stage (Zancanaro et al. 2002). Non-sensory epithelium aligns laterally. Developing blood vessels are seen lateral to non-sensory epithelium (Nagahara et al. 1995). In rat, luminal surface of sensory epithelium exhibits microvilli (Garrosa et al. 1998). By the end of this stage vomeronasal organ becomes a conspicuous structure at the ventral side of the nasal septum.

Late morphogenesis: this is the longest prenatal stage from E15 to birth. Vomeronasal organ elongates to a cigar shape and acquires the adult-like structure. Crescent shaped sensory epithelium becomes multilayered. Oval-shape nuclei of supporting cells make upper layer (towards luminal surface) and the rest of the epithelium is formed by neurons and basal cells. Non-sensory epithelium remains just two-three layers thick (Garrosa et al. 1998). Majority of dividing cells are restricted in corners of crescent shaped sensory epithelium. At the end of this stage few mature neurons can be seen in the sensory epithelium (Tarozzo et al. 1998). Few knobs like structures are seen at luminal surface of sensory epithelium. Sensory neurons and supporting cells protrude microvilli into the lumen. By the end of this phase vomeronasal lumen is formed but its opening duct remains closed until birth (Coppola and O'Connell 1989; Coppola et al. 1993; Garrosa et al. 1998).

In mouse at the time of birth the sensory epithelium consists only of Gαo expressing V2R neurons. Gαi2 expressing V1R neurons are first seen at postnatal day three and by postnatal day thirteenth V1R and V2R are localized respectively in apical and basal parts of sensory epithelium (Berghard and Buck 1996). In mouse, at the time of birth, vomeronasal

organ is comprised of mature neurons, supporting cells and microvilli, however the vomeronasal duct remains close until birth and only a sub-type of neurons is abundant. During further postnatal development the vomeronasal organ attains its functional anatomy to accomplish various physiological roles.

1.3 Canonical olfactory signal transduction

Olfactory signal transduction is a sophisticated mechanism that occurs in olfactory cilia. In cilia different components of signal transduction machinery are specifically compartmentalized to make signal transduction more efficient (Reisert et al. 2003; French et al. 2010). Cilia are immersed in mucus secreted and maintained by Bowman's gland and supporting cells (Menco and Farbman 1992; Menco et al. 1998). Odor molecules pass through mucus to interact with olfactory receptors that are expressed in the ciliary membrane.

Interaction of odor molecules and olfactory receptors triggers a cascade of events that convert chemical stimulus in neural stimuli, i.e. depolarization of olfactory sensory neurons. Olfactory receptors are G-protein coupled receptors (Buck and Axel 1991). The binding of odor molecules to specific olfactory receptors activates them and causes the detachment of Gαolf subunit from Gβ and Gγ subunits and the subsequent activation of adenylyl cyclase III (ACIII) (Jones and Reed 1989; Bakalyar and Reed 1990). Adenylyl cyclase III is a membrane protein and converts adenosine triphosphate (ATP) into cyclic adenosine monophosphate (cAMP). Increase of cAMP concentration in the ciliary lumen results in the opening of cyclic nucleotide gated (CNG) channels. CNG channels are non-selective cationic channels located in the cilia and their opening leads to an influx of sodium and calcium cations in ciliary lumen from the mucus that depolarizes the sensory neurons (Nakamura and Gold 1987; Schild and Restrepo 1998; Pifferi et al. 2006).

The increased calcium concentration in ciliary lumen plays a role in adaptation and activation of chloride channels (Menini 1999; Matthews and Reisert 2003). The chloride concentration in olfactory sensory neurons cilia is similar to the chloride concentration in the mucus and is maintained by $Na^+/Ca^{2+}/2Cl^-$ co-transporter NKCC1 and $Cl^-/HCO3^-$ exchanger SLC4A1 (Nakamura et al. 1997; Reuter et al. 1998; Kaneko et al. 2001, 2004; Reisert et al. 2005; Nickell et al. 2006, 2007; Hengl et al. 2010). Therefore opening of calcium-activated chloride channels cause efflux of anions that correspond to an inward current and further contributes to the depolarization of olfactory sensory neurons (Kleene and Gesteland 1991; Kurahashi and Yau 1993; Lowe and Gold 1993; Kleene 1993). Cation influx depolarizes neurons, however anion efflux is essential for the amplification of the depolarizing current and to increase signal to noise ratio that helps in detection of low concentrations of odor molecules (Lowe and Gold 1993; Kleene 1997). Cation and anion currents could be also

necessary in case of changes in mucus ionic concentration (Kleene and Gesteland 1991; Kurahashi and Yau 1993; Kleene and Pun 1996; Kleene 1999). Odor response recovery includes reestablishment of the resting ionic gradients in cilia. Increased luminal calcium also controls activation of CNG channels by feedback mechanism. A Na^+/Ca^{2+} exchanger NCKX4 and a plasma membrane calcium-ATPase contribute to calcium efflux as the odor response terminates (Noé et al. 1997; Reisert and Matthews, 1998; Antolin et al. 2010; Frings, 2001; Stephan et al. 2012).

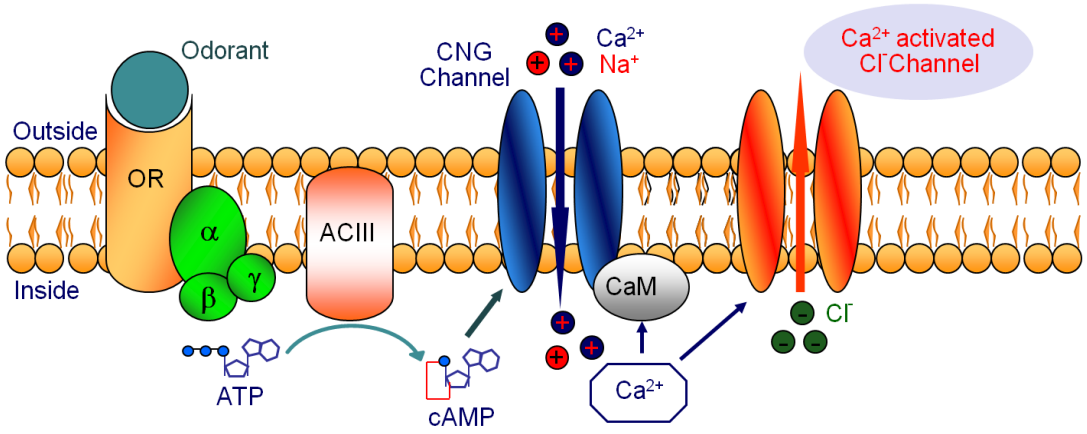

Fig. 4: Canonical olfactory signal transduction in the ciliary membrane of an olfactory sensory neuron. An odorant interacts with the olfactory receptor (OR) and elicits olfactory signal transduction mechanism. Gαolf subunit from the activated G-coupled protein complex detaches and activates the adenylyl cyclase III (ACIII). ACIII facilitates formation of cAMP from ATP. Intra-luminal increase in cAMP concentration leads to opening of cyclic nucleotide gated (CNG) channels. CNG channels are non-selective cationic channel and cause influx of sodium and calcium cations. Cation influx leads to depolarization of the neuron, however the increased calcium concentration in the ciliary lumen also activates calcium-activated chloride channels (CaCCs). Olfactory sensory neurons maintain an unusual chloride concentration so the opening of CaCCs leads to an efflux of chloride ions from the ciliary lumen to mucus. *Modified from Pifferi et al. 2006.*

1.3.a Olfactory receptors

Olfactory receptors are G-protein coupled receptors (GPCRs) (Buck and Axel 1991). Olfactory receptors have seven transmembrane domains with extracellular N-terminal and intracellular C-terminal. N-terminal domain along with transmembrane domains make odorant biding pocket (Strader et al. 1995). Various types of Gα genes (Gαolf, Gαs, Gαo, Gαi2, Gα11, Gα13) are expressed in olfactory sensory neurons but Gαolf is most abundant and genetic ablation of Gαolf results in anosmia, which confirms its importance in signal transduction (Menco et al. 1994; Berghard and Buck 1996; Belluscio et al. 1998). Variable amino acid sequences of transmembrane domains give rise to various types of odorant receptors. In mouse ~1390 olfactory receptor genes are found but only around 1000 are expressed, while the remaining are pseudogenes. In humans around 52% olfactory receptors are pseudogenes (Buck and Axel 1991; Touhara 2009). Olfactory receptor expression is monoallelic and follows the “one receptor one neuron” rule, i.e. one neuron

expresses only one olfactory receptor. Only a small population of olfactory sensory neurons expresses a particular olfactory receptor (Chess et al. 1994; Malnic et al. 1999; Serizawa et al. 2003, 2004; Shykind 2005). The exact mechanism of single olfactory receptor expression is not well known. Some recent studies suggest that in immature neurons aggregated olfactory receptor genes are in silent stage in heterochromatin foci, further one of olfactory receptor expression is activated by lysine demethylase1 (LSD1) (Clowney et al. 2012; Lyons et al. 2013). Earlier expressed olfactory receptor suppresses the expression of other olfactory receptors by PERK-dependent phosphorylation of a translation initiation factor eIF2α (Dalton et al. 2013).

1.3.b Adenylyl cyclase III

Adenylyl cyclase is a key enzyme of transmembrane signaling pathways in many cells including olfactory sensory neuron cilia in amphibians and rodents (Pace et al. 1985; Pfeuffer at al. 1989). It is a family of ten members; three of them are expressed in olfactory epithelium; adenylyl cyclase II, adenylyl cyclase III and adenylyl cyclase IV (Bakalyar and Reed 1990; Feinstein et al. 1991; Sunahara et al. 1996; Wong et al. 2000). Adenylyl cyclase III is expressed in cilia. Adenylyl cyclase III knockout mice are anosmic and the axonal projections of olfactory sensory neurons are miss-routed in these mice (Wong et al. 2000; Col et al. 2007; Zou et al. 2007).

Adenylyl cyclase III is a transmembrane protein with twelve domains and, both N-terminal and C-terminal are cytoplasmic. Once stimulated by Gαolf the catalytic region, between transmembrane domain six and seven, converts adenosine tri-phosphate (ATP) into cyclic adenosine mono-phosphate (cAMP). cAMP is the canonical second messenger of olfactory signal transduction (Lowe et al. 1989; Brunet et al. 1996; Takeuchi and Kurahashi 2003). Odor-induced elevated cAMP is degraded by phosphodiesterases (PDEs). Two phosphodiesterases are expressed in olfactory sensory neurons; PDE1C in cilia and PDE4A in dendrite, cell body and axon terminals but not in cilia (Juilfs et al. 1997). Though PDE1C is expressed in cilia, only in the double knockout mice for PDE1C and PDE4A removal of elevated cAMP is severally effected (Cygnar and Zhao 2009).

1.3.c Cyclic nucleotide gated channel

Cyclic nucleotide gated (CNG) channels are distributed all over cilia but predominantly expressed at the distal part of cilia (Matsuzaki et al. 1999). The CNG channel is a tetramer of two-CNGA2, one-CNGA4 and one-CNGB1b subunits with a central pore region. Each CNG subunit has six transmembrane domains and a cyclic nucleotide binding site close to the C-terminal at the cytoplasmic side. Thus each CNG channel has four cAMP binding sites (Dhallan et al. 1990; Zheng and Zagotta 2004). CNG channel is directly activated by cAMP and permeable to monovalent sodium and potassium and divalent

calcium cations. CNGA2 knockout mice are anosmic for most odorants but have residual response to some odorants (Brunet et al. 1996; Zhao and Reed 2001; Lin et al. 2004). Knockout mouse for CNGA4 or CNGB1b showed alteration in odor adaptation and defective trafficking of other CNG subunits to the cilia (Munger et al. 2001; Bradley et al. 2001; Michalakis et al. 2006).

Modulation of CNG channels by calcium leads to olfactory adaptation. Calcium concentration increases after the opening of CNG channels, via a feedback mechanism increased calcium concentration modulate CNG channels that decrease their sensitivity to cAMP and alter the neuronal response. The modulation of CNG channels by calcium is mediated either by apocalmodulin or calmodulin (Kramer and Siegelbaum 1992; Lynch and Lindemann 1994; Balasubramanian et al.1996; Bradley et al. 2004). Interestingly, deletion of calmodulin binding site in CNGB1b subunit of CNG channels does not affect receptor current adaptation, but termination after response becomes slower (Song et al. 2008).

1.3.d Calcium-activated chloride channels in olfactory sensory neurons

Increase of calcium concentration in the ciliary lumen has various effects including adaptation and activation of chloride channels. Influx of sodium and calcium depolarizes the olfactory sensory neurons, furthermore chloride efflux amplifies the depolarizing current and constitutes up to 90% of total current. In some cases the anion current could be 30 times higher than the cation current (Reisert et al. 2003, 2005; Boccaccio and Menini 2007; Kleene 2008). Calcium-activated chloride currents were first observed in amphibian olfactory sensory neurons and later described in mammalian olfactory neurons (Kleene and Gesteland 1991; Lowe and Gold 1993). Olfactory cilia are always immersed in mucus and ionic composition of mucus is crucial for detection of odor molecules. In amphibians it is hard to maintain mucus ionic integrity in fresh water thus it becomes important to have an additional amplification step in addition to cation influx, i.e. chloride efflux (Kurahashi and Yau 1993; Kleene and Pun 1996). Odor molecules and olfactory receptors have mean dwell time around 1 ms so there is always a possibility that low concentration odor molecules could not be detected due to lack of enough cAMP synthesis and cation current (Bhandawat et al. 2005; Frings 2009). However chloride efflux is thought to amplify depolarization current by providing high gain and low noise amplification (Lowe and Gold 1993; Kleene 1993, 1997).The chloride efflux based signal amplification might increase the possibility to detect odor molecules even at low concentrations and limited interaction with olfactory receptors which make olfactory system efficient (Kleene 2008; Frings 2009).

1.3.e Canonical signal transduction in vomeronasal sensory neurons

Neurons in the vomeronasal organ are organized into apical and basal layers (*described in section* 1.1.b and 1.2.b). In general V1R receptor-positive apical neurons

express Gαi2, whereas V2R receptors-positive basal neurons express Gαo (Rodriguez 2003; Rodriguez and Boehm 2008; Francia et al. 2014). Chemosensory signal transduction mechanism in vomeronasal neurons is quite different from olfactory sensory neurons and not well elucidated. Different components of olfactory signal transduction like Gαolf, ACIII, CNG channel are not expressed in vomeronasal sensory neurons (Berghard and Buck 1996). Genetic ablation of Gαi2 leads in the elimination of ~50% apical neurons, reduction in neuronal activity and changes in maternal behavior (Norlin et al. 2003). But to which extent Gαi2 ablation affects the biophysical properties in these neurons is not known. Gαo has a central role in basal vomeronasal neurons signal transduction machinery. The genetic ablation of Gαo severely affects the detection of peptides, pheromone sensory responses and pheromone-guided behaviors, such as male-male and maternal interaction (Chamero et al. 2011). Signal transduction in vomeronasal sensory neuron involves the activation of transient receptor potential canonical 2 (TRPC2) channels that is mediated by phopholipase C (PLC) dependent synthesis of diacylglycerol (DAG) (Holy et al. 2000; Spehr et al. 2002; Lucas et al. 2003). TRPC2 is a cation channel and its activation causes an influx of sodium and calcium cations in microvilli of vomeronasal sensory neurons. TRPC2 genetic ablation causes 50% and 75% reduction in density of apical and basal neurons, respectively (Stowers et al. 2002). TRPC2$^{-/-}$ mice showed strong reduction in responses against the molecules tested in electro-vomeronasogram. Though apical neuron mediated responses were eliminated in TRPC2$^{-/-}$ mice, however various responses mediated by basal neurons remained unaffected (Leypold et al. 2002; Stowers et al. 2002, Kelliher et al. 2006).

Similarly to olfactory sensory neurons, calcium influx is involved in sensory adaptation and also in activation of chloride channels in vomeronasal sensory neurons (Spehr et al. 2009; Francia et al. 2014). Urine-stimulated responses can be carried up to 80% by calcium-activated chloride channels (Yang and Delay 2010). Calcium-activated chloride currents in vomeronasal sensory neurons were characterized using blockers and focal release of calcium in microvilli (Kim et al. 2011; Dibattista et al. 2012). Thus calcium-activated chloride channels also have a role in the signal transduction mechanism in vomeronasal sensory neurons, but to which extent they influence physiology of these neurons remains elusive.

1.4 Calcium-activated chloride channels: TMEM16A and TMEM16B

Calcium-activated chloride currents were first described in *Xenopus* oocytes and photoreceptor cells. Further they were reported in central and peripheral neurons, olfactory cilia, developing skeletal muscle, cardiac muscle, smooth muscle, lacrimal gland cells, intestinal cells, tracheal cells, kidney cells and pituitary cells (Hartzell et al. 2005; Duran and Hartzell 2011; Huang et al. 2012a). These channels are non-selective anion channels;

however in physiological condition chloride is the most abundant anion so usually these channels are responsible for chloride permeability. In excitable cells, like in neurons, they drive chloride flux depending on the electrochemical gradient. They could be involved in depolarization, hyperpolarization or repolarization (Britton et al. 2010). In secretory and epithelial cells (with high intracellular chloride) calcium-activated chloride efflux is accompanied by passive sodium release and transepithelial water secretion. Thus calcium-activated chloride channels can regulate secretion and hydration at epithelial surface (Kidd and Thorn 2000; Melvin et al. 2005). Because of their interference in various physiological processes calcium-activated chloride channels have been studied for their biophysical and physiological properties, but the molecular identity of the channel and physiological roles remain debatable in various tissues (Hartzell et al. 2005).

In 2008 three groups have found transmembrane protein 16 A (TMEM16A) or anoctamin1 (ANO1) with similar electrophysiological properties as that of native calcium-activated chloride channels (Caputo et al. 2008; Schroeder et al. 2008; Yang et al. 2008). TMEM16A belongs to TMEM16 protein family that is comprised of ten family members (TMEM16A-K, I is excluded from nomenclature). In addition to TMEM16A, another member of this family TMEM16B showed calcium-activated chloride channel properties (Schroeder et al. 2008; Stöhr et al. 2009; Pifferi et al. 2009; Stephan et al. 2009). Interestingly, TMEM16B expression is seen mainly in neuronal tissue, while TMEM16A is expressed ubiquitously in epithelial cells as well as in neuronal tissue (Duran and Hartzell 2011; Pedemonte and Galietta 2014). Another member of this family, TMEM16F showed scrambling activities as well as cation channel properties (Suzuki et al. 2010; Yang et al. 2012). However some other studies described TMEM16F as an anion channel (Martins et al. 2011; Grub et al. 2013; Shimizu et al. 2013). Biophysical properties and physiological role of other members of TMEM16 are unclear.

TMEM16 protein family members have eight putative transmembrane domains with cytoplasmic N-termini and C-termini. The predicted topology of transmembrane domains one-four and seven-eight is constant in different analysis. Topology between transmembrane domains four and seven remains uncertain. Using bioinformatics and hydropathy analysis earlier studies found a re-entrant loop between transmembrane domains five and six (Hahn et al. 2009; Milenkovic et al. 2010). Contrary to this, by using human influenza hemaglutin (HA) epitopes, a new topology was proposed with a re-entrant loop between transmembrane domain six and seven (Yu et al. 2012).

TMEM16A and TMEM16B have different biophysical properties. TMEM16A is more sensitive to calcium than TMEM16B. At positive voltage TMEM16A calcium sensitivity is in the nanomolar range however, for TMEM16B it is in micromolar range. The TMEM16B unitary conductance is also ~10 fold less than that of TMEM16A. Moreover, TMEM16B

channel activation kinetics is faster than that of TMEM16A (Caputo et al. 2008; Yang et al. 2008; Pifferi et al. 2009; Stephan et al. 2009).

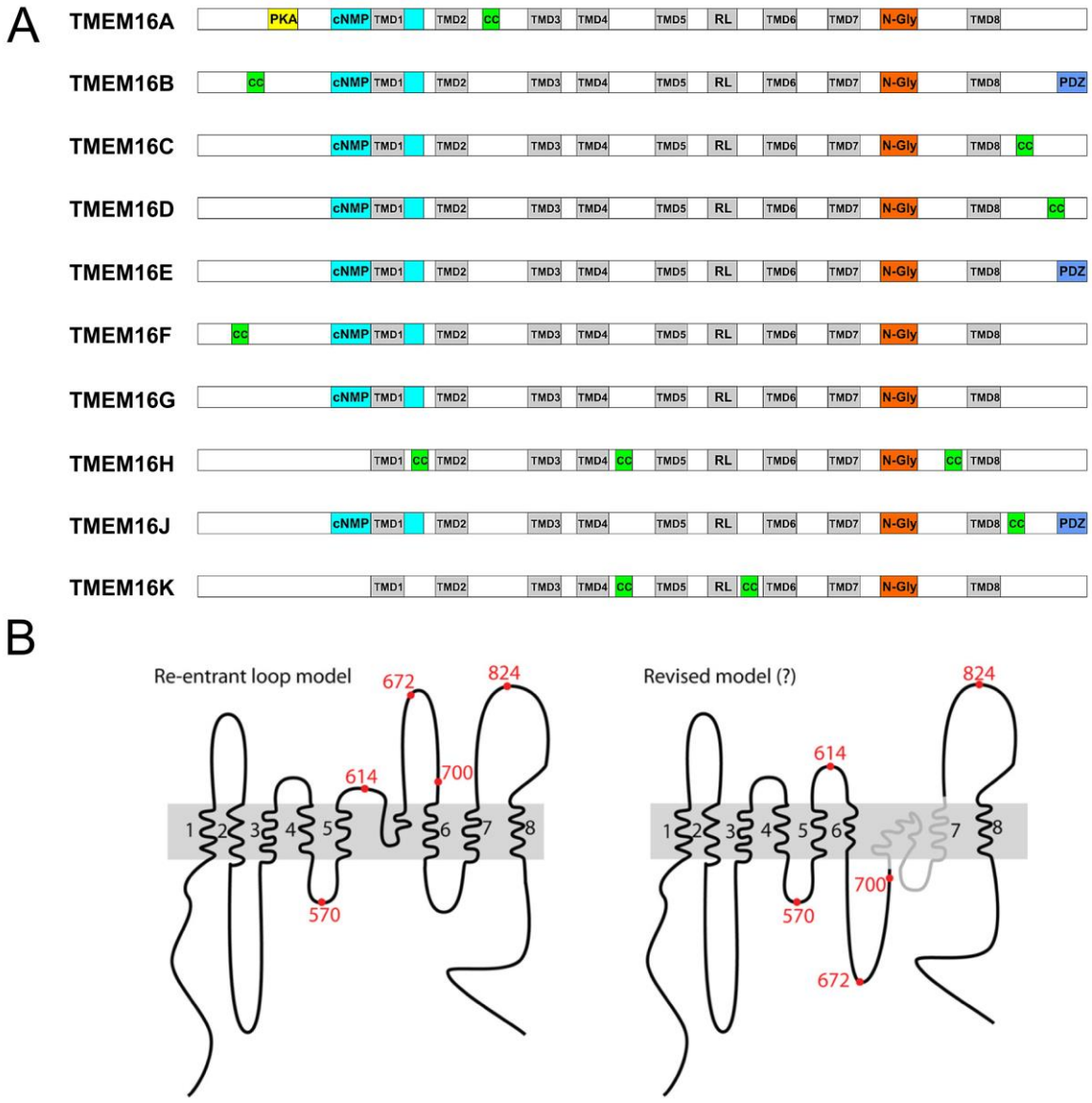

Fig. 5: ***(A)*** Schematic presentation of different domains in TMEM16 protein family members. Predicted membrane topology is based on bioinformatics and hydropathy analysis of 166 vertebrates TMEM16 sequences. All family members have eight putative transmembrane domains (TMD). Between TMD7 and TMD8 an N-glycosilation site (N-Gly) is also predicted in all TMEM16 proteins. Hydropathy plotting also suggests a re-entrant loop between TMD5 and TMD6. Cyclic nucleotide-monophosphate binding domain (c-NMP) is predicted in between TMD1 and TMD2 in all TMEM16 proteins except TMEM16H and TMEM16K. Protein kinase A phosphorylation site (PKA) is predicted only for TMEM16A. Protein-protein interaction domain PDZ is only suggested in c-terminals of TMEM16B, TMEM16E and TMEM1J. Except TMEM16E and TMEM16G, coiled-coil domains (cc) are suggested to be present in other TMEM16 proteins. Number of cc-domains varies from protein to protein. *Modified from Milenkovic et al. 2010*. ***(B)*** Using human influenza hemaglutin (HA) tags old "re-entrant loop model" of mouse TMEM16A is questioned and a new "revised model" has been proposed. Amino acid numbers in red is the site of inserted HA tags. *Adapted from Yu et al. 2012*.

Mouse TMEM16A and TMEM16B have 56.5% sequence similarity and 71.4% amino acid similarity (Huang et al. 2012a). TMEM16A has at least four alternatively spliced segments a*, b, c* and *d* that correspond respectively to an alternative initiation site, exon-6b, exon-13 and exon-15 (Ferrera et al. 2009). Segments *a* and *b* reside in the N-terminal, segments *c* and *d* reside in the first intracellular loop. Thus TMEM16A transcripts can produce multiple protein isoforms; those could have different voltage dependence and calcium sensitivity (Caputo et al. 2008; Ferrera et al. 2009; Xiao et al. 2011). Four amino acids (ERSQ) in TMEM16B correspond to TMEM16A segment *c* (EAVK), in the absence of it the channel becomes inactive at higher calcium concentration, however in the presence of this segment channels are non-inactive even at higher calcium concentration (Vocke et al. 2013). Exon-14 corresponds to ERSQ sequence of TMEM16B and a spliced out variant expresses in mouse olfactory epithelium, however in the retina TMEM16B expresses with the ERSQ sequence (Stephan et al. 2009). TMEM16B channel without exon-4 has shorter N-terminal and remains inactive (Ponissery et al. 2013). Thus in different tissues TMEM16A and TMEM16B play different roles, which correspond to the expressed splice variants and functions of tissue.

1.4.a TMEM16A physiological role

Genetic ablation of TMEM16A is lethal and mice died within few days after birth. The homozygous knockout mouse shows alterations in tracheal cartilage ring formation because of defects in the epithelium or tracheal muscles and mice die due to tracheomalacia (Rock et al. 2008). These mice also show defects in calcium-dependent chloride secretion and accumulation of mucus in airways (Rock et al. 2009; Ousingsawat et al. 2009). In the absence of TMEM16A interstitial cells of Cajal (ICC) fail to generate slow wave activity in gastrointestinal smooth muscles and TMEM16A knockout mice lack proper gut movements (Hwang et al. 2009). Thus TMEM16A is involved in various physiological processes and some are vital for survival of the animal.

Before being identified as a calcium-activated chloride channel, TMEM16A over expression has been reported in different malignant tumors as in gastrointestinal stromal tumors (GISTs), oral and esophageal squamous cell carcinoma. Depending on the tumor it was known as discovered on gastrointestinal stromal tumors protein 1 (DOG-1), oral cancer overexpressed 2 (ORAOV2) and tumor-amplified and overexpressed sequence 2 (TAOS2) (West et al. 2004; Huang et al. 2006; Espinosa et al. 2008; Kashyap et al. 2009).

TMEM16A is involved in proliferation as well as in migration of cells. Proliferation of interstitial cells of cajal is severely affected in TMEM16A knockout mice. Down regulation of TMEM16A by RNAi-mediated silencing and blockers of calcium-activated chloride channels

down regulate the proliferation of TMEM16A expressing cells (Stanich et al. 2011; Duvvuri et al. 2012; Liu et al. 2012; Mazzone et al. 2012; Britschgi et al. 2013).

Along with proliferation, cell migration is also affected by TMEM16A over expression (Ayoub et al. 2010; Liu et al. 2012; Ruiz et al. 2012; Jacobsen et al. 2013). In some cancer cells like SCC-2, BHY, CAL-3 TMEM16A only affects cell migration (Ayoub et al. 2010; Ruiz et al. 2012; Wanitchakool et al. 2014). However screening of thousands of malignant tumors by Ruiz et al. (2012) showed that, not all type of tumors overexpress TMEM16A. A recent report found the overexpression of TMEM16A in GIST cells, but suggests that TMEM16A has a very minor influence on viability and proliferation of cells *in vitro* (Berglund et al. 2014). In heterologous expression systems TMEM16A also regulate ciliogenesis, but it needs to be confirmed *in vivo* (Ruppersburg and Hartzell 2014). Dynamic expression of TMEM16A in various developing tissues has been seen during embryonic development (Rock and Harfe 2008; Gritli-Linde et al. 2009). Thus it seems that TMEM16A expression affects proliferation and migration of cells that depend on the cell types and intracellular factors, but the mechanism still remains elusive.

Chloride secretion is important for the regulation of electrolyte and water balance in secretory cells and secreted mucus. TMEM16A is widely expressed in various secretory epithelium and acinar cells and is supposed to play an important role in chloride regulation across cells. It is evident from the mucus accumulation in the trachea of TMEM16A knockout mice and the reduced transepithelial currents in trachea and colonic epithelium from these mice that TMEM16A is an important chloride secretory channel in epithelial cells (Rock et al. 2009; Ousingsawat et al. 2009). TMEM16A knockout mice or siRNA treated submandibular gland acinar cells showed disrupted chloride and salivary secretion (Ousingsawat et al. 2009). In airway's serous and mucus cells TMEM16A-dependent chloride secretion was also confirmed by other studies (Lee and Foskett 2010; Fischer et al. 2010). In addition to chloride secretion in acinar cells, TMEM16A also regulates bicarbonate anion permeability, so it is possible that TMEM16A could be involved in pH regulation of these cells (Jung et al. 2013; Jang and Oh 2014). TMEM16A is expressed in mucin-secreting cells in the airway epithelium. Asthma rodent model and human asthma samples show increased TMEM16A expression in mucin-secreting cells that can be overcome by calcium-activated chloride channels blockers, supporting the possible role of TMEM16A in regulation of mucin secretion in airway epithelium (Huang et al. 2012b).

TMEM16A expression in the large intestine is compartmentalized; the distal colon expresses TMEM16A while the proximal colon is devoid of it. TMEM16A$^{-/-}$ mice lack TMEM16A stimulated chloride secretion in colon. In distal colon rotavirus toxin NSP4 induced chloride secretion is mediated by TMEM16A. Thus it seems that TMEM16A is involved in rotavirus-mediated gastroenteritis (Ousingsawat et al. 2009, 2011).

During cephalic development TMEM16A is expressed in different parts of the central nervous system, however up to now we have very limited information about TMEM16A's role in the adult nervous system. TMEM16A is expressed in small nociceptive neurons of dorsal root ganglia. siRNA-mediated down regulation of TMEM16A confirms that TMEM16A is involved in bradykinin elicited nociception (Liu et al. 2010). Using siRNA and conditional gene knockdown it was shown that TMEM16A is expressed in dorsal root ganglion neurons and is involved in heat sensation (Cho et al. 2012). Recently TMEM16A and TMEM16B co-expression has been found in vomeronasal sensory neurons, where these channels are supposed to be involved in detection of pheromones and responsible for the calcium-activated chloride currents (Dauner et al. 2012; Dibattista et al. 2012). Thus it seems that TMEM16A is involved in different sensory processes and it is subject to the intracellular factors and extracellular environment.

1.4.b TMEM16B physiological role

TMEM16B is another member of the TMEM16 protein family with calcium-activated chloride channel properties. When expressed in heterologous systems TMEM16B generates calcium-activated chloride currents that are similar to native calcium-activated chloride currents (Schroeder at al. 2008; Pifferi et al. 2009). Contrary to TMEM16A, its expression is found mainly in neuronal tissue like olfactory epithelium, vomeronasal organ, retina and hippocampus (Yu et al. 2005; Stöhr et al. 2009; Rasche et al. 2010; Huang et al. 2012c). TMEM16B transcripts are expressed in adult mouse olfactory epithelium (Yu et al. 2005; Stephan et al. 2009; Rasche et al. 2010; Sagheddu et al. 2010). Proteomic and immunohistochemistry analysis have shown TMEM16B expression in olfactory cilia as well as in microvilli of vomeronasal sensory neurons (Mayer et al. 2009; Stephan et al. 2009; Hengl et al. 2010; Sagheddu et al. 2010; Dauner et al. 2012; Dibattista et al. 2012). Olfactory sensory neuron cilia and vomeronasal sensory neuron microvilli are the site for signal transduction. TMEM16B expression in these sites of sensory neurons confirms its role as calcium-activated chloride channels in the sensory signal transduction cascade. Billig et al. (2011) produced the elimination of calcium-activated chloride currents in TMEM16B knockout mouse. Though in this mouse electro-olfactogram amplitude is diminished only by ~40%, odorant detection and discrimination ability remain the same as in wild type mice (Billig et al. 2011). In olfaction test the concentration of odorants is usually in the range of 1-100 µM but in air many of odorants are in a lower range (Frings 2009). Thus further experiments with lower odorant concentration and altered extracellular ionic conditions are necessary to investigate the physiological importance of TMEM16B in the olfactory system.

At photoreceptor nerve terminals calcium-activated chloride channels regulate the release of glutamate by a local feedback mechanism. TMEM16B is expressed along with

PSD95, VELI3, MPP4 and PMCA in the mouse retina. TMEM16B interact with PSD95 and MPP4 and expresses in presynaptic rod spherules but cone pedicles are devoid of it. Further MPP4 knockout mouse showed abolition of TMEM16B (Stöhr te al. 2009; Dauner et al. 2013). Localization of TMEM16B in photoreceptors and its interaction with presynaptic adaptor proteins suggests that TMEM16B is the possible candidate for the calcium-activated chloride channel in photoreceptors.

In the hippocampus neuronal synaptic transmission between CA3 and CA1 is regulated by a calcium-activated chloride channel. Using blockers and shRNA it was found that TMEM16B is the main calcium-activated chloride channel in the somatodendritic region of postsynaptic CA1 neurons. Depending on the extracellular chloride concentration, TMEM16B could have a dual role with having either inhibitory or excitatory effects on action potentials (Huang et al. 2012c).

2. Aim

Calcium-activated chloride channels have diverse roles in various physiological processes including olfaction. The goal of my work was to decipher their role in olfactory epithelium development by the evaluation of TMEM16A and TMEM16B expression during mouse olfactory epithelium development. The aim of this thesis is summarized below:

(1) To study the expression of calcium-activated chloride channels TMEM16A and TMEM16B in main olfactory epithelium, vomeronasal organ and nasal glands.

(2) To investigate temporal and spatial expression patterns of TMEM16A and TMEM16B in main olfactory epithelium during embryonic development of the mouse.

(3) To evaluate the effect of TMEM16A on the development of the olfactory epithelium and various nasal glands using the TMEM16A knockout mouse model.

3. Material and Methods

Animals

All animals were handled in accordance with the Italian Guidelines for the Use of Laboratory Animals (Decreto Legislativo 27/01/1992, no. 116) and European Union guidelines on animal research (No. 86/609/EEC). Wild-type C57Bl6, OMP-GFP mice [genetically modified mice that express green fluorescent protein (GFP) instead of olfactory marker protein (OMP) in all mature olfactory sensory neurons] and TMEM16A$^{+/-}$ mice were used in this study. OMP-GFP mice were generated by *Potter et al. 2001*, and obtained by Dr. Peter Mombaters, Max Planck institute for Biophysics, Frankfurt, Germany. TMEM16A$^{+/-}$ mice were generated by *Rock et al. 2008*, and obtained by Dr. Luis J. V. Galietta, Istituto Giannina Gaslini, Genova, Italy. Every precaution and care has been taken so that animals suffer least. The mouse colony was maintained in the animal house facility at SISSA, Trieste and housed in a temperature-controlled environment with a twelve hour light/dark cycle and access to food and water *ad libitum*.

For the postnatal mice date of birth was defined as postnatal day 0 (P0). Postnatal mice were anaesthetized by CO_2 inhalation and decapitated. Skin surrounding the skull and jaw were removed without damaging the nose. The nose was separated from the rest of the head and processed further. For the vomeronasal organ processing vomeronasal organs were extracted from the nasal cavity and processed further.

Collection of Embryos

Male and female mice of the same strain were put together for mating in the evening and separated in the next morning. If a vaginal plug was observed in the morning, that day was designated as embryonic day 0.5 (E0.5). Once the mouse was positive for a vaginal

plug, on the prerequisite embryonic day mice were anaesthetized by CO_2 inhalation and further cervical dislocation was performed. To consistent for the age of embryos all dissections were done between 09.00 AM to 11.00 AM. The age of embryos were also compared to the database present at: http://www.emouseatlas.org/Databases/Anatomy/MAstaging.html.

After removing the abdominal skin, abdominal cavity was exposed after removing the peritoneum. Taking extra care the uterus was removed from the abdominal cavity and transferred into sterile PBS (P4417 Sigma, Milano, Italy) in a Petri dish. The uterus was cut in a way that each piece contains single embryo. Before isolation of each embryo from uterine pieces, the uterine pieces were transferred to another Petri dish containing sterile PBS. Uterus wall was cut taking extra care not to damage the embryo and peeled out in such a way that the intact embryo came out from the uterus. Head region with the nose was separated from rest of body and processed further for immunohistochemistry. For E16.5 and E18.5, skin from head region was also removed.

Genotyping of TMEM16A knockout mouse

To check the genotype of mice for *Tmem16a* gene, genotyping for deletion of exon-12 of *Tmem16a* and insertion of PGK-neo cassette was done. Genomic DNA was isolated from the mouse tails by using 5'PRIME Kit (Eppendorf, Milano, Italy), according to manufacturer's protocol. PCR was carried out in a total volume of 25 µl under the following conditions for 40 cycles: 94°C for 5 min (for 1 cycle), 94°C for 30 sec, 60°C for 30 sec and 72°C for 30 sec. The final reaction mixture contained 100 ng of genomic DNA, using Taq Polymerase Master Mix (VWR, Milano, Italy). Two separate PCRs were required to identify homozygous knockout mouse: one for the mutant allele (PGK-neo instead of exon-12) and one for the wild type allele. Wild type allele size was 330 bp and mutant allele was 450 bp. DNA was separated by electrophoresis on 1,5% agarose gel with ethidium bromide.

Primers used:

WT (f): 5'-CCTATGACTGCCAGGGACGCCC-3'

WT (rev): 5'-TGTTCCTGTCCCTGCAATGCGG-3'

Mut (f): 5'-GACGCCCTCCATTGACCC-3'

Mut (rev): 5'-GCAGTAGAAGGTGGCGCGAAG-3'

Dissociation of vomeronasal sensory neurons

Two months old mice were anaesthetized by CO_2 inhalation and decapitated before vomeronasal organ removal. The vomer capsule containing the vomeronasal organ was removed, and vomeronasal sensory neurons were dissociated from the vomeronasal organ with a standard enzymatic-mechanical dissociation protocol. The removed vomer capsule

was immediately transferred to a Petri dish containing divalent-free PBS solution where the vomeronasal organ was extracted. The tissue was cut into three to four small pieces with tiny scissors and further transferred to divalent-free PBS (P4417 Sigma, Milano, Italy) containing collagenase (1mg/ml, Type A). After incubation at 37°C for 10 minutes, tissue was again chopped by tiny scissors for two to three times and re-incubated for 10 min at 37°C. After 2 minutes centrifugation at 1700 rpm the tissue was gently triturated with a fire-polished Pasteur pipette. Cells were re-suspended in 1 ml fresh Ringer solution (120 mM NaCl, 25 mM NHCO3, 5 mM KCl, 1 mM CaCl2, 1 mM MgCl2, 10 mM D-glucose, 10 mM HEPES, pH 7.2) and plated on a glass coverslip, coated with equal volume of poly-L-lysine (10 mg/ml) and concanavalin A (Type V, 10 mg/ml). Cells were allowed to settle down on coverslips for two hours at 4 °C. All chemical were purchased from Sigma, Milano, Italy.

Immunocytochemistry

HEK 293T cells were grown in DMEM (GIBCO) supplemented with 10% FBS, 100 U/ml penicillin, and 100 µg/ml streptomycin at 37ºC in a humidified CO_2 incubator. HEK 293T cells were grown on coverslips and co-transfected with plasmids containing the cDNA sequence of TMEM16A or TMEM16B, and eGFP (Clontech, Mountain View, CA, USA) for fluorescent identification of transfected cells. Transfected cells were fixed in 4% paraformaldehyde for 15 minutes at room temperature and sequentially washed. Next, they were incubated with a quenching solution (0.1 M glycine) for 10 minutes and washed 3 times in PBS each for 5 minutes. Further cells were treated with 0.05% SDS for 10 minutes and washed 3 times in PBS each for 5 minutes. Cells were subsequently incubated for 15 minutes in blocking solution [2% Fetal Bovine serum (v/v), and 0.2% (v/v) Triton X-100 in PBS], followed by incubation with the primary antibody for 3 hours at 4 °C. After washing with PBS-T (0.1% Tween 20 in PBS), cells were incubated for 45 minutes with the secondary antibody, prepared in PBS-T. Finally, cells were incubated with 4'-6-diamidino-2-phenylindole (DAPI) (0.1 µg/ml) for 15 minutes and coverslips were mounted with Vectashield (Vector Laboratories, Burlingame, CA, USA).

Isolated vomeronasal sensory neurons attached to poly-L-lysine and concanavalin-A (Type-V) coated coverslips were fixed for 20 minutes in 4% paraformaldehyde in PBS at room temperature and washed 3 times in PBS each for 5 minutes. Further neurons were incubated in blocking solution [1% BSA (w/v) and 0.3 %(v/v) Triton X-100 in PBS] at room temperature for 20 minutes. This was followed by overnight incubation with primary antibody prepared in blocking solution at 4 °C. Next day neurons were washed 3 times in PBS each for 5 minutes and further incubated with secondary antibody (prepared in PBS-T) for 45 min at room temperature. After washing with PBS for 3 time, neurons were incubated with 4'-6-diamidino-2-phenylindole (DAPI) (0.1 µg/ml) for 15 min and coverslips were mounted with

Vectashield (Vector Laboratories, Burlingame, CA, USA). Unless mentioned, all chemical were purchased from Sigma, Milano, Italy.

Immunohistochemistry

For E12.5 and E14.5 whole head regions and for E16.5, E18.5 and P2-4 mice dissected out noses were fixed in 4% paraformaldehyde prepared in 0.01 M PBS for overnight at 4°C. Fixed tissue was washed in phosphate-buffered saline (PBS), and subsequently equilibrated at 4 °C in 30% (wt/vol) sucrose until the tissue sank to the base of the solution for cryoprotection. Then tissue was embedded in O.C.T. (Bio-optica, Milano, Italy) and stored at −80 °C, before sectioning on cryostat. O.C.T. blocks were kept at −20 °C at least for 12 hours. With a cryostat, 12-14 µm thick coronal sections were cut and stored (−80 °C) for further use. For antigen retrieval, sections were treated with SDS 0.5% (wt/vol) in PBS for 15 minutes. Sections were incubated in a blocking solution [2% FBS (vol/vol) and 0.2% Triton X-100 (vol/vol) in PBS] for 90 minutes, and then with the primary antibody (diluted in the blocking solution) overnight at 4 °C. Sections were then rinsed with 0.1% (vol/vol) Tween 20 in PBS (PBS-T) and incubated with the fluorophore-conjugated secondary antibody (diluted in PBS-T) for 2 hours at room temperature. After washing with PBS-T, sections were treated with 0.1 µg/ml DAPI for 30 minutes, washed with PBS-T, and finally mounted with Vectashield (Vector Laboratories, Burlingame, CA, USA). I have also fixed the embryonic tissue for 3 to 6 hours and did not find any difference in staining pattern of different antibodies used in this study. Postnatal mouse tissue was fixed for 6 hours and incubated overnight in 0.5 M EDTA at 4 °C. Further the postnatal tissue was processed the same as the embryonic tissue. As far as possible different embryonic and postnatal tissue were processed in parallel at the same time to avoid any discrepancies in results. For each age, sections were analyzed from at least three mice obtained from at least two different litters. Unless mentioned, all chemical were purchased from Sigma, Milano, Italy.

Imaging

Immunoreactivity was visualized with a confocal microscope (TCS SP2; Leica) using 40X/1.25NA or 63X/1.4NA oil immersion objectives. Images were acquired using Leica software (at 1,024 × 1,024 pixel resolution). All images were taken either as single plane confocal images or average of z-stacks of 1-2 µm thickness. Images were prepared and assembled in Inkscape version 0.48.2, and images were not modified other than to level illumination. Only DAPI signals were enhanced, to show the anatomy of the olfactory epithelium. In all case, data were not altered with the above adjustments.

Cell counting

To determine cell density, the number of nuclei in 150x150 μm^2 area of epithelium was counted with imageJ 1.48v software. As the olfactory epithelium consists of various shapes of nuclei I counted the cells manually using cell counter tools of imageJ 1.48v. I used the position and shape of the cell nucleus to discriminate the cell types. The sox2 positive oval shape nuclei of supporting cells in the upper one third of the epithelium and the remaining neuronal nuclei were counted as separate subtypes of nuclei in epithelium. During counting of neuronal nuclei we tried to be consistent with shape as much as possible by applying the same criteria of counting to all sections. I have excluded the flat shape nuclei near to basal most layer of the epithelium to avoid counting of basal cells. The number of neurons was estimated by counting all supra-basal round nuclei in the epithelium. The number of supporting cells was estimated by counting the number of oval-shaped sox2 positive nuclei in the most superficial nuclear layer. From each animal eight coronal sections of 16 µm thickness were collected. For E14.5 every third section, for E16.5, E18.5 and neonatal every fifth section was collected. Approximately 40–47 samples were taken from the septum and turbinates in each animal. Samples were chosen randomly at different epithelial thicknesses. In each group at least three animals were used to make final conclusions.

Secondary Antibodies

Secondary antibodies were diluted to 1:500 in PBS-T. The following secondary antibodies were used: donkey anti-rabbit Alexa Fluor 488 (catalog no. A-21206), donkey anti-goat Alexa Fluor 594 (catalog no. A-11058), goat anti-rabbit Alexa Fluor 594 (catalog no. A-11037), goat anti-rabbit Alexa Fluor 488 (catalog no. A-11034), goat anti-rabbit Alexa Fluor 405 (catalog no. A-31556), goat anti-mouse Alexa Fluor 488 (catalog no. A-11001), chicken anti-rabbit Alexa Fluor 594 (catalog no. A-21442), chicken anti-goat Alexa Fluor 488 (catalog no. A-21467), goat anti-guinea pig Alexa Fluor 594 (catalog no. A-11076).

All secondary antibodies were purchased from life technology, Milano, Italy.

TABLE - 1: Primary antibodies used in this study.

Primary antibody	Immunogen	Dilution	Manufacturer/catalog number/lot number or clone
Rabbit polyclonal **TMEM16A**	Cocktail of synthetic peptides corresponding to amino acid residues 424-519, 628-731 & 904-986 of human TMEM16A	1:50	Abcam/ab53212/GR 71118-1 & -3
Goat polyclonal **TMEM16A**	Synthetic peptide corresponding to amino acid residues 825-875 of human TMEM16A	1:50	Santa Cruz Biotech/ sc-69343/ I13111 & H0713
Rabbit polyclonal **TMEM16B**	Synthetic peptide corresponding to amino acid residues 931-1003 of human TMEM16B	1:100	Santa Cruz Biotech/ sc-292004/ A2811
Guinea pig polyclonal **TMEM16B**	Synthetic peptide corresponding to amino acid residues between transmembrane domain 2 and 3 of rat TMEM16B	1:100	*Dauner et al. 2012*.
Rabbit polyclonal **adenylyl cyclase III (ACIII)**	Synthetic peptide corresponding to amino acid residues 1125-1144 of human ACIII	1:100	Santa Cruz Biotech/ sc-588/ K0608
Goat polyclonal **cyclic nucleotide-gated channel A2 (CNGA2)**	Synthetic peptide corresponding to the last 50 amino acids residues at the C-terminus of mouse CNGA2	1:100	Santa Cruz Biotech/ sc-1370/ D0909
Goat polyclonal **olfactory marker protein (OMP)**	Purified rat OMP	1:1000	Wako Chemicals/ 544-10001/ IUP1001
Rabbit polyclonal **β-tubulin III**	Synthetic peptide corresponding to amino acid residues 441-450 of human β-tubulin III	1:800	Sigma/T2200/ 022M4774
Mouse monoclonal **acetylated tubulin**	Acetylated tubulin from the outer arm of *Strongylocentrotus purpuratus*	1:100	Sigma/ T7451/ clone 6-11B-1
Mouse monoclonal **ezrin**	Synthetic peptide corresponding to amino acid residues 362-585 of human ezrin	1:100	Abcam/ab4069/ 3C12
Rabbit monoclonal **Cytokeratin 8**	Synthetic peptide corresponding to amino acid residues 300-350 of human cytokeratin8	1:150	Novus Biologicals/ NB110-56919/EP1628Y
Rabbit polyclonal **Aquaporin 5**	Synthetic peptide corresponding to 17 amino acid sequence in the cytoplasmic region of rat aquaporin5	1:150	Calbiochem/178615/ D00140208
Goat polyclonal **Sox2**	Synthetic peptide corresponding to amino acid residues 277-293 of human sox2	1:50	Santa Cruz Biotech/ sc-17320/ A1314
Goat polyclonal **TRPC2**	Synthetic peptide corresponding to an extracellular domain of mouse TRPC2	1:50	Santa Cruz Biotech/ sc-162356/E0611
Rabbit polyclonal **PDE4A**	Synthetic peptide corresponding to C-terminal of PDE4A	1:50	Abcam/ab14607/GR 20436-6
Rabbit polyclonal **Gαo**	Synthetic peptide corresponding divergent domain of rat origin	1:100	Santa Cruz Biotech/ sc-387/D2709

4. Results

JGP
The Journal of General Physiology
Vol 140 • No 1 • July 2012

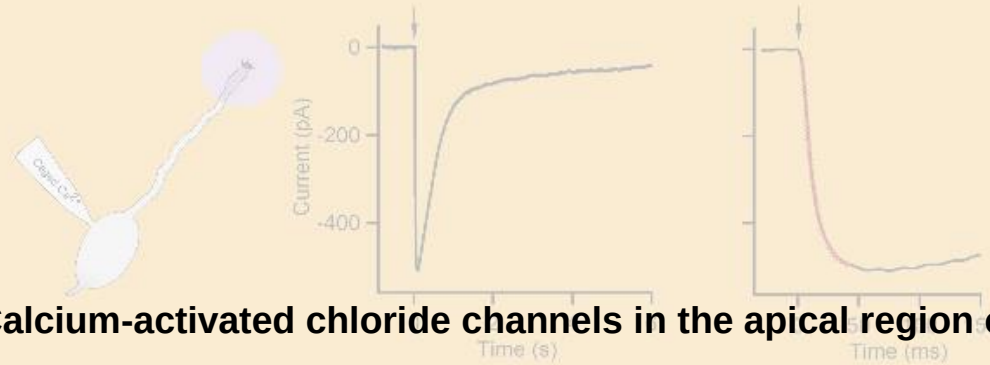

4.1 Calcium-activated chloride channels in the apical region of mouse vomeronasal sensory neurons

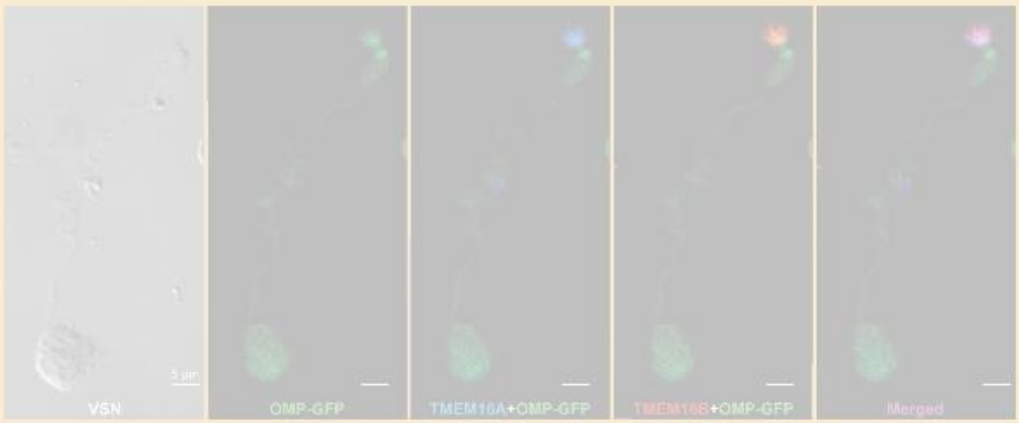

Abstracts of Papers at the 66th Annual Meeting of the Society of General Physiologists
www.jgp.org

Published June 25, 2012

Calcium-activated chloride channels in the apical region of mouse vomeronasal sensory neurons

Michele Dibattista,[1] Asma Amjad,[1] Devendra Kumar Maurya,[1] Claudia Sagheddu,[1] Giorgia Montani,[2] Roberto Tirindelli,[2] and Anna Menini[1]

[1]Neurobiology Sector and Italian Institute of Technology Unit, Scuola Internazionale Superiore di Studi Avanzati (SISSA), 34136 Trieste, Italy

[2]Department of Neuroscience, University of Parma, and Brain Center for Social and Motor Cognition, Italian Institute of Technology, 43121 Parma, Italy

The rodent vomeronasal organ plays a crucial role in several social behaviors. Detection of pheromones or other emitted signaling molecules occurs in the dendritic microvilli of vomeronasal sensory neurons, where the binding of molecules to vomeronasal receptors leads to the influx of sodium and calcium ions mainly through the transient receptor potential canonical 2 (TRPC2) channel. To investigate the physiological role played by the increase in intracellular calcium concentration in the apical region of these neurons, we produced localized, rapid, and reproducible increases in calcium concentration with flash photolysis of caged calcium and measured calcium-activated currents with the whole cell voltage-clamp technique. On average, a large inward calcium-activated current of −261 pA was measured at −50 mV, rising with a time constant of 13 ms. Ion substitution experiments showed that this current is anion selective. Moreover, the chloride channel blockers niflumic acid and 4,4′-diisothiocyanatostilbene-2,2′-disulfonic acid partially inhibited the calcium-activated current. These results directly demonstrate that a large chloride current can be activated by calcium in the apical region of mouse vomeronasal sensory neurons. Furthermore, we showed by immunohistochemistry that the calcium-activated chloride channels TMEM16A/anoctamin1 and TMEM16B/anoctamin2 are present in the apical layer of the vomeronasal epithelium, where they largely colocalize with the TRPC2 transduction channel. Immunocytochemistry on isolated vomeronasal sensory neurons showed that TMEM16A and TMEM16B coexpress in the neuronal microvilli. Therefore, we conclude that microvilli of mouse vomeronasal sensory neurons have a high density of calcium-activated chloride channels that may play an important role in vomeronasal transduction.

INTRODUCTION

Many social behaviors in animals are triggered by molecules with various chemical structures. In mammals, several chemosensory organs, such as the main olfactory epithelium, the vomeronasal organ (VNO), the septal organ, and the Grüneberg ganglion, are involved in chemical detection (Brennan and Zufall, 2006; Zufall and Leinders-Zufall, 2007; Brennan, 2009; Ma, 2009; Munger et al., 2009; Tirindelli et al., 2009; Touhara and Vosshall, 2009). Among these, the two main systems are represented by the main olfactory epithelium and the VNO. In both sensory systems, signal transduction occurs in bipolar sensory neurons and leads to membrane depolarization, although different transduction cascades are involved.

In most olfactory sensory neurons of the main olfactory epithelium, signal transduction occurs in the cilia protruding from the neurons' apical surface. The binding of molecules to odorant receptors leads to cAMP production and to the opening of CNG channels in the ciliary membrane. Na^+ and Ca^{2+} influx through CNG channels produces a depolarization of the neuron, and the increase in cytoplasmic Ca^{2+} concentration in the cilia has several effects, including a role in adaptation and the activation of Cl^- channels (Schild and Restrepo, 1998; Pifferi et al., 2006, 2009b; Kleene, 2008; Frings, 2009a,b; Reisert and Zhao, 2011).

In most vomeronasal sensory neurons, signal transduction occurs in microvilli that are present at the neurons' apical surface. The binding of molecules to vomeronasal receptors activates a phospholipase C signaling cascade, leading to the opening of ion channels that allow Na^+ and Ca^{2+} influx. The transient receptor potential canonical 2 (TRPC2) channel is expressed in the neurons' microvilli (Liman et al., 1999) and is mainly responsible for such cation influx (Zufall et al., 2005;

Correspondence to Anna Menini: menini@sissa.it

M. Dibattista's present address is Monell Chemical Senses Center, Philadelphia, PA 19104.

Abbreviations used in this paper: DAPI, 4′-6-diamidino-2-phenylindole; DIDS, 4,4′-diisothiocyanatostilbene-2,2′-disulfonic acid; MeS^-, methanesulfonate; NFA, niflumic acid; PDE4A, phosphodiesterase 4A; SCN^-, isothiocyanate; TRPC2, transient receptor potential canonical 2; VNO, vomeronasal organ.

The Rockefeller University Press $30.00
J. Gen. Physiol. Vol. 140 No. 1 3–15
www.jgp.org/cgi/doi/10.1085/jgp.201210780

Published June 25, 2012

Munger et al., 2009). Several studies demonstrated that vomeronasal sensory neurons respond to stimuli with the generation of action potentials and an increase in intracellular Ca^{2+} concentration (Holy et al., 2000; Leinders-Zufall et al., 2000, 2004, 2009; Spehr et al., 2002; Chamero et al., 2007). However, the role played by cytoplasmic Ca^{2+} elevation in the microvilli is still largely unknown. Spehr et al. (2009) have recently shown that Ca^{2+} in combination with calmodulin is responsible for sensory adaptation. In addition, other studies suggested that intracellular Ca^{2+} might also activate ion channels involved in the transduction process, although it is still a matter of debate whether these channels are cation or anion selective. Indeed, Ca^{2+}-activated nonselective cation currents have been measured in hamster (Liman, 2003) or mouse vomeronasal sensory neurons (Spehr et al., 2009). In the whole cell configuration, currents of about −177 pA at −80 mV were activated by dialysis of 0.5 or 2 mM Ca^{2+} (Liman, 2003). In excised inside-out patches, the dose–response relation indicated that half-activation of the channels occurred at 0.5 mM Ca^{2+} at −80 mV (Liman, 2003). It has been suggested that this Ca^{2+}-activated nonselective cation channel could directly mediate vomeronasal sensory transduction or amplify the primary sensory response (Liman, 2003), but at present its role and its molecular identity are still unknown. Other studies suggested that a significant portion of the response to urine in mouse vomeronasal sensory neurons is carried by Ca^{2+}-activated Cl^- channels (Yang and Delay, 2010; Kim et al., 2011). However, these studies used indirect ways to activate channels, as the increase in cytoplasmic Ca^{2+} concentration was a secondary effect of urine stimulation.

Thus, at present, it is still unclear whether nonselective cation and/or Cl^- channels activated by Ca^{2+} are expressed in the apical region of vomeronasal sensory neurons and may be involved in vomeronasal transduction. To contribute to the resolution of this debate, we directly recorded and characterized currents by producing rapid and repeatable increases in intracellular Ca^{2+} concentration using flash photolysis of caged Ca^{2+}, while recording the induced current in the whole cell voltage-clamp configuration (Boccaccio et al., 2011). The use of photolysis of caged Ca^{2+} to produce an increase in Ca^{2+} concentration, instead of dialysis of Ca^{2+} into the neuron or the production of a secondary Ca^{2+} increase, allowed us to release Ca^{2+} in a temporally and spatially defined manner into an intact neuron because we could precisely deliver a flash of UV light at the apical region of a vomeronasal sensory neuron. We measured an average inward Ca^{2+}-activated current of −261 pA at the holding potential of −50 mV and showed that this current is anion selective. Furthermore, both niflumic acid (NFA) and 4,4′-diisothiocyanatostilbene-2,2′-disulfonic acid (DIDS), two very well known Cl^- channel blockers (Frings et al., 2000; Hartzell et al., 2005), partially blocked the Ca^{2+}-activated current in vomeronasal sensory neurons.

To the best of our knowledge, these are the first recordings providing a direct demonstration that a large Cl^- current can be directly activated by Ca^{2+} in the apical region of mouse vomeronasal sensory neurons, as this demonstration can only be obtained by using a method that provides a temporal and spatial control of Ca^{2+} release, such as photolysis of caged Ca^{2+}.

Recent studies indicated that at least two members of the TMEM16/anoctamin family, TMEM16A/anoctamin1 and TMEM16B/anoctamin2, are Ca^{2+}-activated Cl^- channels (Caputo et al., 2008; Schroeder et al., 2008; Yang et al., 2008; Pifferi et al., 2009a, 2012; Stephan et al., 2009; Stöhr et al., 2009; Scudieri et al., 2012). We studied the expression of members of this family in the VNO and found that both TMEM16A and TMEM16B are expressed in the apical region of the VNO, in agreement with recent studies (Rasche et al., 2010; Billig et al., 2011; Dauner et al., 2012). However, microvilli both from vomeronasal sensory neurons and from supporting cells are present at the apical surface of the vomeronasal epithelium, and they are not clearly distinguishable. We therefore investigated the localization of TMEM16A and TMEM16B in isolated vomeronasal sensory neurons and found that these channels are expressed in neurons' microvilli. Because microvilli are the site where transduction events take place, the presence of Ca^{2+}-activated Cl^- channels indicates that they may be involved in signal transduction in the VNO. A complete understanding of conductances present in vomeronasal sensory neurons will help to elucidate the molecular mechanisms involved in the generation of the vomeronasal transduction current and the production of action potentials.

MATERIALS AND METHODS

Preparation of isolated vomeronasal sensory neurons

All animals were handled in accordance with the Italian Guidelines for the Use of Laboratory Animals (Decreto Legislativo 27/01/1992, no. 116) and European Union guidelines on animal research (no. 86/609/EEC). For experiments, 2-mo-old mice were anaesthetized by CO_2 inhalation and decapitated before VNO removal. The vomer capsule containing the VNO was removed as described previously (Liman and Corey, 1996; Dean et al., 2004; Shimazaki et al., 2006; Arnson et al., 2010), and vomeronasal sensory neurons were dissociated from the VNO with a standard enzymatic–mechanical dissociation protocol (Dibattista et al., 2008). In brief, the removed vomer capsule was rapidly transferred to a Petri dish containing divalent-free PBS (Sigma-Aldrich) solution where the VNO was extracted. The tissue was cut into small pieces with tiny scissors, transferred to divalent-free PBS containing 1 mg/ml collagenase (type A), incubated at 37°C for 10 min, cut into small pieces with tiny scissors, and reincubated for 10 min at 37°C. After a 2-min centrifugation at 1,700 rpm, the tissue was gently triturated with a fire-polished Pasteur pipette. Cells were resuspended in 1 ml of fresh Ringer's solution and plated on a glass coverslip (World Precision

Published June 25, 2012

Instruments) coated with poly-L-lysine and concanavalin A (type V; Sigma-Aldrich). Cells were stored at 4°C for up to 7 h before experiments.

Patch-clamp recordings

Vomeronasal sensory neurons were observed using an inverted microscope (IX 70; Olympus) with an oil immersion ×100 objective (Carl Zeiss). Currents in whole cell voltage-clamp configuration were recorded using an Axopatch 200B patch-clamp amplifier controlled by Clampex 8 connected with a Digidata 1322A (Molecular Devices). Patch pipettes were made using borosilicate capillaries (World Precision Instruments) and were pulled by a two-stage vertical puller (PP-83; Narishige). Pipette resistance was around 3–6 MΩ. Currents were low-pass filtered at 1 kHz and acquired at 2 kHz. All the experiments were performed at room temperature (20–24°C).

Ionic solutions, photolysis of caged Ca^{2+}, and perfusion system

The extracellular mammalian Ringer's solution contained (in mM): 140 NaCl, 5 KCl, 1 $CaCl_2$, 1 $MgCl_2$, 10 HEPES, 10 glucose, and 1 sodium pyruvate, pH 7.4. For flash photolysis of caged compounds, we used a xenon flash–lamp system (JML-C2; Rapp OptoElectronic) coupled with the epifluorescence port of the inverted microscope with a quartz light guide, as described previously (Boccaccio et al., 2006, 2011; Boccaccio and Menini, 2007). The light spot had a diameter of ∼15 µm and was focused on the microvilli and dendritic knob of isolated vomeronasal sensory neurons. The flash duration was <1.5 ms and was kept constant for each experiment. The interval between flashes was at least 2 min. At the beginning of each experiment, the stability of the response was checked by applying repetitive flashes at intervals of 2 min. Neurons that did not reach a stable response to at least two consecutive flashes were discarded.

The intracellular recording solution for the photorelease of caged Ca^{2+} contained (in mM): 3 DMNP-EDTA, 1.5 $CaCl_2$, 140 CsCl, and 10 HEPES, pH 7.4. DMNP-EDTA was purchased from Invitrogen, and $CaCl_2$ was adjusted with a 0.1-M standard solution from Fluka. Aliquots were stored at −20°C and kept refrigerated in the dark during the experiment.

For ionic selectivity experiments, NaCl was replaced with equimolar NMDG-Cl, or Cl^- was substituted with other anions, such as methanesulfonate (MeS^-) or isothiocyanate (SCN^-), by replacing NaCl on an equimolar basis with NaX, where X is the substituted anion.

The bath was grounded through a 1-M KCl agar bridge connected to an Ag-AgCl reference electrode. Liquid junction potentials were calculated using the Clampex's Junction Potential Calculator (Molecular Devices), based on the JPCalc program developed by Barry (1994), and applied membrane potentials were corrected offline for the calculated liquid junction potentials, as described previously (Sagheddu et al., 2010).

NFA was prepared in DMSO as stock solutions at 200 mM and diluted to the final concentration of 300 µM. DMSO alone did not modify the currents. DIDS was directly dissolved in the bathing solution to 1 mM.

Bathing solutions were changed by using a gravity-fed perfusion system with a slow perfusion rate, adjusted in such a way that the position of the neuron was not perturbed. A complete solution change was obtained in ∼10 s. To measure blocker effects, current recordings were obtained before blocker application until a stable response was obtained (control), 2 min after delivery of the solution with the blocker, and 2–5 min after perfusion with Ringer's solution without the blocker (wash).

Chemicals, unless otherwise stated, were purchased from Sigma-Aldrich.

Analysis of electrophysiological data

Data analysis and figures were made using Clampfit and IGOR software (WaveMetrics). Current recordings at each holding potential were plotted by subtracting the value of the baseline measured before photorelease of caged Ca^{2+}. Data are given as mean ± SEM and the total number of neurons (n). Statistical significance was tested with a Student's t test. $P < 0.05$ was considered statistically significant.

RNA extraction and RT-PCR

RNA was extracted from the VNO of FVB mice. Methods and primers for the amplification of TMEM16/anoctamins cDNA were the same as described previously (Sagheddu et al., 2010). All amplicons were gel extracted, subcloned, and sequenced for confirmation.

Immunofluorescence

HEK 293T cells were grown on coverslips and cotransfected with plasmids containing the cDNA sequence of TMEM16A or TMEM16B (RZPD) and enhanced GFP (Takara Bio Inc.) for fluorescent identification of transfected cells, as described previously (Pifferi et al., 2009a). Transfected cells were fixed in 4% paraformaldehyde for 15 min at room temperature and sequentially washed. Next, they were incubated with a quenching solution (0.1 M glycine) for 10 min and then treated with 0.05% SDS for antigen retrieval for 10 min. Cells were subsequently incubated for 15 min in blocking solution (2% [vol/vol] FBS and 0.2% [vol/vol] Triton X-100 in PBS), followed by incubation with the primary antibody for 3 h at 4°C. After washing with PBS-T (0.1% Tween 20 in PBS), cells were incubated for 45 min with the secondary antibody, prepared in PBS-T. Finally, cells were incubated with 0.1 µg/ml 4′-6-diamidino-2-phenylindole (DAPI) for 15 min, and coverslips were mounted with Vectashield (Vector Laboratories).

For immunohistochemistry on tissue sections, the mouse nasal regions or the VNOs extracted from the nasal cavity were fixed in 4% paraformaldehyde (for 4 h at 4°C), then decalcified in 0.5 M EDTA for 12 h at 4°C, and subsequently equilibrated overnight (4°C) in 30% (wt/vol) sucrose for cryoprotection. 14-µm coronal sections were cut with a cryostat and stored (−80°C) for further use. For antigen retrieval, sections were treated with SDS 0.5% (wt/vol) in PBS for 15 min. Sections were incubated in a blocking solution (2% [vol/vol] FBS and 0.2% [vol/vol] Triton X-100 in PBS) for 2 h, and then with the primary antibody (diluted in the blocking solution) overnight at 4°C. Sections were then rinsed with 0.1% (vol/vol) Tween 20 in PBS (PBS-T) and incubated with the fluorophore-conjugated secondary antibody (diluted in PBS-T) for 2 h at room temperature. After washing with PBS-T, sections were treated with 0.1 µg/ml DAPI for 30 min, washed with PBS-T, and mounted with Vectashield (Vector Laboratories).

Immunocytochemistry on isolated vomeronasal sensory neurons was performed as described previously (Fieni et al., 2003). Dissociated vomeronasal sensory neurons were prepared as for electrophysiological experiments. Glass-attached vomeronasal neurons were gently perfused with 4% paraformaldehyde and then washed in PBS. Cells were blocked in 1% albumin and 0.3% Triton X-100 in PBS for 20 min and incubated overnight with the primary antibody. Cells were then washed in PBS and further incubated with the secondary antibody, prepared in PBS. In some experiments, cells were also incubated with 0.1 µg/ml DAPI for 15 min. Coverslips were mounted with Vectashield (Vector Laboratories).

Wild-type C57BL6 or genetically modified mice that express GFP in all mature olfactory and vomeronasal sensory neurons (OMP-GFP mice; provided by P. Mombaerts, Max Planck Institute of Biophysics, Frankfurt, Germany) were used.

The following primary antibodies were used: rabbit anti-TMEM16A (1:50; Abcam), rabbit anti-TMEM16B (1:100; Santa Cruz Biotechnology, Inc.), guinea pig anti-TMEM16A and guinea

Published June 25, 2012

pig anti-TMEM16B (provided by S. Frings, Heidelberg University, Heidelberg, Germany; Dauner et al., 2012), goat anti-TRPC2 (1:50; Santa Cruz Biotechnology, Inc.), rabbit anti-Gαo (1:100; Santa Cruz Biotechnology, Inc.), and rabbit anti–phosphodiesterase 4A (PDE4A; 1:50; Abcam). The following secondary antibodies, obtained from Invitrogen, were used: goat anti–guinea pig Alexa Fluor 594 (1:500), goat anti–rabbit Alexa Fluor 488 (1:500), goat anti–rabbit Alexa Fluor 594 (1:500), goat anti–rabbit Alexa Fluor 405 (1:500), chicken anti–rabbit Alexa Fluor 594 (1:500), and chicken anti–goat Alexa Fluor 488 (1:500).

Immunoreactivity was visualized with a confocal microscope (TCS SP2; Leica). Images were acquired using Leica software (at 1,024 × 1,024–pixel resolution) and were not modified other than to balance brightness and contrast. Control experiments without the primary antibodies gave no signal.

RESULTS

Whole cell currents activated by photolysis of caged Ca^{2+} at the apical region of mouse vomeronasal sensory neurons

We obtained whole cell voltage-clamp recordings from isolated mouse vomeronasal sensory neurons and directly measured Ca^{2+}-activated currents by rapidly elevating the Ca^{2+} concentration in the apical region (dendritic knob and microvilli) by localized photorelease of caged Ca^{2+} (Fig. 1 A). Fig. 1 B shows a typical current response at the holding potential of −50 mV. An inward current rapidly developed upon the flash release, reaching a peak amplitude of −508 pA, and then slowly returned to baseline. The rising phase of the Ca^{2+}-activated current was well described by a single-exponential function with a time constant of 9.5 ms (Fig. 1 C). Similar results were obtained from a total of 59 neurons with an average time constant value of 12.6 ± 6.0 ms (n = 59; range of 3–26 ms). We observed a large variability in Ca^{2+}-activated current amplitudes in different neurons with absolute values ranging between 50 pA and 1 nA at −50 mV, and a mean amplitude of −261 ± 37 pA (n = 59). Such variability has also been observed in recording Ca^{2+}-activated currents in the ciliary region of olfactory sensory neurons, where absolute values ranging from 50 pA up to ∼1 nA were also recorded (Boccaccio et al., 2006; Boccaccio and Menini, 2007). The amplitude variability can originate both from the illumination conditions in the neuron that may differ between experiments as well as from various numbers or densities of channels that may vary in different neurons. Similarly to olfactory sensory neurons, we also found a large variability in the time necessary for the current to return to baseline in vomeronasal sensory neurons (Figs. 1 B and 3, A and B). This is likely to be the result of differences in the time necessary for the decrease in Ca^{2+} concentration by Ca^{2+} extrusion and/or by diffusion to other neuronal compartments.

To investigate the ionic nature of the Ca^{2+}-activated currents, we measured the reversal potential in various ionic conditions. Currents were recorded at various holding potentials with different ionic compositions in the extracellular solution. In a first set of experiments, we used our standard intracellular and extracellular solutions, in which Cs^+ was chosen as the intracellular monovalent cation to avoid contributions from Ca^{2+}-activated K^+ currents, and Na^+ was the main extracellular monovalent cation. Moreover, the intracellular and extracellular Cl^- concentrations were almost symmetrical. Fig. 2 A shows the responses induced by photorelease of Ca^{2+} at the indicated holding potentials. The reversal potential calculated from the current–voltage relation was +0.5 mV, with an average value of +0.3 ± 3.5 mV (n = 6; Fig. 2 E). Because the cation concentrations were $[Na^+]_o$ = 149 mM and $[Cs^+]_i$ = 143 mM, and the Cl^- concentrations were $[Cl^-]_o$ = 149 mM and $[Cl^-]_i$ = 143 mM, a reversal potential value close to 0 mV is consistent both with a nonselective cation current and with an anion-selective current.

To distinguish between the two types of currents, we performed a first set of experiments by replacing Na^+ in the extracellular solution with $NMDG^+$, a large organic monovalent cation largely impermeant in cation channels. If the measured Ca^{2+}-activated currents were carried by cations, the replacement of Na^+ by $NMDG^+$ should produce a shift of the reversal potential toward negative values. Fig. 2 B shows that the reversal potential in the presence of 140 mM NMDG-Cl was +0.3 mV, with an average value of +0.5 ± 3.8 mV (n = 3; Fig. 2 E), indicating that the Ca^{2+}-activated current was not carried by cations.

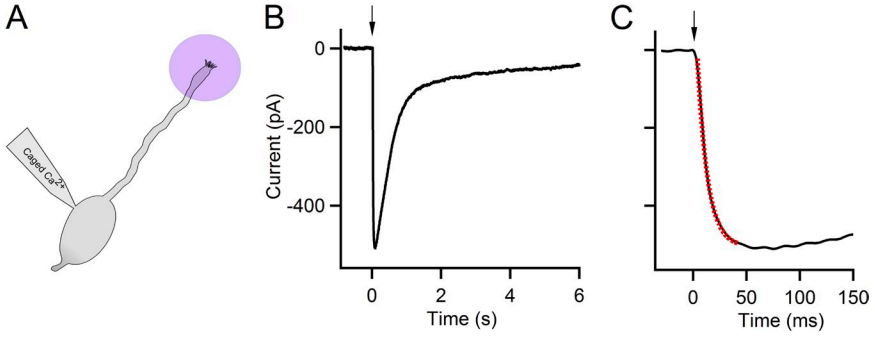

Figure 1. Current responses induced by photorelease of Ca^{2+} in the apical region of mouse vomeronasal sensory neurons. (A) Schematic drawing of a vomeronasal sensory neuron showing the location of application of the UV flash to photorelease Ca^{2+}. (B) Whole cell current induced by photorelease of Ca^{2+} at the holding potential of −50 mV. A flash was applied at time t = 0 (indicated by an arrow). (C) Expanded timescale shows the rapid increase in the current upon Ca^{2+} photorelease. The current rising phase was well fitted by a single exponential (red dotted line) with a τ value of 9.5 ms.

Published June 25, 2012

In a second set of experiments, we tested whether the Ca^{2+}-activated current was carried by Cl^- by substituting most of the extracellular Cl^- with MeS^-, an anion known to be almost impermeant in Cl^- channels. Fig. 2 C shows that, when we replaced 140 NaCl with NaMeS, the reversal potential was +18 mV, with an average value of +20.2 ± 1.5 mV (n = 3; Fig. 2 E). The average reversal potential in the low extracellular Cl^- solution was shifted toward more positive values, as expected if MeS^- is much less permeant than Cl^-. Furthermore, because most Cl^- channels are more permeable to SCN^- than to Cl^-, we measured the reversal potential after replacing 140 mM NaCl with NaSCN: the reversal potential shifted toward more negative values, −20 mV (Fig. 2 D), with an average value of −18 ± 3 mV (n = 8; Fig. 2 E). These results demonstrate that the Ca^{2+}-activated current is an anion current and that these ion channels have higher permeability for SCN^- over Cl^-, as in most Cl^- channels (Hartzell et al., 2005).

To further characterize these channels, we measured the extracellular blockage by NFA and DIDS, two compounds commonly used to partially block Ca^{2+}-activated Cl^- currents in various tissues (Frings et al., 2000). Fig. 3 A shows the blocking effect by 300 µM NFA of the current elicited by photolysis of caged Ca^{2+} at −50 mV. The maximal inward current decreased from −1,022 to −221 pA upon NFA application, corresponding to 22% of its value before blocker application. The blocking effect was partially reversible after perfusion with Ringer's solution without NFA, as the current amplitude recovered to −505 pA, 50% of the control value. On average, the current amplitude in the presence of 300 µM NFA at −50 mV was 27% (n = 5) of the value before blocker application (Fig. 3 C). After perfusion with Ringer's

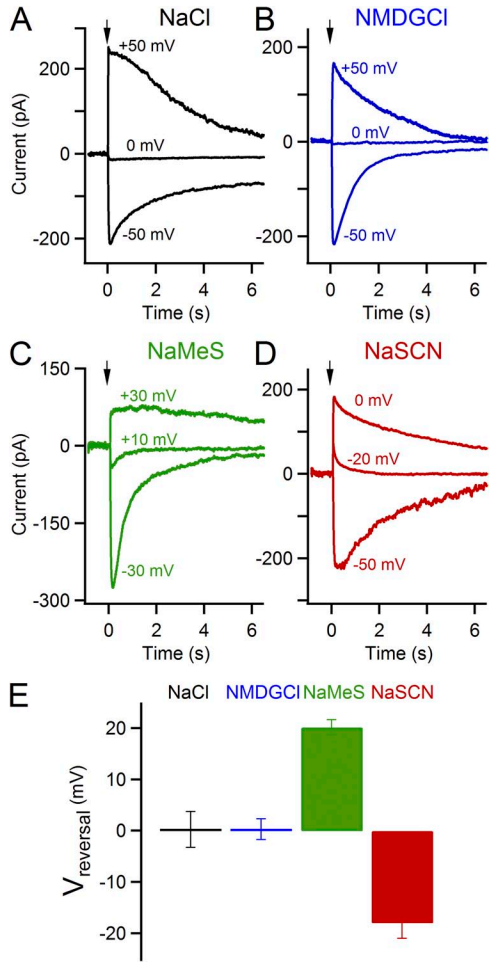

Figure 2. Ion selectivity of the Ca^{2+}-activated current. Whole cell currents from vomeronasal sensory neurons induced by photorelease of Ca^{2+} into the apical region recorded at the indicated holding potentials. A UV flash was applied at the time t = 0 (indicated by an arrow). Recordings in the presence of extracellular Ringer's solution containing 140 mM: (A) NaCl, (B) NMDG-Cl, (C) NaMeS, and (D) NaSCN, each from a different neuron. (E) Average reversal potentials measured in the presence of the indicated ionic solutions: NaCl (n = 6), NMDG-Cl (n = 3), NaMeS (n = 3), and NaSCN (n = 8).

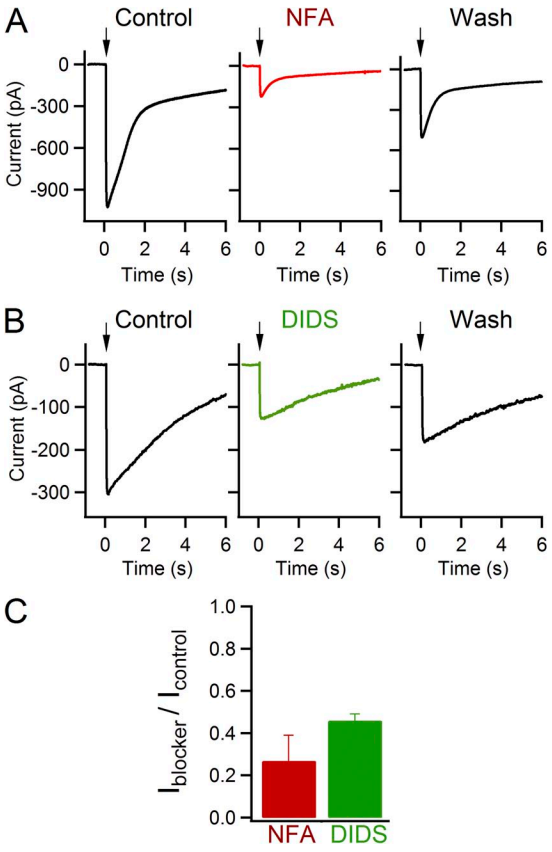

Figure 3. Blockage of the Ca^{2+}-activated Cl^- current. Whole cell currents induced by photorelease of Ca^{2+} into the apical region of vomeronasal sensory neurons. The holding potential was −50 mV. Current recordings were obtained before blocker application (control), 2 min after application of the indicated blockers, and 2 min after the removal of blockers (wash). The following blockers were used: (A) 300 µM NFA and (B) 1 mM DIDS. (C) Average values of the current in the presence of 300 µM NFA (n = 5) or 1 mM DIDS (n = 3) normalized to the current in control conditions ($P < 0.05$).

Published June 25, 2012

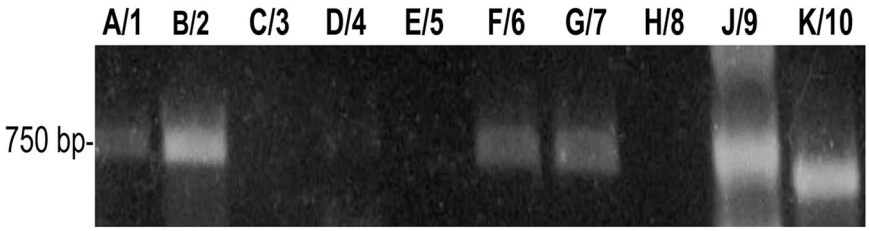

Figure 4. Expression of TMEM16s/anoctamins in mouse VNO. TMEM16/anoctamin isoforms A–J (1–10) were amplified from VNO cDNA by RT-PCR. A/1, B/2, F/6, G/7, J/9, and K/10 are expressed in the VNO.

solution without the blocker, the current recovered on average to 68% of its control value.

Fig. 3 B shows recordings from a vomeronasal sensory neuron in which the extracellular addition of 1 mM DIDS produced a block to 42% of its control value. After washout with Ringer's solution, the current amplitude reached 60% of the value before blocker application. On average, the current amplitude in the presence of 1 mM DIDS was 46% ($n = 3$) of the control value (Fig. 3 C). After perfusion with Ringer's solution without DIDS, the current was on average 60% of its control value.

Collectively, these results show that a sudden increase in the intracellular Ca^{2+} concentration can rapidly activate a large anion current, demonstrating the expression of a high density of Ca^{2+}-activated Cl^- channels in the apical region of vomeronasal sensory neurons.

Expression of TMEM16s/anoctamins in mouse VNOs

Having measured Ca^{2+}-activated Cl^- currents in the apical region of mouse vomeronasal sensory neurons, we sought to investigate which members of the TMEM16/anoctamin family that are known to function as Ca^{2+}-activated Cl^- channels are expressed in the VNO.

To analyze the expression of each TMEM16/anoctamin, we performed RT-PCR on cDNA obtained from mouse VNOs. mRNAs of TMEM16A/anoctamin1, B/2, F/6, G/7, J/9, and K/10 were found to be significantly expressed in the VNO (Fig. 4).

Because antibodies against TMEM16A and TMEM16B are commercially available, we first tested their specificity on HEK 293T cells transiently transfected with plasmids containing the cDNA sequence of TMEM16A or TMEM16B and GFP. Fig. 5 shows that cells transfected with TMEM16A (Fig. 5, A–F) or TMEM16B (Fig. 5, G–L)

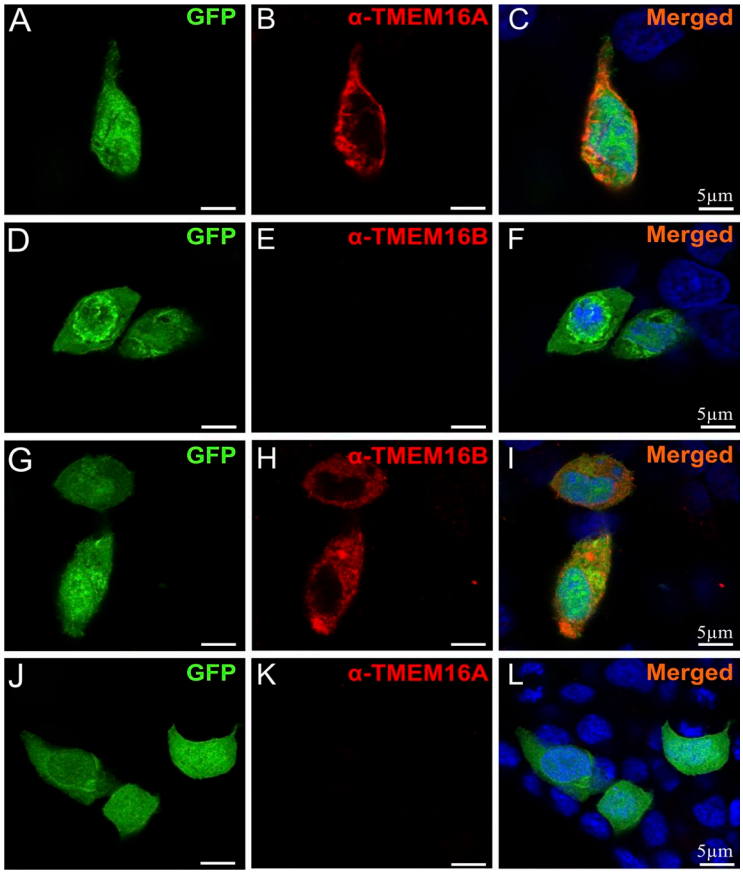

Figure 5. Specificity of rabbit anti-TMEM16A and anti-TMEM16B antibodies in HEK 293T cells expressing TMEM16A or TMEM16B. (A–F) Fluorescence images of the staining with anti-TMEM16A or anti-TMEM16B antibodies (indicated with the prefix α) of HEK 293T cells transiently cotransfected with TMEM16A and GFP cDNA. Specific staining was observed only with anti-TMEM16A (B), whereas no immunoreactivity was detected with anti-TMEM16B (E) antibody. (G–L) Fluorescence images of the staining with anti-TMEM16B or anti-TMEM16A antibodies of HEK 293T cells transiently cotransfected with TMEM16B and GFP cDNA. Specific staining was observed only with anti-TMEM16B (H), whereas no immunoreactivity was detected with anti-TMEM16A (K) antibody. Cell nuclei were stained by DAPI (blue). Bars, 5 μm.

Published June 25, 2012

cDNA produced a strong and specific immunoreactivity exclusively to their respective antibody.

We further investigated the specificity of the two antibodies on the olfactory epithelium. Indeed, it is well established that TMEM16B is expressed in the apical layer of the olfactory epithelium but not in the respiratory epithelium (Hengl et al., 2010; Rasche et al., 2010; Billig et al., 2011). We used genetically modified OMP-GFP mice that express GFP in all mature olfactory and vomeronasal sensory neurons (Potter et al., 2001) and confirmed that TMEM16B was expressed at the apical surface of the olfactory epithelium but not in the respiratory epithelium (Fig. 6, D–F), and that TMEM16A immunoreactivity was absent (Fig. 6, A–C). Collectively, these experiments indicate that these antibodies specifically recognized their epitopes and did not show cross-reactivity.

We therefore used the same antibodies to examine the localization of TMEM16A and TMEM16B in the vomeronasal epithelium of OMP-GFP mice and detected immunoreactivity at the luminal surface of the sensory epithelium (Fig. 7, A–F). High magnification images show that both anti-TMEM16A (Fig. 7 G) and anti-TMEM16B (Fig. 7 H) staining lies above the knobs of the vomeronasal sensory neurons, where microvilli are located. We also costained VNO sections with an antibody against the cation channel TRPC2, which is involved in vomeronasal transduction, and observed staining in the microvillar region (Fig. 8, B and E) that largely colocalized with TMEM16A and TMEM16B immunoreactivity (Fig. 8, A, C, D, and F), indicating that cation (TRPC2) and anion channels (TMEM16A and TMEM16B) coexpress. However, the microvillar region is composed of microvilli of both sensory neurons and supporting cells (Höfer et al., 2000; Dauner et al., 2012), and they cannot be distinguished in immunosignals from VNO coronal sections.

To unequivocally establish whether TMEM16A and/or TMEM16B are expressed in the microvilli of sensory neurons, the compartment responsible for signal transduction, we performed immunocytochemistry on isolated vomeronasal sensory neurons using combinations of the commercially available antibodies raised in rabbit and of those raised in guinea pigs (provided by S. Frings; Dauner et al., 2012). Figs. 9 and 10 illustrate that TMEM16A and TMEM16B are both expressed in the microvilli of vomeronasal sensory neurons. Moreover, Fig. 9 clearly shows the coexpression of TMEM16A and TMEM16B in the microvilli of the same neuron from an OMP-GFP mouse. After dissociation and immunocytochemistry procedures, we obtained 34 intact isolated vomeronasal sensory neurons from four OMP-GFP mice, and 62 intact neurons from 10 wild-type mice. Every intact vomeronasal sensory neuron, both from OMP-GFP and wild-type mice, showed coexpression of TMEM16A and TMEM16B in the microvilli. For coexpression, both combinations of rabbit anti-TMEM16A with guinea pig anti-TMEM16B and guinea pig anti-TMEM16A with rabbit anti-TMEM16B produced the same result. Unfortunately, in our preparation of dissociated

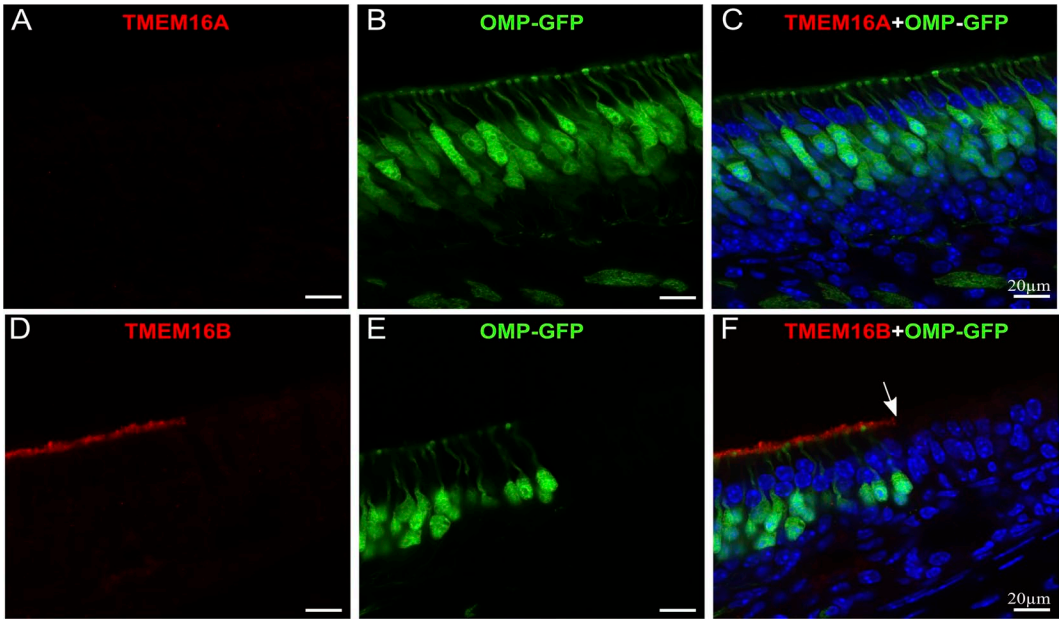

Figure 6. TMEM16A and TMEM16B immunoreactivity in the olfactory epithelium. (A–C) Confocal images of coronal sections of the olfactory epithelium from an OMP-GFP mouse showing the absence of TMEM16A immunoreactivity. (D–F) Confocal images of the transition region between the olfactory and the respiratory epithelium (absence of OMP-GFP–expressing neurons). The arrow indicates the transition between the two epithelia. TMEM16B is expressed at the apical surface of the olfactory but not of the respiratory epithelium. Cell nuclei were stained by DAPI (blue). Bars, 20 µm.

Published June 25, 2012

vomeronasal cells, we were not able to clearly identify supporting cells; therefore, we cannot exclude the possibility that TMEM16A and/or TMEM16B are also expressed in microvilli of these cells.

The rodent VNO has two major neuronal populations, apical and basal neurons, characterized by their location in the VNO and by the expression of specific proteins and receptors (Berghard and Buck, 1996; Jia and Halpern, 1996; Ryba and Tirindelli, 1997; Lau and Cherry, 2000; Leinders-Zufall et al., 2004; Liberles et al., 2009; Rivière et al., 2009). Apical neurons are located near the lumen of the VNO and express the G protein α subunit Gαi2, the PDE4A, and receptors of the V1R or formyl peptide receptor family. Basal neurons are close to the basal lamina and express the G protein α subunit Gαo and receptors of the V2R or formyl peptide receptor family. The finding that TMEM16A and TMEM16B are expressed in the microvilli of neurons raises the question of whether the expression of these proteins is restricted to any of these two neuronal subsets. We used specific markers to identify whether neurons expressing TMEM16A or TMEM16B are basal or apical. We performed immunocytochemistry on isolated vomeronasal sensory neurons using rabbit anti-PDE4A antibody, a marker for apical neurons, or rabbit anti-Gαo antibody, a marker for basal neurons (Lau and Cherry, 2000; Leinders-Zufall et al., 2004), together with the guinea pig anti-TMEM16A or anti-TMEM16B. Fig. 10 shows that TMEM16A and TMEM16B are localized in the microvilli of both apical (Fig. 10, A–C and G–I) and basal (Fig. 10, D–F and J–L) vomeronasal sensory neurons from wild-type mice. These results show that TMEM16A and TMEM16B are expressed in microvilli of both the apical and basal neuronal populations.

DISCUSSION

In this study, we have provided the first direct demonstration that a large Cl^- current can be directly activated by Ca^{2+} in the apical region of mouse vomeronasal sensory neurons. Indeed, photolysis of caged Ca^{2+} allowed us to obtain a precise temporal and spatial control of cytoplasmic Ca^{2+} elevation while recording the current in the whole cell voltage-clamp mode. Moreover, we have demonstrated that TMEM16A and TMEM16B largely colocalize with TRPC2 at the apical surface of the vomeronasal epithelium, and that TMEM16A and TMEM16B are coexpressed in microvilli of both apical and basal isolated vomeronasal sensory neurons, therefore suggesting that these two anion channels are likely to be involved in vomeronasal transduction.

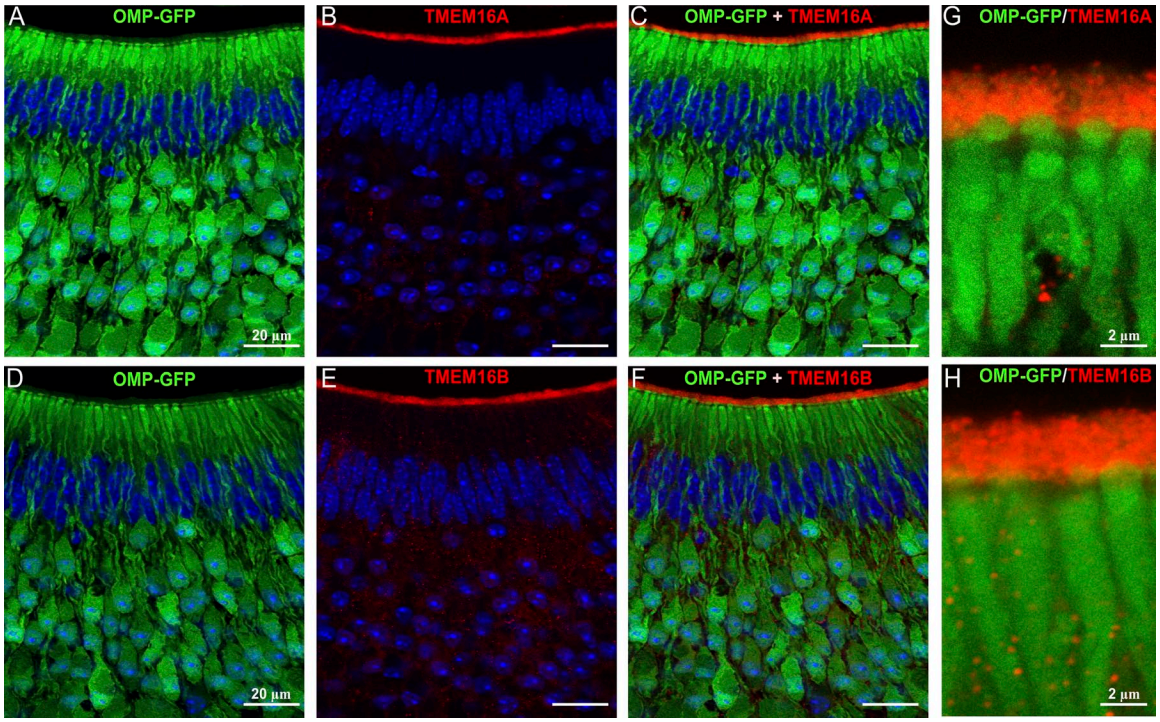

Figure 7. TMEM16A and TMEM16B are expressed at the apical surface of the vomeronasal epithelium. (A–H) Immunostaining of sections of VNO from an OMP-GFP mouse. (A and D) Endogenous GFP fluorescence of mature vomeronasal sensory neurons. TMEM16A (B) and TMEM16B (E) are expressed at the luminal surface of the vomeronasal sensory epithelium. (G and H) High magnification image of the apical portion of the VNO showing that TMEM16A and TMEM16B are expressed at the apical surface. Cell nuclei were stained by DAPI (blue). Bars: (A–F) 20 µm; (G and H) 2 µm.

Published June 25, 2012

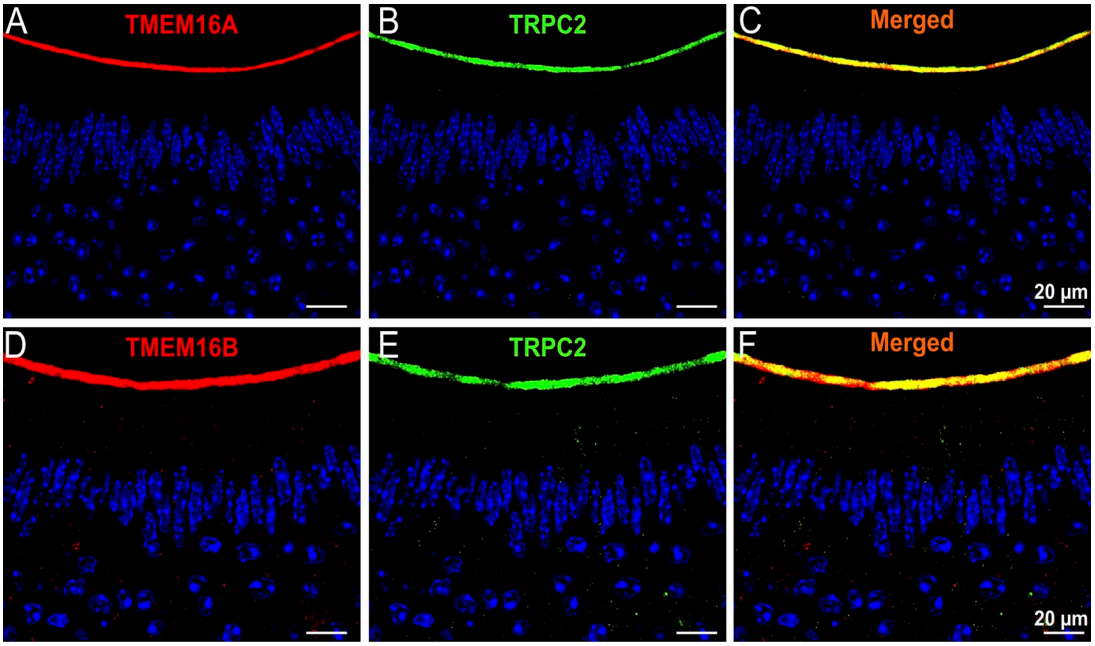

Figure 8. TMEM16A and TMEM16B are coexpressed with TRPC2. Double-label immunohistochemistry in tissue sections of VNO from a wild-type mouse showing the coexpression of TRPC2 with TMEM16A (A–C) and TMEM16B (D–F) at the luminal surface of the vomeronasal sensory epithelium. Cell nuclei were stained by DAPI (blue). Bars, 20 µm.

Expression of TMEM16A and TMEM16B in the vomeronasal epithelium

Two recent reports (Billig et al., 2011; Dauner et al., 2012) have shown that both TMEM16A and TMEM16B are expressed in the microvillar surface of the VNO. However, as pointed out by Dauner et al. (2012), the VNO apical surface layer contains the microvilli of both sensory neurons and supporting cells (Höfer et al., 2000). Thus, immunohistochemistry on coronal sections of the VNO does not allow for the distinction between these two microvillar subsets. By performing high resolution confocal imaging on isolated vomeronasal sensory neurons, we were able to detect both TMEM16A and TMEM16B in microvilli of the same neuron, thus providing the first unequivocal evidence of coexpression of these two anion channels in the same cell.

Ca^{2+}-activated currents in vomeronasal sensory neurons

Previous reports showed the presence of Ca^{2+}-activated nonselective cation currents in vomeronasal sensory

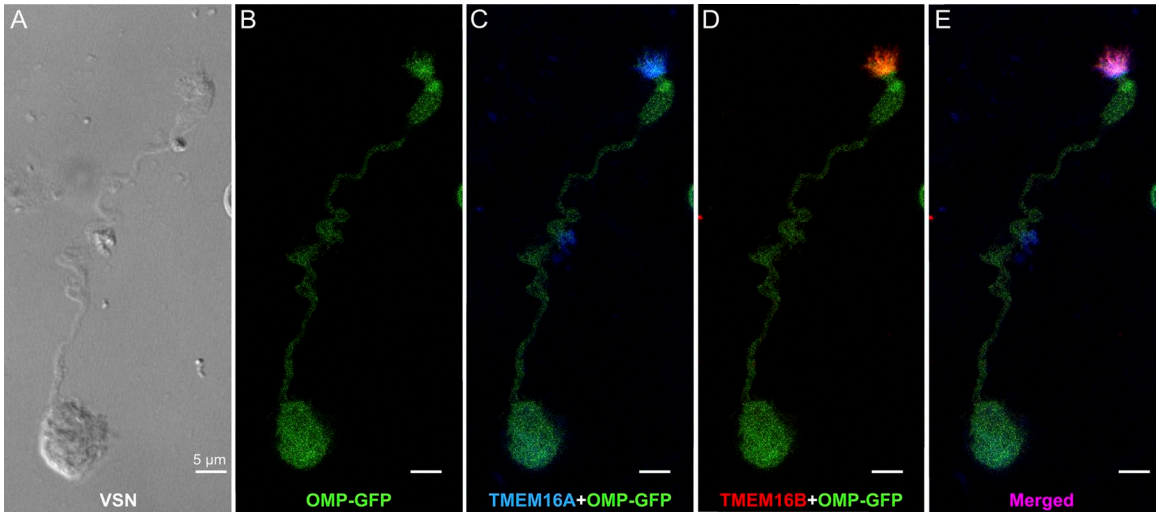

Figure 9. TMEM16A and TMEM16B are coexpressed in the microvilli of vomeronasal sensory neurons. (A) Bright field image of a vomeronasal sensory neuron isolated from an OMP-GFP mouse (B). The same neuron was stained with (C) rabbit anti-TMEM16A and (D) guinea pig anti-TMEM16B, showing the coexpression of the two anion channels in the microvilli (E). Cell nuclei were stained by DAPI (blue). Bars, 5 µm.

Published June 25, 2012

neurons (Liman, 2003; Spehr et al., 2009). In our experiments, with intracellular Cs^+ and extracellular Na^+ as the main monovalent cations, we did not detect any cation current. However, it must be pointed out that the anion and cation channels are likely to be activated in two very different ranges of Ca^{2+} concentration. Liman (2003) reported that half-activation of the nonselective cation channel occurred at a very high Ca^{2+} concentration: 0.5 mM at −80 mV. The Ca^{2+}-activated Cl^- channels TMEM16A and TMEM16B, located in the microvilli of vomeronasal sensory neurons, are half-activated at <5 µM (Pifferi et al., 2009a; Stephan et al., 2009; Xiao et al., 2011), a Ca^{2+} concentration that is 100-fold lower than that required to activate the nonselective cation currents. Moreover, although we did not directly measure the Ca^{2+} concentration photoreleased in the microvilli, estimates from our previous studies in olfactory sensory neurons obtained by comparing the normalized currents at various flash intensities (Boccaccio et al., 2006) with the dose–response relation for the native olfactory Ca^{2+}-activated Cl^- channels (Pifferi et al., 2009b) indicate that the maximal photoreleased concentration of Ca^{2+} is likely to be ∼10–20 µM. Thus, a Ca^{2+} concentration range lower than that necessary to activate the nonselective cation channels may explain the lack of detectable cation currents in our experiments.

Liman (2003) also stimulated inside-out patches from dendritic knobs of hamster vomeronasal sensory neurons with 2 mM Ca^{2+} and showed that the activated current was almost entirely cationic. Similar results were obtained by Spehr et al. (2009) by activating patches from mouse VNO neurons with 50 µM Ca^{2+}. It is likely that the explanation of the absence of the chloride component in these inside-out experiments is related to a rapid decrease of the current. Indeed, it has been shown that Ca^{2+}-activated Cl^- channels have a fast run-down in activity after patch excision from the dendritic knob of rat olfactory sensory neurons (Reisert et al., 2003) and that a detectable chloride current is present only in 75% of the patches from mouse olfactory sensory neurons (Fig. 6 C of Pifferi et al., 2009b).

A few recent studies have also provided some evidence for the presence of Ca^{2+}-activated Cl^- channels in vomeronasal sensory neurons. Yang and Delay (2010) used the perforated patch-clamp recordings with gramicidin, a technique that does not modify the intracellular Cl^- concentration, and demonstrated that 80% of the urine-induced current was carried by Ca^{2+}-activated Cl^- channels. These authors also showed that Ca^{2+} influx is

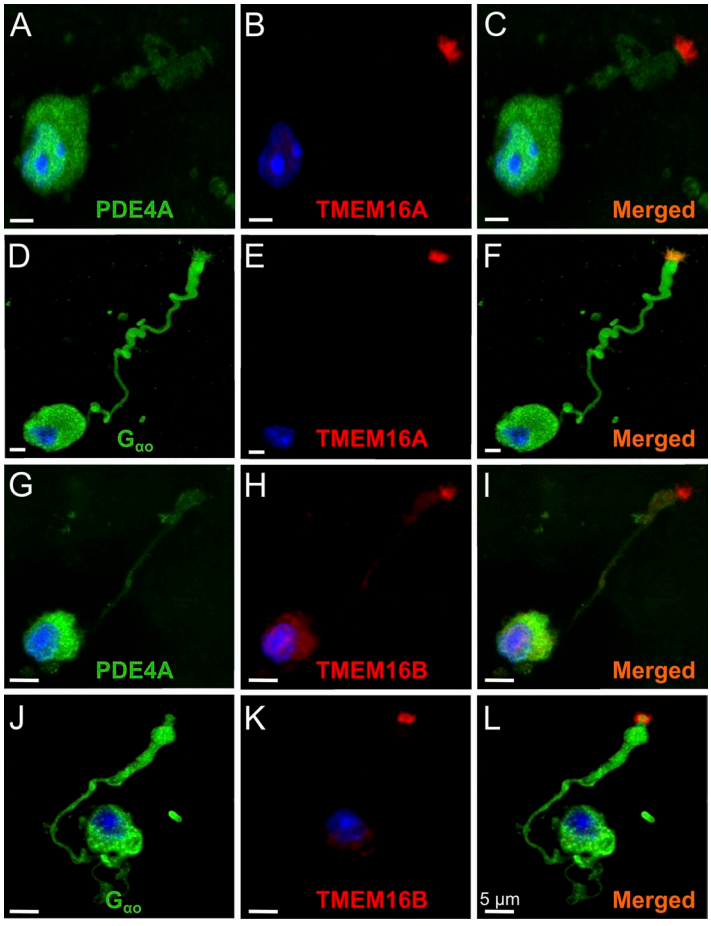

Figure 10. TMEM16A and TMEM16B are expressed in the microvilli of both apical and basal vomeronasal sensory neurons. TMEM16A (guinea pig antibody) is expressed in the microvilli of both apical neurons, as shown by PDE4A (A–C) immunoreactivity, and basal neurons, labeled with rabbit anti-Gαo antibody (D–F). TMEM16B (guinea pig antibody) is also located in the microvilli of both apical (G–I) and basal (J–L) neurons. Cell nuclei were stained by DAPI (blue). Bars, 5 µm.

Published June 25, 2012

necessary to activate the Cl^- channels. In another study, Kim et al. (2011) confirmed the previous study of Yang and Delay (2010) showing that a Ca^{2+}-activated Cl^- current contributes to urine response, but they also suggested that this current can be activated both by Ca^{2+} influx through the TRPC2 channel and by Ca^{2+} release from intracellular stores. Indeed, they also showed that knockout mice for TRPC2 still have a Ca^{2+}-activated Cl^- component in the response to urine that is blocked by compounds that inhibit intracellular Ca^{2+} release, thus suggesting that a TRPC2-independent signaling pathway may be operating in the VNO and that the Ca^{2+}-activated Cl^- current may play a relevant role in transduction.

Billig et al. (2011) compared whole cell recordings in vomeronasal sensory neurons from wild-type ($n = 7$) or knockout mice for TMEM16B ($Ano2^{-/-}$; $n = 6$) obtained with 1.5 µM Ca^{2+} or 0 Ca^{2+} in the pipette and reported that "currents of most $Ano2^{-/-}$ VSNs were indistinguishable from those we observed without Ca^{2+} (Fig. 5n), but a few cells showed currents up to twofold larger. Averaged current/voltage curves revealed that Ca^{2+}-activated Cl^- currents of VSNs depend predominantly on Ano2 (Fig. 5l). Although Ano1 is expressed in the VNO (Fig. 3a), its contribution to VSN currents seems minor." Thus, although most of the Ca^{2+}-activated current was abolished in knockout mice for TMEM16B, a residual current was still present in some neurons. It is likely that the residual current is carried by TMEM16A channels. Indeed, both TMEM16A and TMEM16B are known to independently function as Ca^{2+}-activated Cl^- channels (Scudieri et al., 2012), and we have demonstrated that TMEM16A and TMEM16B coexpress in microvilli of vomeronasal sensory neurons. Further experiments are necessary to unequivocally establish the origin of the residual current and to determine whether TMEM16A and TMEM16B form heteromeric channels and, if so, what the functional properties of the heteromeric channels are.

Physiological role of Ca^{2+}-activated Cl^- channels in vomeronasal and olfactory transduction

What is, then, the physiological role of Ca^{2+}-activated Cl^- channels in vomeronasal sensory neurons? Depending on the Cl^- equilibrium potential, these channels may contribute to the neuron depolarization or hyperpolarization. In vomeronasal sensory neurons, estimates of the Cl^- concentration inside the neurons and in the fluid filling its lumen are not available yet. However, experiments with the perforated patch-clamp recordings with gramicidin showed that the Ca^{2+}-activated Cl^- current acts to further amplify a primary inward depolarizing current (Yang and Delay, 2010), indicating that the intracellular Cl^- concentration was relatively high. In addition, the same authors showed that bumetanide, a specific blocker for the sodium potassium–chloride cotransporter NKCC1, significantly decreased the urine-induced inward current, indicating that NKCC1 is involved in chloride accumulation.

In olfactory sensory neurons, direct measurements of Cl^- concentrations showed that these neurons maintain an unusually high internal concentration of Cl^- of ~50 mM, which is similar to the Cl^- concentration present in the mucus at the external side of the ciliary membrane (Reuter et al., 1998; Kaneko et al., 2001, 2004). Therefore, in physiological conditions, the opening of Ca^{2+}-activated Cl^- channels causes an efflux of Cl^- ions from the cilia, which contributes to neuron depolarization. Up to 80% of the transduction current can be carried by Cl^-. Furthermore, studies from several laboratories indicated that TMEM16B is the main constituent of the Ca^{2+}-activated Cl^- channels involved in olfactory transduction. Indeed, it has been shown that TMEM16B is expressed in the ciliary layer of the olfactory epithelium, that currents in olfactory sensory neurons and in HEK 293T cells transfected with TMEM16B have very similar characteristics, and that knockout mice for TMEM16B did not show any detectable Ca^{2+}-activated Cl^- current (Pifferi et al., 2012). However, Billig et al. (2011) found that disruption of TMEM16B did not reduce mouse performance in some classical olfactory behavioral tasks, suggesting that Ca^{2+}-activated Cl^- channels may be dispensable for near-normal olfaction. Future experiments will have to establish whether Ca^{2+}-activated Cl^- channels are involved in more subtle aspects of olfactory sensing not detected in previous experiments.

It is of interest to note that, despite their differences in the molecular mechanisms of transduction, both olfactory and vomeronasal neurons express members of the TMEM16 family at the site of transduction, indicating that these channels are likely to play a physiological role in sensory transduction.

Conclusions

Our data contribute to the present understanding of the molecular mechanisms of vomeronasal transduction by providing the first direct evidence of the presence of a large Ca^{2+}-activated Cl^- current in the apical region of mouse vomeronasal sensory neurons and of the coexpression of the two Ca^{2+}-activated Cl^- channels TMEM16A and TMEM16B in the microvilli of the same sensory neurons. These observations suggest that TMEM16A and TMEM16B are likely to be responsible for the Cl^- current reported in this work.

In conclusion, collectively with previous studies indicating the presence of a Ca^{2+}-activated Cl^- component in urine response (Yang and Delay, 2010; Kim et al., 2011), our results contribute to the indication that Ca^{2+}-activated Cl^- channels could play a role in vomeronasal transduction. Future studies in mice in which the TMEM16A and/or TMEM16B gene are deleted will increase our understanding of the role of intracellular Ca^{2+} elevation in vomeronasal transduction.

We thank Stephan Frings (Heidelberg University, Heidelberg, Germany) for providing guinea pig antibodies against TMEM16A and TMEM16B, Peter Mombaerts (Max Planck Institute of Biophysics, Frankfurt, Germany) for providing OMP-GFP mice, Johannes Reisert for helpful discussions, Simone Pifferi and Anna Boccaccio for comments on the manuscript, and all members of the laboratories for discussions.

This study was supported by grants from the Italian Ministry of Education, University and Research, and from the Italian Institute of Technology.

Edward N. Pugh Jr. served as editor.

Submitted: 2 February 2012
Accepted: 6 June 2012

REFERENCES

Arnson, H.A., X. Fu, and T.E. Holy. 2010. Multielectrode array recordings of the vomeronasal epithelium. *J. Vis. Exp.* 1845.

Barry, P.H. 1994. JPCalc, a software package for calculating liquid junction potential corrections in patch-clamp, intracellular, epithelial and bilayer measurements and for correcting junction potential measurements. *J. Neurosci. Methods.* 51:107–116. http://dx.doi.org/10.1016/0165-0270(94)90031-0

Berghard, A., and L.B. Buck. 1996. Sensory transduction in vomeronasal neurons: evidence for G alpha o, G alpha i2, and adenylyl cyclase II as major components of a pheromone signaling cascade. *J. Neurosci.* 16:909–918.

Billig, G.M., B. Pál, P. Fidzinski, and T.J. Jentsch. 2011. Ca^{2+}-activated Cl^- currents are dispensable for olfaction. *Nat. Neurosci.* 14:763–769. http://dx.doi.org/10.1038/nn.2821

Boccaccio, A., and A. Menini. 2007. Temporal development of cyclic nucleotide-gated and Ca^{2+} -activated Cl^- currents in isolated mouse olfactory sensory neurons. *J. Neurophysiol.* 98:153–160. http://dx.doi.org/10.1152/jn.00270.2007

Boccaccio, A., L. Lagostena, V. Hagen, and A. Menini. 2006. Fast adaptation in mouse olfactory sensory neurons does not require the activity of phosphodiesterase. *J. Gen. Physiol.* 128:171–184. http://dx.doi.org/10.1085/jgp.200609555

Boccaccio, A., C. Sagheddu, and A. Menini. 2011. Flash photolysis of caged compounds in the cilia of olfactory sensory neurons. *J. Vis. Exp.* e3195.

Brennan, P.A. 2009. Pheromones and mammalian behavior. *In* The Neurobiology of Olfaction. A. Menini, editor. CRC Press, Boca Raton, FL. 157–179.

Brennan, P.A., and F. Zufall. 2006. Pheromonal communication in vertebrates. *Nature.* 444:308–315. http://dx.doi.org/10.1038/nature05404

Caputo, A., E. Caci, L. Ferrera, N. Pedemonte, C. Barsanti, E. Sondo, U. Pfeffer, R. Ravazzolo, O. Zegarra-Moran, and L.J.V. Galietta. 2008. TMEM16A, a membrane protein associated with calcium-dependent chloride channel activity. *Science.* 322:590–594. http://dx.doi.org/10.1126/science.1163518

Chamero, P., T.F. Marton, D.W. Logan, K. Flanagan, J.R. Cruz, A. Saghatelian, B.F. Cravatt, and L. Stowers. 2007. Identification of protein pheromones that promote aggressive behaviour. *Nature.* 450:899–902. http://dx.doi.org/10.1038/nature05997

Dauner, K., J. Lissmann, S. Jeridi, S. Frings, and F. Möhrlen. 2012. Expression patterns of anoctamin 1 and anoctamin 2 chloride channels in the mammalian nose. *Cell Tissue Res.* 347:327–341. http://dx.doi.org/10.1007/s00441-012-1324-9

Dean, D.M., A. Mazzatenta, and A. Menini. 2004. Voltage-activated current properties of male and female mouse vomeronasal sensory neurons: sexually dichotomous? *J. Comp. Physiol. A Neuroethol. Sens. Neural Behav. Physiol.* 190:491–499. http://dx.doi.org/10.1007/s00359-004-0513-8

Dibattista, M., A. Mazzatenta, F. Grassi, R. Tirindelli, and A. Menini. 2008. Hyperpolarization-activated cyclic nucleotide-gated channels in mouse vomeronasal sensory neurons. *J. Neurophysiol.* 100:576–586. http://dx.doi.org/10.1152/jn.90263.2008

Fieni, F., V. Ghiaroni, R. Tirindelli, P. Pietra, and A. Bigiani. 2003. Apical and basal neurones isolated from the mouse vomeronasal organ differ for voltage-dependent currents. *J. Physiol.* 552:425–436. http://dx.doi.org/10.1113/jphysiol.2003.052035

Frings, S. 2009a. Chloride-based signal amplification in olfactory sensory neurons. *In* Physiology and Pathology of Chloride Transporters and Channels in the Nervous System. From Molecules to Diseases. F. J. Alvarez-Leefmans and E. Delpire, editors. Elsevier-Academic Press, San Diego, CA. 413–424.

Frings, S. 2009b. Primary processes in sensory cells: current advances. *J. Comp. Physiol. A Neuroethol. Sens. Neural Behav. Physiol.* 195:1–19. http://dx.doi.org/10.1007/s00359-008-0389-0

Frings, S., D. Reuter, and S.J. Kleene. 2000. Neuronal Ca^{2+}-activated Cl^- channels—homing in on an elusive channel species. *Prog. Neurobiol.* 60:247–289. http://dx.doi.org/10.1016/S0301-0082(99)00027-1

Hartzell, C., I. Putzier, and J. Arreola. 2005. Calcium-activated chloride channels. *Annu. Rev. Physiol.* 67:719–758. http://dx.doi.org/10.1146/annurev.physiol.67.032003.154341

Hengl, T., H. Kaneko, K. Dauner, K. Vocke, S. Frings, and F. Möhrlen. 2010. Molecular components of signal amplification in olfactory sensory cilia. *Proc. Natl. Acad. Sci. USA.* 107:6052–6057. http://dx.doi.org/10.1073/pnas.0909032107

Höfer, D., D.W. Shin, and D. Drenckhahn. 2000. Identification of cytoskeletal markers for the different microvilli and cell types of the rat vomeronasal sensory epithelium. *J. Neurocytol.* 29:147–156. http://dx.doi.org/10.1023/A:1026548020851

Holy, T.E., C. Dulac, and M. Meister. 2000. Responses of vomeronasal neurons to natural stimuli. *Science.* 289:1569–1572. http://dx.doi.org/10.1126/science.289.5484.1569

Jia, C., and M. Halpern. 1996. Subclasses of vomeronasal receptor neurons: differential expression of G proteins (Gi alpha 2 and G(o alpha)) and segregated projections to the accessory olfactory bulb. *Brain Res.* 719:117–128. http://dx.doi.org/10.1016/0006-8993(96)00110-2

Kaneko, H., T. Nakamura, and B. Lindemann. 2001. Noninvasive measurement of chloride concentration in rat olfactory receptor cells with use of a fluorescent dye. *Am. J. Physiol. Cell Physiol.* 280:C1387–C1393.

Kaneko, H., I. Putzier, S. Frings, U.B. Kaupp, and T. Gensch. 2004. Chloride accumulation in mammalian olfactory sensory neurons. *J. Neurosci.* 24:7931–7938. http://dx.doi.org/10.1523/JNEUROSCI.2115-04.2004

Kim, S., L. Ma, and C.R. Yu. 2011. Requirement of calcium-activated chloride channels in the activation of mouse vomeronasal neurons. *Nat Commun.* 2:365. http://dx.doi.org/10.1038/ncomms1368

Kleene, S.J. 2008. The electrochemical basis of odor transduction in vertebrate olfactory cilia. *Chem. Senses.* 33:839–859. http://dx.doi.org/10.1093/chemse/bjn048

Lau, Y.E., and J.A. Cherry. 2000. Distribution of PDE4A and G(o) alpha immunoreactivity in the accessory olfactory system of the mouse. *Neuroreport.* 11:27–32. http://dx.doi.org/10.1097/00001756-200001170-00006

Leinders-Zufall, T., A.P. Lane, A.C. Puche, W. Ma, M.V. Novotny, M.T. Shipley, and F. Zufall. 2000. Ultrasensitive pheromone detection by mammalian vomeronasal neurons. *Nature.* 405:792–796. http://dx.doi.org/10.1038/35015572

Leinders-Zufall, T., P. Brennan, P. Widmayer, P.C. S, A. Maul-Pavicic, M. Jäger, X.H. Li, H. Breer, F. Zufall, and T. Boehm. 2004. MHC class I peptides as chemosensory signals in the vomeronasal organ. *Science.* 306:1033–1037. http://dx.doi.org/10.1126/science.1102818

Published June 25, 2012

Leinders-Zufall, T., T. Ishii, P. Mombaerts, F. Zufall, and T. Boehm. 2009. Structural requirements for the activation of vomeronasal sensory neurons by MHC peptides. *Nat. Neurosci.* 12:1551–1558. http://dx.doi.org/10.1038/nn.2452

Liberles, S.D., L.F. Horowitz, D. Kuang, J.J. Contos, K.L. Wilson, J. Siltberg-Liberles, D.A. Liberles, and L.B. Buck. 2009. Formyl peptide receptors are candidate chemosensory receptors in the vomeronasal organ. *Proc. Natl. Acad. Sci. USA.* 106:9842–9847. http://dx.doi.org/10.1073/pnas.0904464106

Liman, E.R. 2003. Regulation by voltage and adenine nucleotides of a Ca^{2+}-activated cation channel from hamster vomeronasal sensory neurons. *J. Physiol.* 548:777–787. http://dx.doi.org/10.1113/jphysiol.2002.037119

Liman, E.R., and D.P. Corey. 1996. Electrophysiological characterization of chemosensory neurons from the mouse vomeronasal organ. *J. Neurosci.* 16:4625–4637.

Liman, E.R., D.P. Corey, and C. Dulac. 1999. TRP2: a candidate transduction channel for mammalian pheromone sensory signaling. *Proc. Natl. Acad. Sci. USA.* 96:5791–5796. http://dx.doi.org/10.1073/pnas.96.10.5791

Ma, M. 2009. Multiple olfactory subsystems convey various sensory signals. *In* The Neurobiology of Olfaction. A. Menini, editor. CRC Press, Boca Raton, FL. 225–240.

Munger, S.D., T. Leinders-Zufall, and F. Zufall. 2009. Subsystem organization of the mammalian sense of smell. *Annu. Rev. Physiol.* 71:115–140. http://dx.doi.org/10.1146/annurev.physiol.70.113006.100608

Pifferi, S., A. Boccaccio, and A. Menini. 2006. Cyclic nucleotide-gated ion channels in sensory transduction. *FEBS Lett.* 580:2853–2859. http://dx.doi.org/10.1016/j.febslet.2006.03.086

Pifferi, S., M. Dibattista, and A. Menini. 2009a. TMEM16B induces chloride currents activated by calcium in mammalian cells. *Pflugers Arch.* 458:1023–1038. http://dx.doi.org/10.1007/s00424-009-0684-9

Pifferi, S., M. Dibattista, C. Sagheddu, A. Boccaccio, A. Al Qteishat, F. Ghirardi, R. Tirindelli, and A. Menini. 2009b. Calcium-activated chloride currents in olfactory sensory neurons from mice lacking bestrophin-2. *J. Physiol.* 587:4265–4279. http://dx.doi.org/10.1113/jphysiol.2009.176131

Pifferi, S., V. Cenedese, and A. Menini. 2012. Anoctamin 2/TMEM16B: a calcium-activated chloride channel in olfactory transduction. *Exp. Physiol.* 97:193–199.

Potter, S.M., C. Zheng, D.S. Koos, P. Feinstein, S.E. Fraser, and P. Mombaerts. 2001. Structure and emergence of specific olfactory glomeruli in the mouse. *J. Neurosci.* 21:9713–9723.

Rasche, S., B. Toetter, J. Adler, A. Tschapek, J.F. Doerner, S. Kurtenbach, H. Hatt, H. Meyer, B. Warscheid, and E.M. Neuhaus. 2010. Tmem16b is specifically expressed in the cilia of olfactory sensory neurons. *Chem. Senses.* 35:239–245. http://dx.doi.org/10.1093/chemse/bjq007

Reisert, J., and H. Zhao. 2011. Perspectives on: Information and coding in mammalian sensory physiology: Response kinetics of olfactory receptor neurons and the implications in olfactory coding. *J. Gen. Physiol.* 138:303–310. http://dx.doi.org/10.1085/jgp.201110645

Reisert, J., P.J. Bauer, K.W. Yau, and S. Frings. 2003. The Ca-activated Cl channel and its control in rat olfactory receptor neurons. *J. Gen. Physiol.* 122:349–363. http://dx.doi.org/10.1085/jgp.200308888

Reuter, D., K. Zierold, W.H. Schröder, and S. Frings. 1998. A depolarizing chloride current contributes to chemoelectrical transduction in olfactory sensory neurons in situ. *J. Neurosci.* 18:6623–6630.

Rivière, S., L. Challet, D. Fluegge, M. Spehr, and I. Rodriguez. 2009. Formyl peptide receptor-like proteins are a novel family of vomeronasal chemosensors. *Nature.* 459:574–577. http://dx.doi.org/10.1038/nature08029

Ryba, N.J., and R. Tirindelli. 1997. A new multigene family of putative pheromone receptors. *Neuron.* 19:371–379. http://dx.doi.org/10.1016/S0896-6273(00)80946-0

Sagheddu, C., A. Boccaccio, M. Dibattista, G. Montani, R. Tirindelli, and A. Menini. 2010. Calcium concentration jumps reveal dynamic ion selectivity of calcium-activated chloride currents in mouse olfactory sensory neurons and TMEM16b-transfected HEK 293T cells. *J. Physiol.* 588:4189–4204. http://dx.doi.org/10.1113/jphysiol.2010.194407

Schild, D., and D. Restrepo. 1998. Transduction mechanisms in vertebrate olfactory receptor cells. *Physiol. Rev.* 78:429–466.

Schroeder, B.C., T. Cheng, Y.N. Jan, and L.Y. Jan. 2008. Expression cloning of TMEM16A as a calcium-activated chloride channel subunit. *Cell.* 134:1019–1029. http://dx.doi.org/10.1016/j.cell.2008.09.003

Scudieri, P., E. Sondo, L. Ferrera, and L.J. Galietta. 2012. The anoctamin family: TMEM16A and TMEM16B as calcium-activated chloride channels. *Exp. Physiol.* 97:177–183. http://dx.doi.org/10.1113/expphysiol.2011.058198

Shimazaki, R., A. Boccaccio, A. Mazzatenta, G. Pinato, M. Migliore, and A. Menini. 2006. Electrophysiological properties and modeling of murine vomeronasal sensory neurons in acute slice preparations. *Chem. Senses.* 31:425–435. http://dx.doi.org/10.1093/chemse/bjj047

Spehr, M., H. Hatt, and C.H. Wetzel. 2002. Arachidonic acid plays a role in rat vomeronasal signal transduction. *J. Neurosci.* 22:8429–8437.

Spehr, J., S. Hagendorf, J. Weiss, M. Spehr, T. Leinders-Zufall, and F. Zufall. 2009. Ca^{2+}-calmodulin feedback mediates sensory adaptation and inhibits pheromone-sensitive ion channels in the vomeronasal organ. *J. Neurosci.* 29:2125–2135. http://dx.doi.org/10.1523/JNEUROSCI.5416-08.2009

Stephan, A.B., E.Y. Shum, S. Hirsh, K.D. Cygnar, J. Reisert, and H. Zhao. 2009. ANO2 is the cilial calcium-activated chloride channel that may mediate olfactory amplification. *Proc. Natl. Acad. Sci. USA.* 106:11776–11781. http://dx.doi.org/10.1073/pnas.0903304106

Stöhr, H., J.B. Heisig, P.M. Benz, S. Schöberl, V.M. Milenkovic, O. Strauss, W.M. Aartsen, J. Wijnholds, B.H.F. Weber, and H.L. Schulz. 2009. TMEM16B, a novel protein with calcium-dependent chloride channel activity, associates with a presynaptic protein complex in photoreceptor terminals. *J. Neurosci.* 29:6809–6818. http://dx.doi.org/10.1523/JNEUROSCI.5546-08.2009

Tirindelli, R., M. Dibattista, S. Pifferi, and A. Menini. 2009. From pheromones to behavior. *Physiol. Rev.* 89:921–956. http://dx.doi.org/10.1152/physrev.00037.2008

Touhara, K., and L.B. Vosshall. 2009. Sensing odorants and pheromones with chemosensory receptors. *Annu. Rev. Physiol.* 71:307–332. http://dx.doi.org/10.1146/annurev.physiol.010908.163209

Xiao, Q., K. Yu, P. Perez-Cornejo, Y. Cui, J. Arreola, and H.C. Hartzell. 2011. Voltage- and calcium-dependent gating of TMEM16A/Ano1 chloride channels are physically coupled by the first intracellular loop. *Proc. Natl. Acad. Sci. USA.* 108:8891–8896. http://dx.doi.org/10.1073/pnas.1102147108

Yang, C., and R.J. Delay. 2010. Calcium-activated chloride current amplifies the response to urine in mouse vomeronasal sensory neurons. *J. Gen. Physiol.* 135:3–13. http://dx.doi.org/10.1085/jgp.200910265

Yang, Y.D., H. Cho, J.Y. Koo, M.H. Tak, Y. Cho, W.-S. Shim, S.P. Park, J. Lee, B. Lee, B.-M. Kim, et al. 2008. TMEM16A confers receptor-activated calcium-dependent chloride conductance. *Nature.* 455:1210–1215. http://dx.doi.org/10.1038/nature07313

Zufall, F., K. Ukhanov, P. Lucas, E.R. Liman, and T. Leinders-Zufall. 2005. Neurobiology of TRPC2: from gene to behavior. *Pflugers Arch.* 451:61–71.

Zufall, F., and T. Leinders-Zufall. 2007. Mammalian pheromone sensing. *Curr. Opin. Neurobiol.* 17:483–489. http://dx.doi.org/10.1016/j.conb.2007.07.012

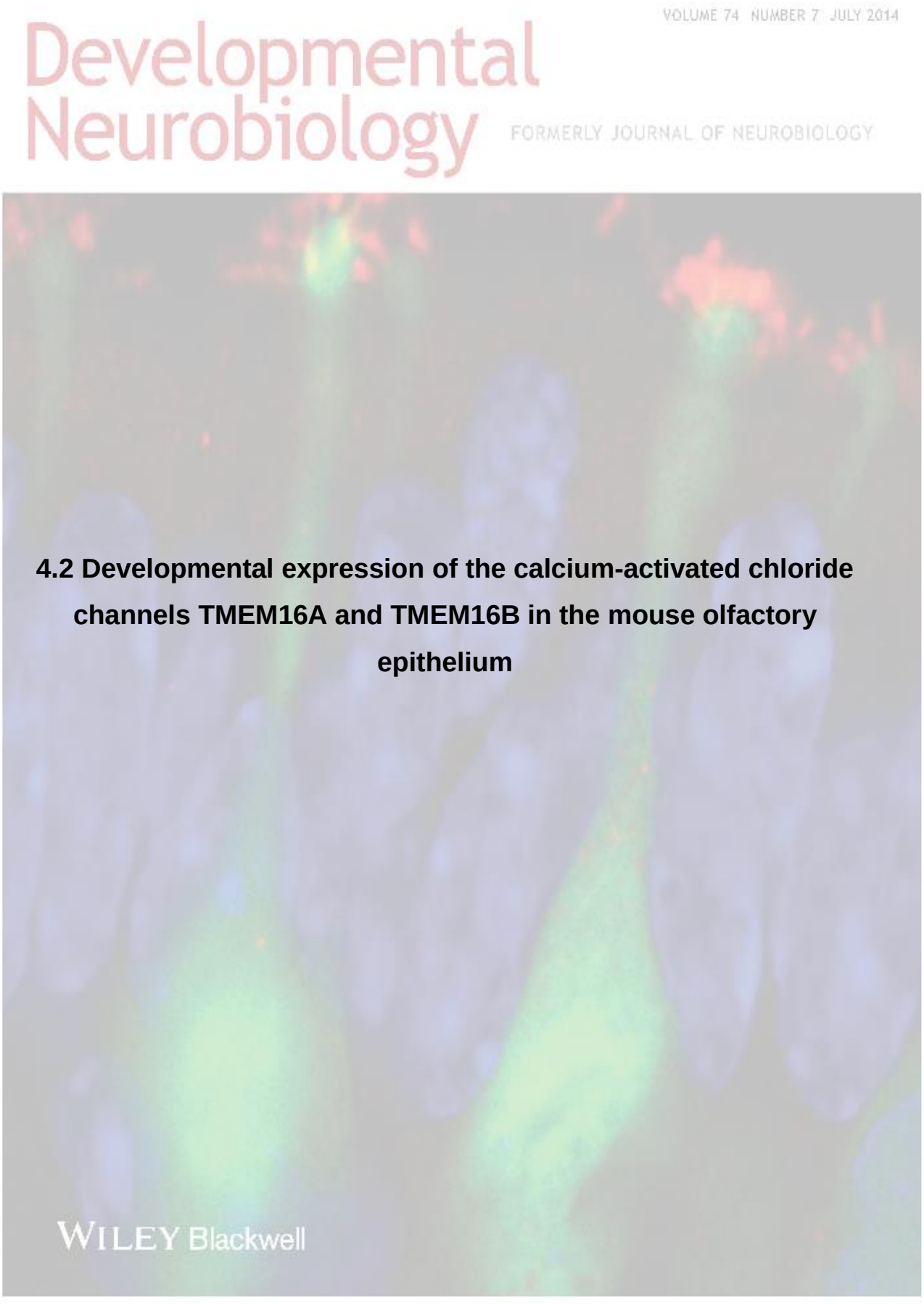

4.2 Developmental expression of the calcium-activated chloride channels TMEM16A and TMEM16B in the mouse olfactory epithelium

Developmental Expression of the Calcium-Activated Chloride Channels TMEM16A and TMEM16B in the Mouse Olfactory Epithelium

Devendra Kumar Maurya, Anna Menini

Laboratory of Olfactory Transduction, SISSA, International School for Advanced Studies, Via Bonomea 265, Trieste 34136, Italy

Received 11 November 2013; revised 2 December 2013; accepted 3 December 2013

ABSTRACT: **Calcium-activated chloride channels are involved in several physiological processes including olfactory perception. TMEM16A and TMEM16B, members of the transmembrane protein 16 family (TMEM16), are responsible for calcium-activated chloride currents in several cells. Both are present in the olfactory epithelium of adult mice, but little is known about their expression during embryonic development. Using immunohistochemistry we studied their expression in the mouse olfactory epithelium at various stages of prenatal development from embryonic day (E) 12.5 to E18.5 as well as in postnatal mice. At E12.5, TMEM16A immunoreactivity was present at the apical surface of the entire olfactory epithelium, but from E16.5 became restricted to a region near the transition zone with the respiratory epithelium, where localized at the apical part of supporting cells and in their microvilli. In contrast, TMEM16B immunoreactivity was present at E14.5 at the apical surface of the entire olfactory epithelium, increased in subsequent days, and localized to the cilia of mature olfactory sensory neurons. These data suggest different functional roles for TMEM16A and TMEM16B in the developing as well as in the postnatal olfactory epithelium. The presence of TMEM16A at the apical part and in microvilli of supporting cells is consistent with a role in the regulation of the chloride ionic composition of the mucus covering the apical surface of the olfactory epithelium, whereas the localization of TMEM16B to the cilia of mature olfactory sensory neurons is consistent with a role in olfactory signal transduction.** Develop Neurobiol 74: 657–675, 2014

Keywords: **olfaction; OSN; supporting cell; ANO1; ANO2**

INTRODUCTION

Calcium-activated chloride channels are expressed in many cell types and play several different physiological functions, but their molecular identity has been elusive until 2008, when TMEM16A (also named anoctamin1 or ANO1) was identified as a calcium-activated chloride channel (Caputo et al., 2008; Schroeder et al., 2008; Yang et al., 2008). An additional member of the same family, TMEM16B (also named anoctamin2 or ANO2), has also been shown to function as a calcium-activated chloride channel (Schroeder et al., 2008; Pifferi et al., 2009a; Stephan et al., 2009; for recent reviews, see Huang et al., 2012a; Scudieri et al., 2012).

In adult mice, TMEM16A and TMEM16B are both expressed in the olfactory epithelium and allow the flow of anions in or out of cells upon increases in intracellular calcium concentration. However, their precise physiological functions in the cells of the olfactory epithelium are still unclear and little is known about their expression during embryonic development.

The olfactory epithelium is a pseudostratified epithelium composed of several types of cells: olfactory sensory neurons in various stages of maturation, supporting or sustentacular cells, basal cells, and some

Correspondence to: A. Menini (menini@sissa.it).

Contract grant sponsor: Italian Ministry of Education, University and Research (MIUR).

Published online 9 December 2013 in Wiley Online Library (wileyonlinelibrary.com).
DOI 10.1002/dneu.22159

subpopulations of microvillous cells. Olfactory sensory neurons are bipolar neurons with an axon that projects to the olfactory bulb and a dendritic process ending in a dendritic knob from which several cilia protrude at the apical surface of the epithelium (Cuschieri and Bannister, 1975a,b). Cilia are immersed in a mucus layer composed of water, ions, and proteins secreted by Bowman's glands and supporting cells (Menco and Farbman, 1992, Menco et al., 1998). The process of olfactory transduction occurs in the cilia of olfactory sensory neurons, when molecules from the external environment reach the olfactory epithelium and bind to specific odorant receptors in the cilia. Subsequently, a G protein and adenylyl cyclase III (ACIII) are activated, causing a rise of intraciliary cAMP and the opening of cyclic nucleotide-gated (CNG) channels located in the ciliary membrane (Schild and Restrepo, 1998; Pifferi et al., 2006; Frings, 2009). Calcium and sodium influx through CNG channels produces a depolarization, and the increase in intracellular calcium activates chloride channels. In the presence of an elevated intracellular chloride concentration, these channels can contribute to a further depolarization of olfactory sensory neurons (for reviews, see Kleene, 2008; Frings, 2010; Pifferi et al., 2010, 2012; Reisert and Zhao, 2011). The presence of both the cationic CNG channels and the anionic calcium-activated chloride channels may have at least two physiological roles. By acting in combination, the two channels may preserve odorant detection even if the extracellular ionic environment changes, as it was suggested for amphibians (Kleene and Gesteland, 1991; Kleene, 1993; Kurahashi and Yau, 1993; Kleene and Pun, 1996). Another possible role is the amplification of the primary cationic current by the anionic current, which may be relevant for the detection of very low odorant concentrations (Lowe and Gold, 1993; Kleene, 1997; Reisert et al., 2005; Boccaccio et al. 2006; Boccaccio and Menini 2007).

In the olfactory epithelium, supporting or sustentacular cells have columnar cell bodies and several microvilli on their apical side that extend in the mucus (Nomura et al., 2004). These apically located cells function both as epithelial and glia cells, i.e., they electrically isolate olfactory sensory neurons (Breipohl et al., 1974) and regulate the balance between salt and water in the mucus layer (Mendoza, 1993; Menco et al., 1998; Rochelle, 2000). Basal cells are responsible for the regeneration of olfactory sensory neurons throughout the animal life. Several subpopulations of microvillous cells, different from supporting cells, are also present and some of them may contribute to odorant detection (Elsaesser et al., 2005; Lin et al., 2007; Hanse and Finger, 2008; Ma, 2010).

The mRNA of TMEM16B is expressed in adult mouse olfactory epithelium (Yu et al., 2005; Stephan et al., 2009; Rasche et al., 2010; Sagheddu et al., 2010; Billig et al., 2011). Moreover, TMEM16B is a prominent protein in the olfactory ciliary proteome (Mayer et al., 2009; Stephan et al., 2009), and immunohistochemistry showed that it is strongly expressed in the ciliary layer of olfactory sensory neurons (Hengl et al., 2010; Rasche et al., 2010; Sagheddu et al., 2010; Billig et al., 2011; Dauner et al., 2012; Dibattista et al., 2012). From a functional perspective, striking similarities have been observed between native calcium-activated chloride currents in olfactory sensory neurons and currents in HEK 293 cells transfected with TMEM16B (Stephan et al., 2009; Sagheddu et al., 2010). Finally, recordings from TMEM16B knockout mice showed that calcium-activated chloride currents in olfactory sensory neurons were undetectable, confirming that TMEM16B is the principal subunit of the ciliary calcium-activated chloride channel in olfactory neurons (Billig et al., 2011). However, the physiological role of this current is still enigmatic, as adult TMEM16B knockout mice have a near-normal olfactory behavior (Billig et al., 2011); this indicates that TMEM16B may not be necessary for olfactory perception in normal conditions, although additional studies with altered extracellular ionic conditions and/or with low odorant concentrations have not been performed yet and may produce different behavioral results.

The mRNA of TMEM16A is expressed in adult mouse olfactory epithelium (Gritli-Linde et al., 2008; Rasche et al., 2010; Sagheddu et al., 2010; Billig et al., 2011), while the expression of the protein TMEM16A has been less studied. In adult mice, TMEM16A was not expressed in olfactory sensory neurons (Billig et al., 2011; Dauner et al., 2012; Dibattista et al., 2012) but was present in supporting cells and in Bowman's glands (Dauner et al., 2012). Knockout mice for TMEM16A die soon after birth (Rock et al., 2008) thus preventing functional and behavioral studies in adult mice.

During embryonic development of the olfactory epithelium, the expression of TMEM16B has not been investigated, whereas the expression of TMEM16A has been studied by *in situ* hybridization (Gritli-Linde et al., 2009), revealing a dynamic high expression level of TMEM16A. Thus, the precise developmental patterns of TMEM16A and TMEM16B in the olfactory epithelium are still unknown.

The goal of this study is to identify with immunohistochemistry the temporal and cellular expression

of TMEM16A and TMEM16B in the olfactory epithelium during mouse embryonic development and at postnatal age, with the aim to contribute to the understanding of the functional roles of these recently discovered proteins. We found different temporal and cellular expressions for the two proteins.TMEM16B was expressed at embryonic day 14.5 (E14.5) in the cilia of mature olfactory sensory neurons, where the process of olfactory transduction occurs, indicating its likely involvement in olfactory transduction. TMEM16A was already expressed at E12.5 at the apical surface of the olfactory epithelium, but from E16.5 it was found only in a region of the olfactory epithelium near the transition zone with the respiratory epithelium, where it was expressed in microvilli of supporting cells, suggesting a possible role in the regulation of the chloride ionic composition of the olfactory mucus.

METHODS

Animals

All animals were handled in accordance with the Italian Guidelines for the Use of Laboratory Animals (Decreto Legislativo 27/01/1992, no. 116) and European Union guidelines on animal research (No. 86/609/EEC). Wild-type C57Bl6 or genetically modified mice that express the green fluorescent protein (GFP) instead of the olfactory marker protein (OMP) in all mature olfactory sensory neurons were used (OMP–GFP mice; provided by Dr. Peter Mombaerts, Max Planck Institute of Biophysics, Frankfurt, Germany). Male and female mice of the same strain were put together for mating in the evening and separated the next morning. If a vaginal plug was observed in the morning, that day was designated as embryonic day 0.5 (E0.5). For postnatal mice, the date of birth was defined as P0. Postnatal mice were anaesthetized by CO_2 inhalation and decapitated. Embryos were removed from the uterus and decapitated. The age of each embryo was also compared to the database at: http://www.emouseatlas.org/Databases/Anatomy/MAstaging.html.

Immunohistochemistry

Heads of embryonic mice, or nasal regions of postnatal mice, were fixed in 4% paraformaldehyde at 4°C (4–12 h). For postnatal mice over P15, the nasal region was additionally decalcified in 0.5 M EDTA, pH 8.0, for 48 h at 4°C (Pifferi et al., 2009b; Sagheddu et al., 2010). For cryoprotection, tissues of embryonic or postnatal mice were subsequently equilibrated in 30% (w/v) sucrose at 4°C. Tissues were frozen in OCT compound (Bio-optica, Milano, Italy) and stored at −80°C before sectioning on cryostat. Coronal sections (12–14 μm thick) were cut with a cryostat, and stored at −80°C for further use. For antigen retrieval, sections were treated with SDS 0.5 % (w/v) in PBS for 15 min at room temperature. Sections were incubated in a blocking solution [2% FBS (v/v), and 0.2% (v/v) Triton X-100 in PBS] for 2 h, and then with the primary antibody (diluted in the blocking solution) overnight at 4°C. Sections were then rinsed with 0.1% (v/v) Tween 20 in PBS (PBS-T), and incubated with the chosen fluorophore-conjugated secondary antibody (diluted in PBS-T) for 2 h at room temperature. After washing with PBS-T, sections were treated with DAPI (0.1 μg/mL) for 30 min, washed with PBS-T, and mounted with Vectashield (Vector Laboratories, Burlingame, CA).

All chemicals, unless otherwise stated, were purchased from Sigma.

For each age, sections were analyzed from at least three mice obtained from at least two different litters.

Antibody Characterization

The antibodies used in this study are listed in Table 1.

The TMEM16A polyclonal antibody was raised in rabbit (Abcam, ab53212) against a cocktail of three different peptides in the following range of amino acids: 424–519, 628–731, and 904–986 of TMEM16A of human origin. The specificity of the rabbit TMEM16A antibody has been demonstrated by the absence of labeling in colon tissue from TMEM16A knockout mice when compared to wild-type animals (Gomez-Pinilla et al., 2009). In addition, we have recently tested the specificity of the rabbit TMEM16A antibody on HEK 293T cells transiently transfected with plasmids containing the cDNA sequence of TMEM16A or TMEM16B, and showed that this antibody specifically detected TMEM16A and showed no cross-reactivity to TMEM16B (Dibattista et al., 2012).

The TMEM16A polyclonal antibody (S-20) raised in goat (Santa Cruz Biotechnology, sc-69343) recognizes an epitope in the range of amino acids 825–875 within an internal region of TMEM16A of human origin. The specificity of the goat TMEM16A antibody has been characterized by Sun et al. (2012) in pulmonary artery protein lysates. Western blot analysis detected a band of about 114 kDa, the predicted size of TMEM16A. The specificity of the antibody against TMEM16A was verified with the blocking peptide (Sun et al., 2012). In addition, Davis et al. (2013) showed that this antibody inhibited TMEM16A function as calcium-activated chloride channel by 90%. Moreover, we observed that the goat TMEM16A antibody produced in the olfactory epithelium the same immunohistochemical staining pattern as the rabbit TMEM16A antibody (data not shown).

The TMEM16B polyclonal antibody (H-73) raised in rabbit (Santa Cruz Biotechnology, sc-292004) recognizes an epitope at the C-terminus in the range of amino acids 931–1003 of TMEM16B of human origin. We have recently tested the specificity of the rabbit TMEM16B antibody on HEK 293T cells transiently transfected with plasmids containing the cDNA sequence of TMEM16A or

Table 1 Primary Antibodies Used in this Study

Primary Antibody	Immunogen	Dilution	Manufacturer/Catalog Number/Lot Number or Clone
Rabbit polyclonal TMEM16A	Synthetic peptides corresponding to amino acid ranges 424–519, 628–731 and 904–986 of human TMEM16A	1:50	Abcam/ab53212/GR71118-1
Goat polyclonal TMEM16A	Synthetic peptide corresponding to amino acid range 825–875 of human TMEM16A	1:50	Santa Cruz Biotech Inc (Santa Cruz) /sc-69343/I13111
Rabbit polyclonal TMEM16B	Synthetic peptide corresponding to amino acid range 931–1003 of human TMEM16B	1:100	Santa Cruz Biotech Inc (Santa Cruz) /sc-292004/A2811
Rabbit polyclonal adenylyl cyclase III (ACIII)	Synthetic peptide corresponding to amino acid range 1125–1144 of human ACIII	1:100	Santa Cruz Biotech Inc (Santa Cruz) /sc-588/K0608
Goat polyclonal cyclic nucleotide-gated channel A2 (CNGA2)	Synthetic peptide corresponding to the last 50 amino acids residues at the C-terminus of mouse CNGA2	1:100	Santa Cruz Biotech Inc (Santa Cruz) /sc-1370/D0909
Goat polyclonal olfactory marker protein (OMP)	Purified natural rat OMP	1:1000	Wako Chemicals/544-10001/ IUP1001
Rabbit polyclonal β-tubulin III	Synthetic peptide corresponding to amino acid residues 441–450 of human β-tubulin III (Ala^{446} to Ser^{446} substitution) with N-terminal added cysteine, conjugated to KLH	1:800	Sigma/T2200/022M4774
Mouse monoclonal acetylated tubulin	Acetylated tubulin from the outer arm of *Strongylocentrotus purpuratus*	1:100	Sigma/T7451/clone 6–11B-1
Mouse monoclonal ezrin	Recombinant fragment corresponding to amino acid residues 362–585 of human ezrin	1:100	Abcam/ab4069/3C12

TMEM16B, and showed that this antibody specifically recognized TMEM16B and showed no cross-reactivity to TMEM16A (Dibattista et al., 2012).

The ACIII polyclonal antibody (C-20) raised in rabbit (Santa Cruz Biotechnology, sc-588) recognizes an epitope at the C-terminus in the range of amino acids 1125–1144 of human origin. The specificity of the rabbit ACIII antibody has been demonstrated by the absence of labeling in the olfactory epithelium from ACIII knockout mice when compared to wild-type animals (Wong et al., 2000; Col et al., 2007; Zou et al., 2007).

The cyclic nucleotide-gated channel A2 (CNGA2) polyclonal antibody (M-20) raised in goat (Santa Cruz Biotechnology, sc-13700) recognizes an epitope in the range of the last 50 amino acids at the C-terminus of CNGA2 of mouse origin. We tested the specificity of this antibody on HEK 293T cells transiently transfected with plasmid containing the cDNA sequence of CNGA2, and showed that this antibody specifically recognized CNGA2 (data not shown). Moreover, the same antibody was used by Michalakis et al. (2006) to identify the expression of CNGA2 in the olfactory epithelium of wild-type and knockout mice for CNGB1.

The goat OMP antibody (Wako Chemicals, 544-10001) was used to immunostain mature olfactory sensory neurons (Keller and Margolis, 1975). Baker et al. (1989) showed that this antibody recognized a single band at 19 kDa on a Western blot of mouse brain and that pre-absorption blocked all staining. This antibody has been previously extensively characterized as a marker for mature olfactory sensory neurons (Rodriguez-Gil and Greer, 2008; Miller et al., 2010; Eckler et al., 2011; Marcucci et al., 2011).

The β-tubulin III polyclonal antibody raised in rabbit (Sigma, T2200) was used to immunostain neurons in the olfactory epithelium. This antibody recognizes an epitope at the C-terminus corresponding to amino acids 441–450 of β-tubulin III of human origin. This antibody has been characterized by Furmanski et al. (2009), and Martín-Ibáñez et al. (2010).

The acetylated tubulin monoclonal antibody (clone 6-11B-1) raised in mouse (Sigma, T7451) was used to identify olfactory cilia. This antibody is derived from a hybridoma produced by the fusion of mouse myeloma cells and splenocytes from a mouse immunized with acetylated tubulin from the outer arm of *Strongylocentrotus purpuratus* (sea urchin), and its specificity has been previously characterized by Piperno and Fuller (1985). This antibody has been previously used to identify cilia (Ross et al., 2005; Cygnar and Zhao, 2009).

The ezrin monoclonal antibody (3C12) raised in mouse (Abcam, ab4069), was used to immunostain microvilli of supporting cells in the olfactory epithelium. This antibody

was raised against a recombinant fragment corresponding to amino acids 362–585 of ezrin of human origin. Its specificity has been demonstrated by the absence of staining in the microvilli of retinal pigment epithelium from rats in which ezrin was silenced when compared to control or to rats over-expressing ezrin (Chuang et al., 2010).

Secondary Antibodies

The following secondary antibodies obtained from Invitrogen, Eugene, OR, were used: donkey anti-rabbit Alexa Fluor 488 (1:500; catalog no. A21206), donkey anti-goat Alexa Fluor 594 (1:500; catalog no. A11058), goat anti-rabbit Alexa Fluor 594 (1:500; catalog no. A11037), goat anti-mouse Alexa Fluor 488 (1:500; catalog no. A11001).

Imaging

Immunoreactivity was visualized with a confocal microscope (TCS SP2; Leica) using 40×/1.25NA or 63×/1.4NA oil immersion objectives. Images were acquired using Leica software (at 1,024 × 1,024 pixel resolution). All images were taken as single plane confocal images, except for the images in Figure 1, which were taken as average of *z*-stacks of 1-μm thickness. Images were prepared and assembled in Inkscape version 0.48.2, images were not modified other than to level illumination. Only DAPI signals were enhanced, to show the anatomy of the olfactory epithelium. In any case, data were not altered with the above adjustments.

Control Experiments

Control experiments, conducted by incubating the sections with secondary antibodies without primary antibodies, showed no significant staining.

RESULTS

Expression of TMEM16B in the Olfactory Epithelium

Coronal sections of the mouse olfactory epithelium were obtained during embryonic development from E12.5, when the nasal cavity is formed and the olfactory epithelium can be anatomically distinguished (Cuschieri and Bannister, 1975a; Treloar et al., 2010). We used β-tubulin III and the OMP as markers to visualize olfactory sensory neurons at different stages of maturation. β-tubulin III is a good marker to identify immature olfactory sensory neurons, as it is strongly expressed in their cell bodies (Lee and Pixely, 1994; Roskams et al., 1998; Wei et al., 2013), while β-tubulin III expression decreases dramatically in mature neurons, where it is mainly present in dendrites but not in the cell bodies (Wei et al., 2013). OMP is a typical marker for mature olfactory sensory neurons (Keller and Margolis, 1975).

In Figures 1 and 2 we used genetically modified OMP-GFP mice that express GFP instead of OMP in all mature olfactory sensory neurons (Potter et al., 2001). Figures 1(A–C) shows that at E12.5 numerous immature olfactory sensory neurons were present, but no mature neurons were detected. At E14.5 the number of mature neurons was very small [Fig. 1(E)], but markedly increased at E16.5 and E18.5 [Fig. 1(H,K)]. Thus, with development, the number of mature versus immature neurons increased [Fig. 1(C,F,I,L)]. Similar images were obtained from various areas of the olfactory epithelium. These results are in agreement with the previous study by Graziadei et al. (1980), which showed that between E10 and E13 olfactory sensory neurons of wild-type mice became numerous but were devoid of immunoreactivity for OMP, while OMP expression began at E14 in a very small number of neurons and increased with development.

We next compared the expression during embryonic development of TMEM16B with some critical proteins involved in the olfactory transduction cascade, ACIII and CNGA2. Arrow heads in Figure 2(A) indicate that small clusters of ACIII immunoreactivity were already detected at E12.5 at the apical surface of the olfactory epithelium, before the appearance of mature olfactory sensory neurons. At E14.5 and subsequent days, ACIII immunoreactivity increased and was mainly observed around the dendritic swellings (knobs) of mature neurons [Fig. 2(B–D)].

In contrast to ACIII, which was already expressed at E12.5, CNGA2 immunoreactivity was first observed at E16.5 [Fig. 2(E–G)]. Immunopositive signals were seen at the apical surface of the olfactory epithelium mainly around the knobs of mature neurons [Fig. 2(G)]. At E18.5, the number of neurons expressing CNGA2 markedly increased [Fig. 2(H)].

For TMEM16B, immunopositive signals were first observed at E14.5 [Fig. 2(I,J,M,N)]. In addition, the number of neurons expressing TMEM16B increased with development [Fig. 2(K,L)] The expression of TMEM16B was clearly observed in the cilia of mature neurons and in some of their dendritic knobs [Fig. 2(O,P)]. Similar images for ACIII, CNGA2, and TMEM16B were obtained from various areas of the olfactory epithelium, indicating that these figures are representative of the distributions across the tissue.

Taken together, these results show that both CNGA2 and TMEM16B are expressed around the knobs and in the cilia of mature neurons at similar embryonic days, E16.5 for CNGA2 and E14.5 for TMEM16B, indicating that by E16.5 both channels are present to participate in their olfactory functions.

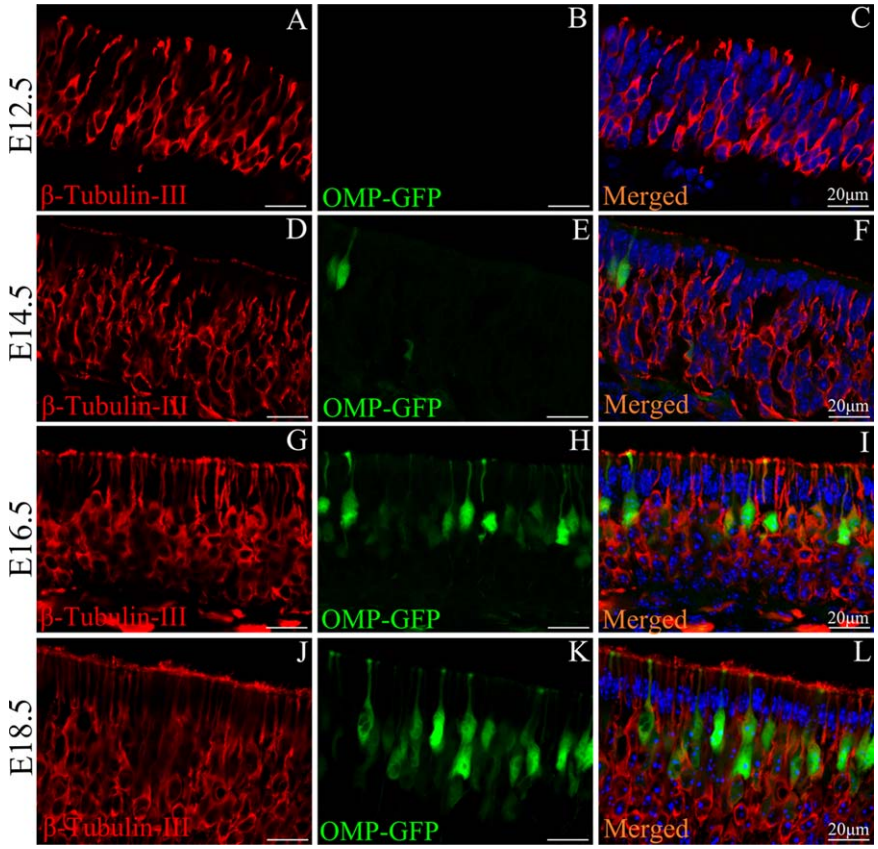

Figure 1 Olfactory sensory neurons in the developing olfactory epithelium of OMP-GFP mice. In these mice, mature olfactory sensory neurons express GFP instead of OMP, so that mature neurons are denoted as OMP-GFP. A-L: Confocal images of coronal sections of the olfactory epithelium at E12.5, E14.5, E16.5 and E18.5. Early in development at E12.5 the olfactory epithelium was devoid of mature neurons (B) and the developing neuronal population expressed β-tubulin III (A). Mature neurons were first seen at E14.5 (E), and their number progressively increased at E16.5 and E18.5 (H,K). Images are averages of z-stacks of 1 μm thickness. Cell nuclei were stained by DAPI. Scale bars = 20 μm. [Color figure can be viewed in the online issue, which is available at wileyonlinelibrary.com.]

To further characterize the expression pattern of TMEM16B in the cilia of olfactory sensory neurons in wild-type mice, we used anti-acetylated tubulin, a canonical marker to identify cilia, and performed a double immunostaining along with anti-TMEM16B. At E14.5, acetylated tubulin was expressed in small clusters at the apical surface of the olfactory epithelium and largely coexpressed with TMEM16B [Fig. 3(A–C)]. As seen from acetylated tubulin immunoreactivity, cilia elongated during development [Fig. 3(B,E,H)] and, in postnatal mice, cilia formed a layer parallel to the apical surface of the olfactory epithelium [Fig. 3(K,N)]. TMEM16B immunoreactivity also increased during development [Fig. 3(A,D,G,J,M)] and the two proteins were largely coexpressed [Fig. 3(C,F,I,L,O)]. Figure 3(L–O) indicates that TMEM16B was mainly localized to the proximal part of the cilia and also to some dendritic knobs [see also Fig. 2(O,P)] of olfactory sensory neurons.

These results show that TMEM16B was expressed at E14.5 (but not at E12.5) in the cilia of mature olfactory sensory neurons and that the number of neurons expressing TMEM16B increased with development, both in OMP–GFP (Fig. 2) and in wild-type mice (Fig. 3). Other proteins involved in olfactory transduction appeared at the apical surface of the olfactory epithelium at different days during embryonic development, ACIII at E12.5 and CNGA2 at E16.5, in agreement with previous studies (Sullivan et al., 1995; Treloar et al., 2005; Col et al., 2007).

Expression of TMEM16A in the Olfactory Epithelium

To examine the expression and localization of TMEM16A in comparison with TMEM16B, we performed a double immunostaining in wild-type mice. At E12.5, TMEM16A immunoreactivity was uniform

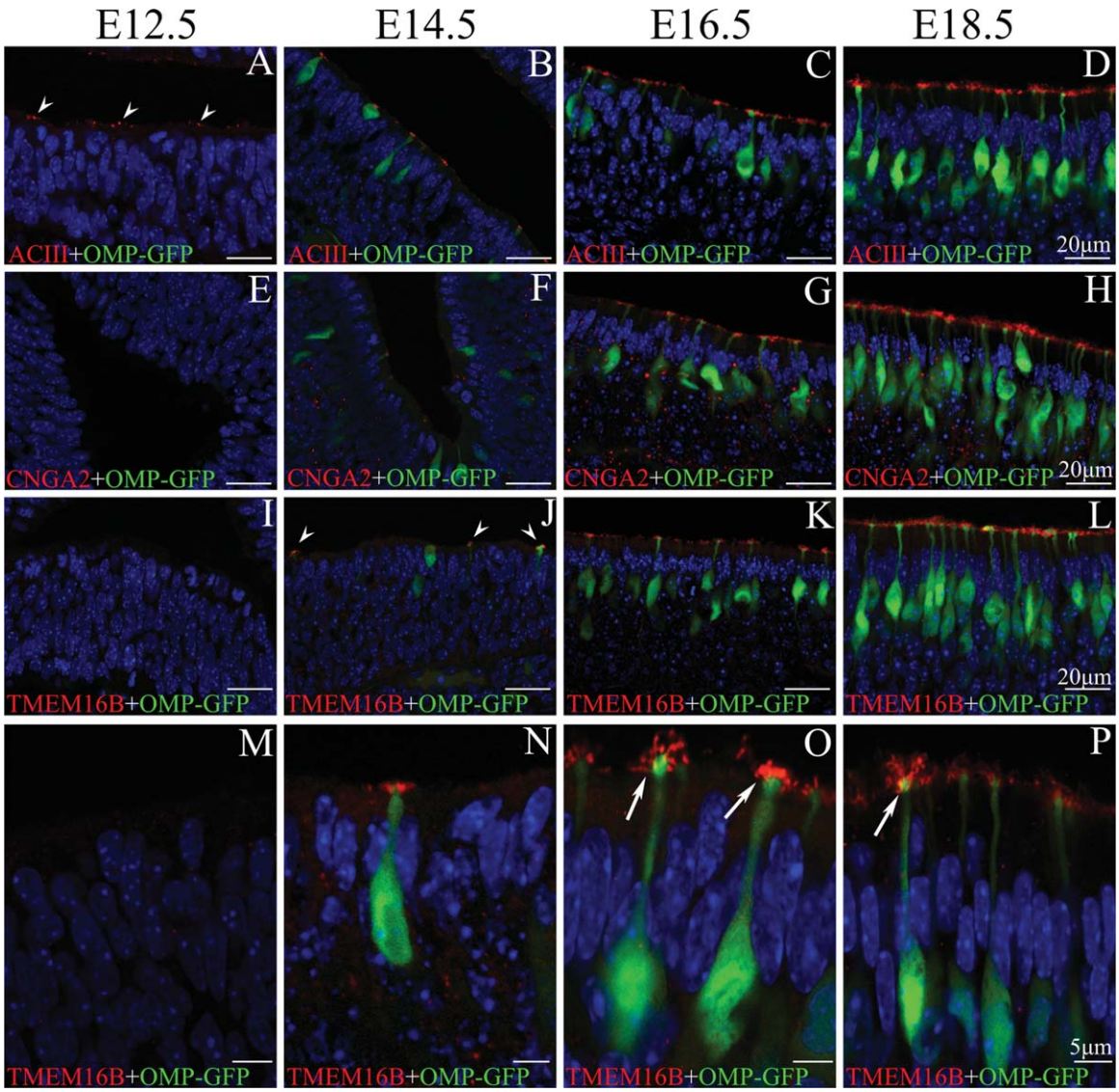

Figure 2 Expression of proteins involved in olfactory transduction in the developing olfactory epithelium of OMP-GFP mice. In these mice, as in Figure 1, mature olfactory sensory neurons express GFP instead of OMP, and mature neurons are denoted as OMP-GFP. Confocal images of coronal sections of the olfactory epithelium at E12.5, E14.5, E16.5 and E18.5. A-D: adenylyl cyclase III (ACIII) was already expressed in immature olfactory sensory neurons at E12.5 (arrowheads) as well as in mature neurons at subsequent days. E-H: cyclic nucleotide-gated channel A2 (CNGA2) was first expressed at E16.5 (G). I-P: TMEM16B was first expressed at E14.5 (J,N) and its expression increased in the following days. M-P: higher magnification images show the expression of TMEM16B in mature neurons. TMEM16B was expressed in the cilia and in some knobs (arrows in O,P). Cell nuclei were stained by DAPI. Scale bars: A-L = 20μm; M-P = 5μm.

over the entire apical surface of the olfactory epithelium [Fig. 4(A,A1,A2)] and of the respiratory epithelium [Fig. 4(A,A3)], whereas TMEM16B immunoreactivity was not yet present. A similar expression for TMEM16A was observed at E14.5 (data not shown). At E16.5, TMEM16A immunoreactivity was not longer uniform, but began to be restricted only to a ventral region toward the transition zone between the olfactory and the respiratory epithelium [Fig. 4(B,B1,B2)]. At P2, the expression of TMEM16A was further restricted toward the respiratory epithelium [Fig. 4(C,C1,C2)], and a similar expression was observed also at later postnatal days (data not shown). Both at E16.5 and in postnatal

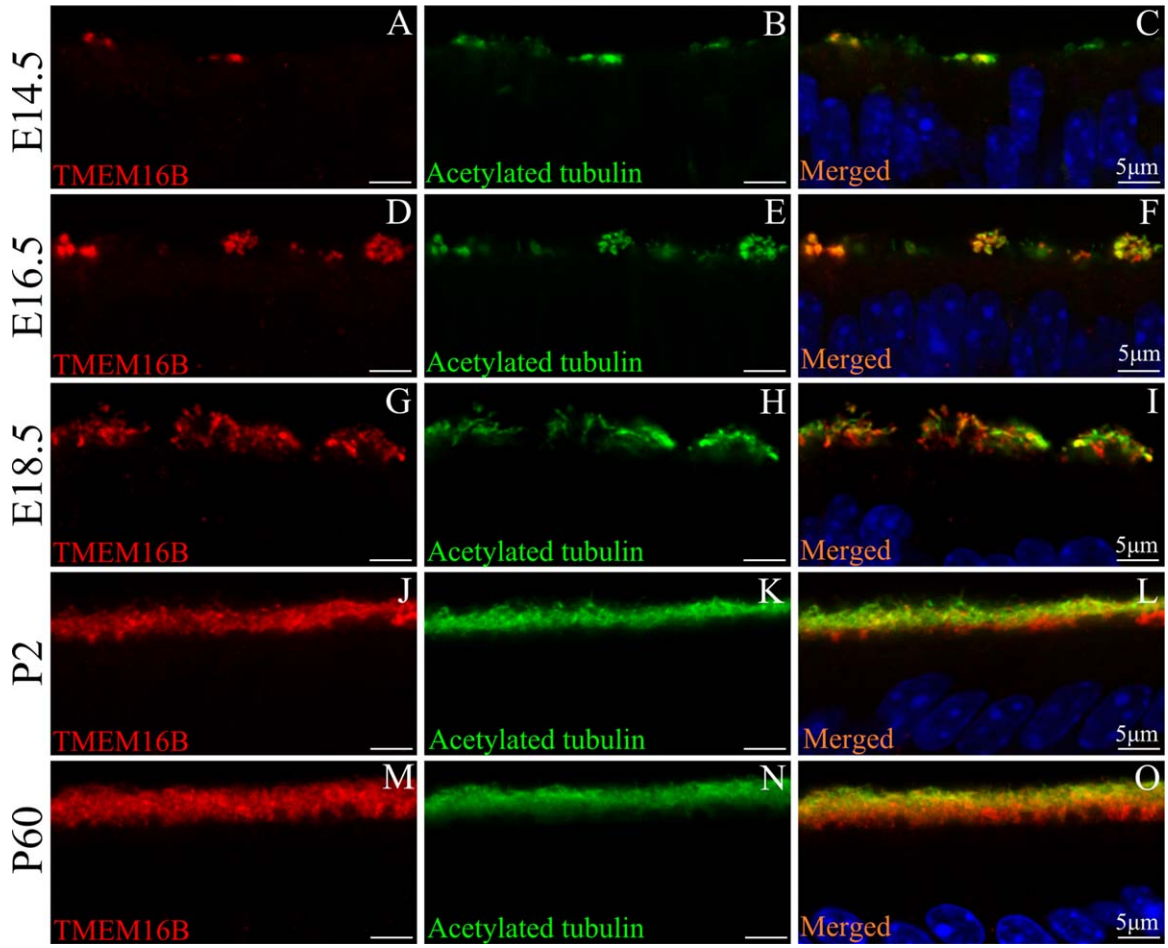

Figure 3 Expression of TMEM16B and acetylated tubulin in the olfactory epithelium of wild-type mice. Confocal images of coronal sections of the olfactory epithelium at E14.5, E16.5, E18.5, P2 and P60. A-L: both TMEM16B and acetylated tubulin, a marker for cilia, were expressed at E14.5 and during the subsequent days of development. In postnatal mice cilia form a layer at the surface of the olfactory epithelium (K,N). TMEM16B was expressed in this layer along with acetylated tubulin (J-O). At P2 (J-L) and P60 (M-O) TMEM16B was mainly expressed in the proximal part of the cilia, and also below the cilia, presumably in the dendritic knobs of olfactory sensory neurons [see also Fig. 2(O,P)]. Cell nuclei were stained by DAPI. Scale bars = 5µm. [Color figure can be viewed in the online issue, which is available at wileyonlinelibrary.com.]

mice, the dorsal region of the olfactory epithelium expressed TMEM16B but not TMEM16A [Fig. 4(B,B1,C,C1)]. The expression of TMEM16B was uniform across the entire olfactory epithelium, whereas no TMEM16B immunoreactivity was detected in the respiratory epithelium.

Figure 5 shows high magnification images for double immunostaining of TMEM16A and TMEM16B from E14.5 to P60 in a region of the olfactory epithelium near the transition zone with the respiratory epithelium. From E14.5 to P60, both TMEM16A and TMEM16B were expressed at the apical surface of the olfactory epithelium but, importantly, the staining for these proteins did not overlap.

Similar results were obtained from double immunolabeling of ACIII with TMEM16A in a region of the olfactory epithelium near the transition zone with the respiratory epithelium at different stages of development. At E14.5 both ACIII and TMEM16A were expressed at the apical surface of the olfactory epithelium, with ACIII present in clusters and TMEM16A expressed in a prominent layer just below the ACIII clusters [Fig. 6(A–C)]. At subsequent days of development the two antibodies stained distinct layers close to the apical surface, with ACIII expressed in a layer directly above the TMEM16A layer: no overlap between them was detectable [Fig. 6(D–O)].

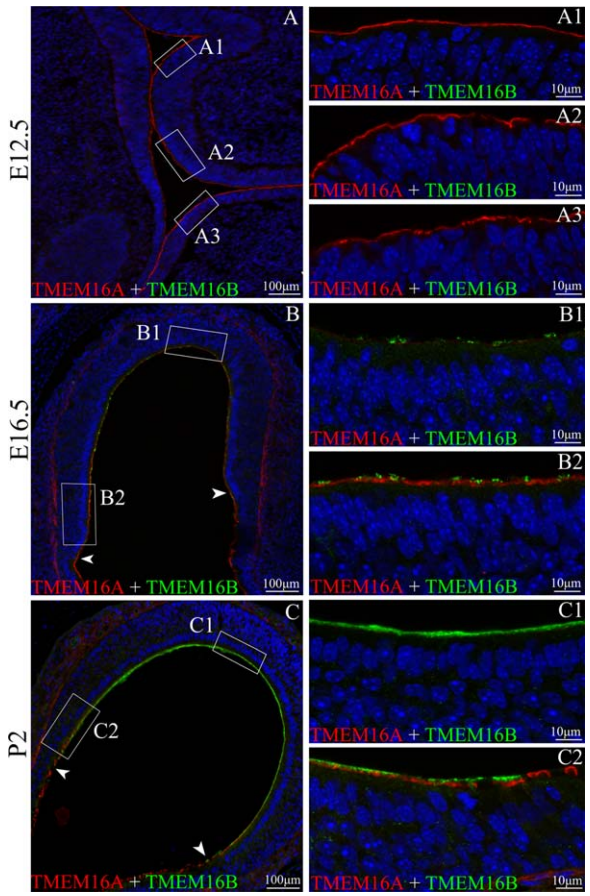

Figure 4 Expression of TMEM16A and TMEM16B in the developing olfactory epithelium of wild-type mice. Confocal images of coronal sections of the olfactory epithelium at E12.5, E16.5, and P2. A: at E12.5, TMEM16A (goat anti-TMEM16A) was expressed at the surface of the olfactory epithelium (A1,A2) as well as at the surface of the respiratory epithelium (A3), whereas no TMEM16B signal was detected. Higher magnification images taken from the boxed areas are shown in A1, A2 and A3. B: at E16.5, TMEM16A expression was not uniform and immunoreactivity was present in the regions toward the respiratory epithelium and at the surface of the respiratory epithelium itself. Arrowheads indicate the transition from olfactory to respiratory epithelium. Higher magnification images taken from the boxed areas are shown in B1 and B2. No signal for TMEM16A was present in B1, TMEM16B was expressed in clusters. C: in neonatal mice TMEM16A expression was even more restricted toward the respiratory epithelium and at the surface of the respiratory epithelium itself. TMEM16B immunoreactivity increased at the apical surface of the olfactory epithelium, but was not present in the respiratory epithelium. Higher magnification images taken from the boxed areas are shown in C1 and C2. No signal for TMEM16A was present in C1. Cell nuclei were stained by DAPI. Scale bars: A-C = 100μm; A1-A3, B1-B2, C1-C2 = 10μm. [Color figure can be viewed in the online issue, which is available at wileyonlinelibrary.com.]

Similar results were obtained with acetylated tubulin (data not shown). At every stage of embryonic development, TMEM16A and acetylated tubulin immunoreactivity never overlapped.

Taken together, these results clearly show that TMEM16A did not coexpress with TMEM16B, but was expressed in a prominent layer below TMEM16B. Moreover, at any stage of development, TMEM16A was not expressed in the cilia of olfactory sensory neurons.

To further investigate whether TMEM16A was expressed in olfactory sensory neurons, we analyzed its expression during development in OMP–GFP mice [Fig. 7(A–H)]. High magnification images [Fig. 7(E–H)] showed a strong-layered immunopositive signal of TMEM16A at the apical surface of the olfactory epithelium, which was interrupted by the dendritic swellings (knobs) of mature neurons, clearly demonstrating that TMEM16A was not expressed in mature neurons of OMP–GFP mice.

Furthermore, to establish whether TMEM16A was expressed in immature olfactory sensory neurons, we costained the olfactory epithelium of wild-type mice at E12.5 with β-tubulin III. As illustrated in Figure 7(I–K), TMEM16A did not colocalize with β-tubulin III, showing that TMEM16A was not expressed in immature olfactory sensory. As an additional control of the possible expression of TMEM16A in mature olfactory sensory neurons, we used neonatal wild-type mice instead of OMP–GFP mice (which express GFP instead of OMP). In wild-type mice, costaining of TMEM16A and OMP further confirmed the absence of expression of TMEM16A in mature neurons [Fig. 7(L–N)].

Thus, TMEM16A was not expressed in olfactory sensory neurons of wild-type or OMP–GFP mice during embryonic development and after birth.

As the apical surface of the olfactory epithelium is covered both by cilia of olfactory sensory neurons and by microvilli of supporting cells, we examined the cellular localization of TMEM16A by costaining the olfactory epithelium with an antibody against ezrin, a marker for microvilli (see Fig. 8). At E16.5, TMEM16A and ezrin immunopositive signals largely overlapped [Fig. 8(A–C)]. At E18.5 and in postnatal mice, TMEM16A and ezrin immunoreactivity partially overlapped, with TMEM16A immunoreactivity restricted only to the lower portion of ezrin immunoreactivity [Fig. 8(D–L)]. This clearly shows that TMEM16A was mainly localized to the proximal part of microvilli of supporting cells and to the apical part of supporting cells. As an additional control for the expression of TMEM16B, we also double-labeled the olfactory epithelium with TMEM16B and ezrin

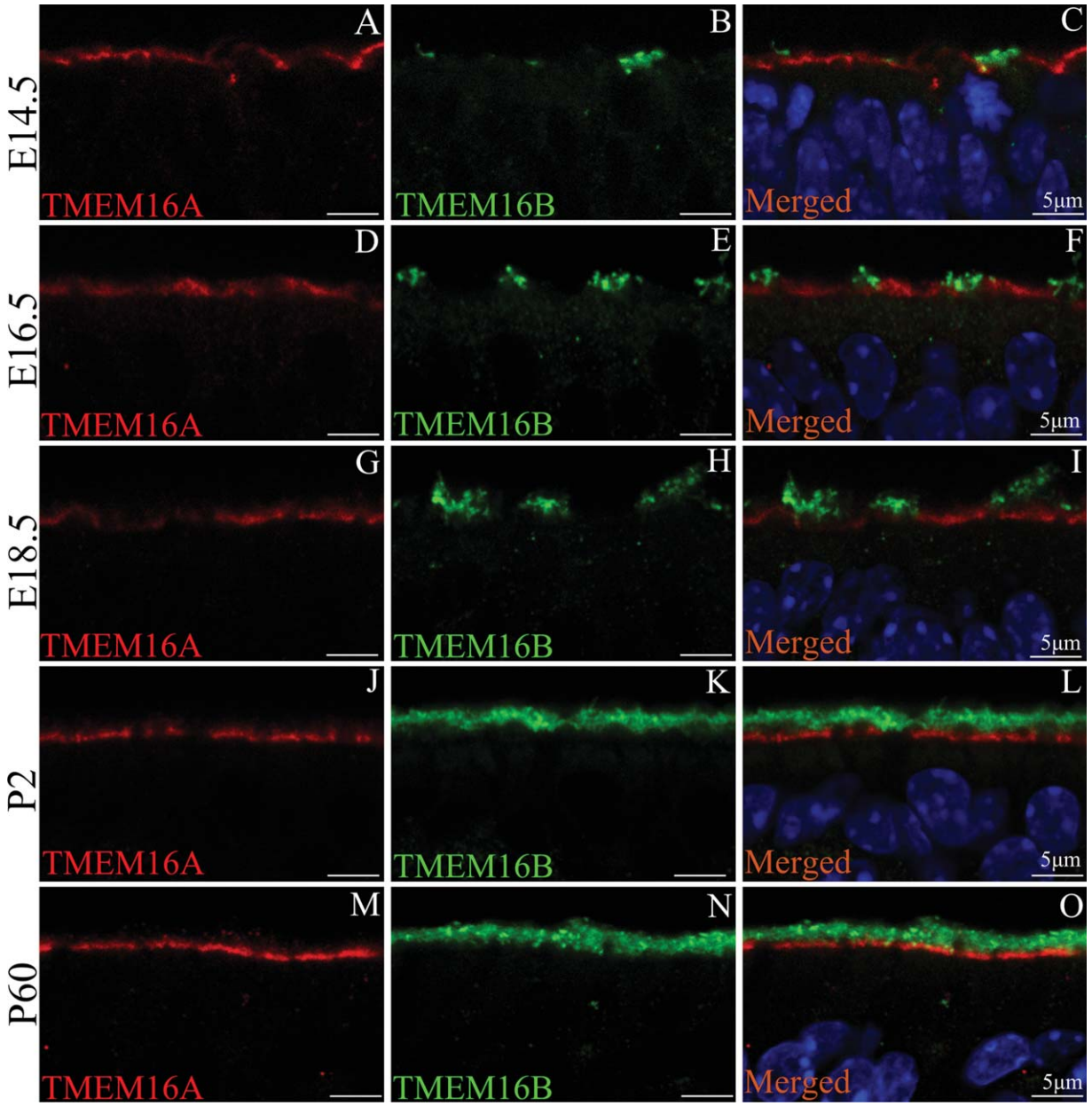

Figure 5 Expression of TMEM16A and TMEM16B in a region of the olfactory epithelium near the transition zone with the respiratory epithelium of wild-type mice. Confocal images of coronal sections of the olfactory epithelium at E14.5, E16.5, E18.5, P2 and P60. A-L: at each stage of development, TMEM16A (goat anti-TMEM16A) did not colocalize with TMEM16B. At P2 and P60, TMEM16A was expressed in a prominent layer just below TMEM16B (J-O). Cell nuclei were stained by DAPI. Scale bars = 5µm. [Color figure can be viewed in the online issue, which is available at wileyonlinelibrary.com.]

(see Fig. 9). At E16.5 and E18.5, ezrin was expressed in a layer below TMEM16B. At P2 and P60 mice, some overlapping was observed [Fig. 9(I,L)]. However, we argue that the overlapping is likely to originate from the partial superimposition of cilia (expressing TMEM16B) and microvilli (expressing ezrin), rather than from the coexpression of the two proteins. Indeed, schematic drawings of the apical surface of the olfactory epithelium based on electron micrograph at different developmental stages, show that cilia of olfactory sensory neurons and microvilli of supporting cells do not superimpose in embryos [Fig. 9(M), based on Fig. 29c from Cuschieri and Bannister, 1975b], while both cilia and microvilli

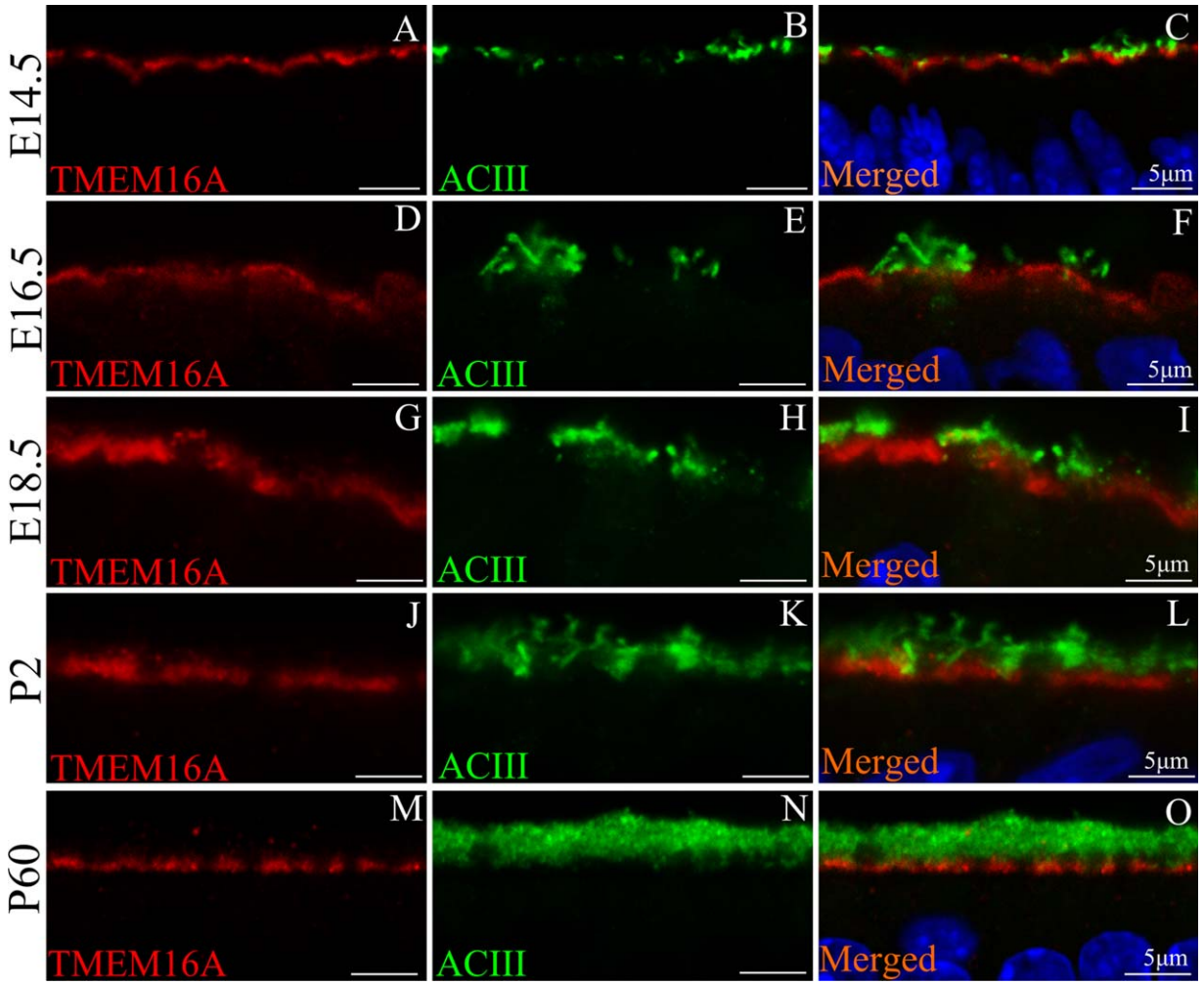

Figure 6 Expression of TMEM16A and ACIII in a region of the olfactory epithelium near the transition zone with the respiratory epithelium of wild-type mice. Confocal images of coronal sections of the olfactory epithelium at E14.5, E16.5, E18.5, P2 and P60. A-O: TMEM16A (goat anti-TMEM16A) expression did not overlap with ACIII and was expressed below ACIII. Cell nuclei were stained by DAPI. Scale bars = 5µm. [Color figure can be viewed in the online issue, which is available at wileyonlinelibrary.com.]

elongate during development and partially superimpose in postnatal mice [Fig. 9(N), based on Fig. 1 from Menco, 1995].

These results show that TMEM16A was not expressed in olfactory sensory neurons, did not colocalize with TMEM16B, and it was mainly localized to the proximal part of microvilli of supporting cells and to the apical part of supporting cells.

DISCUSSION

In this study, we have obtained for the first time immunohistochemistry data showing the temporal and spatial expression in the olfactory epithelium of the calcium-activated chloride channels TMEM16A and TMEM16B during mouse embryonic development. TMEM16A was already expressed at E12.5 at the apical surface of the olfactory epithelium but from E16.5 onward became restricted to a region near the respiratory epithelium. TMEM16B was expressed at E14.5 and its expression increased with development. Moreover, we showed that these two proteins never colocalized. TMEM16B localized to the cilia of mature olfactory sensory neurons, suggesting a role for this anion channel in olfactory transduction. In contrast, TMEM16A was not expressed in olfactory sensory neurons, but was found in microvilli of supporting cells and at the apical part of supporting cells, consistent with a role in the maintenance of ionic balance in the mucus layer.

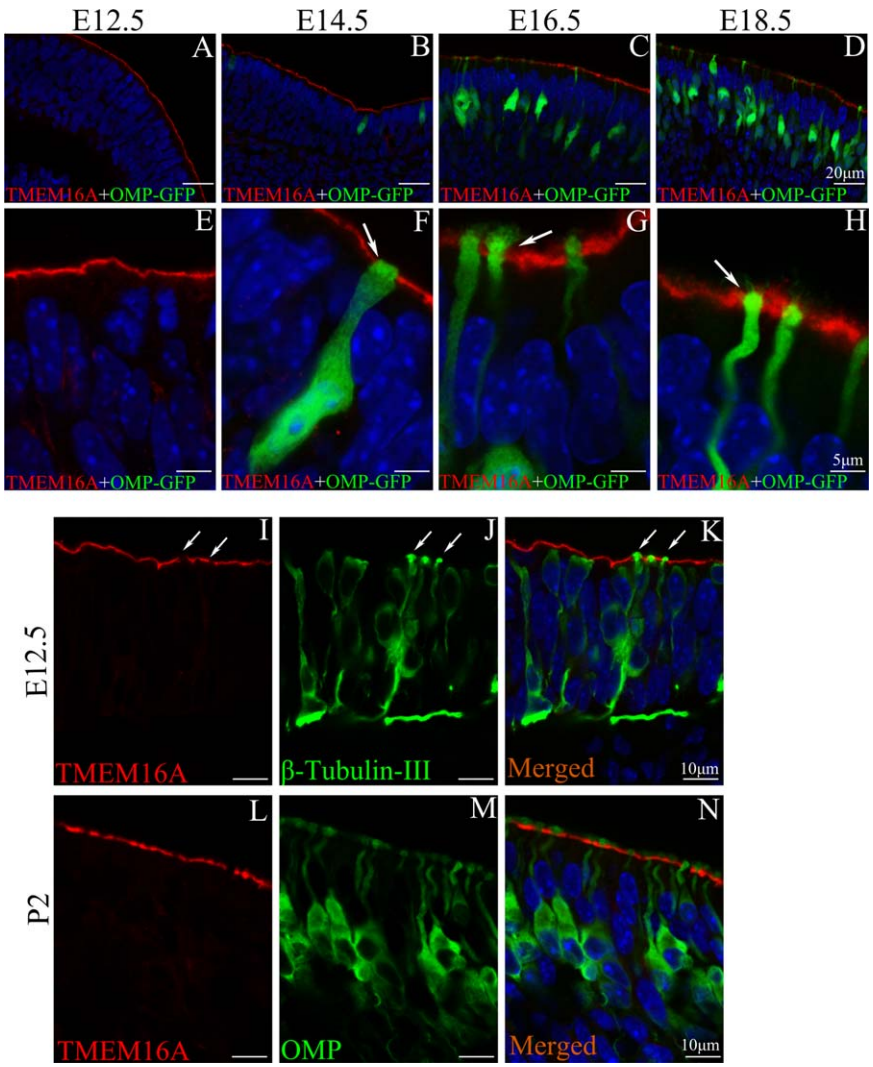

Figure 7 Expression of TMEM16A in a region of the olfactory epithelium near the transition zone with the respiratory epithelium of OMP-GFP or wild-type mice. A-H: confocal images of coronal sections of the olfactory epithelium of OMP-GFP mice at E12.5, E14.5, E16.5 and E18.5. In OMP-GFP mice, as in Figures (1 and 2), mature olfactory sensory neurons express GFP instead of OMP, and mature neurons are denoted as OMP-GFP. TMEM16A was expressed at E12.5 and subsequent days (rabbit anti-TMEM16A). E-H: higher magnification images showing the expression of TMEM16A at the apical part of the olfactory epithelium. TMEM16A was not expressed in mature olfactory sensory neurons of OMP-GFP mice. I-N: confocal images of coronal sections of the olfactory epithelium of wild-type mice at E12.5 and P2. At E12.5 the olfactory epithelium is devoid of mature neurons [see Fig. 1(A–C)]. Developing neurons expressing β-tubulin III (J) did not show TMEM16A immunoreactivity (I-K, goat anti-TMEM16A). Indeed, dendritic knobs (indicated by arrows) of developing neurons did not express TMEM16A. In neonatal wild-type mice, most neurons are mature and express OMP (M). TMEM16A did not colocalize with OMP in wild-type mice (L-N, rabbit anti-TMEM16A). Cell nuclei were stained by DAPI. Scale bars: A-D = 20μm; E-H = 5μm; I-N = 10μm. [Color figure can be viewed in the online issue, which is available at wileyonlinelibrary.com.]

TMEM16B and Olfactory Transduction

As noted, this is the first report investigating the expression of TMEM16B in the olfactory epithelium during embryonic development. Previous studies only reported the expression of TMEM16B in the olfactory epithelium in adult mice and are in agreement with our results.

During mouse embryonic development, TMEM16B was not expressed at E12.5, but was present at E14.5

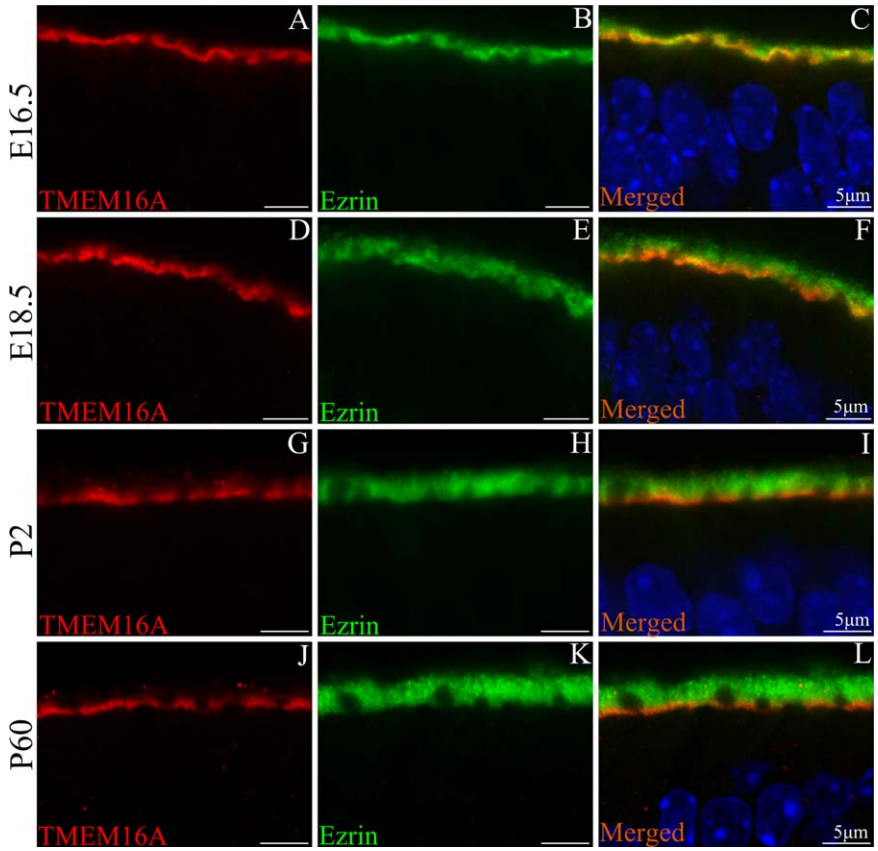

Figure 8 Expression of TMEM16A and ezrin in a region of the olfactory epithelium near the transition zone with the respiratory epithelium of wild-type mice. Confocal images of coronal sections of the olfactory epithelium at E16.5, E18.5, P2 and P60. A-L: coimmunostaining for TMEM16A (rabbit anti-TMEM16A) and the microvilli marker ezrin. At E16.5, immunoreactivity for TMEM16A and ezrin largely overlapped at the surface of the olfactory epithelium (A-C). At E18.5, P2 and P60, TMEM16A was mainly localized to the proximal part of the microvilli and to the apical part of supporting cells (D-L). Cell nuclei were stained by DAPI. Scale bars = 5μm. [Color figure can be viewed in the online issue, which is available at wileyonlinelibrary.com.]

in mature olfactory sensory neurons. TMEM16B immunoreactivity increased in the following days both because the number of mature neurons increased and the cilia elongated with development. Indeed, it has been reported that at E14.5 cilia are short (∼1 to 2 μm) and with development elongate reaching a length of up to 60 μm before birth (Noda and Harda, 1981; Schwarzenbacher et al., 2005; McEwen et al., 2008). From E16.5 onwards, acetylated tubulin immunoreactivity clearly indicated that several cilia protruded from dendritic knobs and that their length increased with development. TMEM16B immunoreactivity largely overlapped with acetylated tubulin immunoreactivity, indicating that TMEM16B expression was correlated with ciliary growth (Fig. 3). Moreover, TMEM16B was also seen in the dendritic knobs of some mature olfactory sensory neurons (Fig. 2). During development and in postnatal mice, we did not find any immunoreactivity for TMEM16B in the respiratory epithelium (Fig. 4) indicating that TMEM16B expression was restricted to the olfactory epithelium. The subcellular expression of TMEM16B, restricted to the cilia of mature olfactory sensory neurons is consistent with a role in olfactory transduction.

At which age can embryonic mice detect odorants? Lam and Mombaerts (2013) showed that at E16.5, (but not at E15.5 or E14.5) olfactory sensory neurons expressing the odorant receptor genes S1 or MOR23 responded to the corresponding odor ligands. There is also evidence from behavioral studies for prenatal olfaction and learning. Embryos receive odorant information from the amniotic fluid, which fills their nasal cavity. When one of two odorants, iso-amyl acetate or iso-valeric acid, was introduced into the nasal

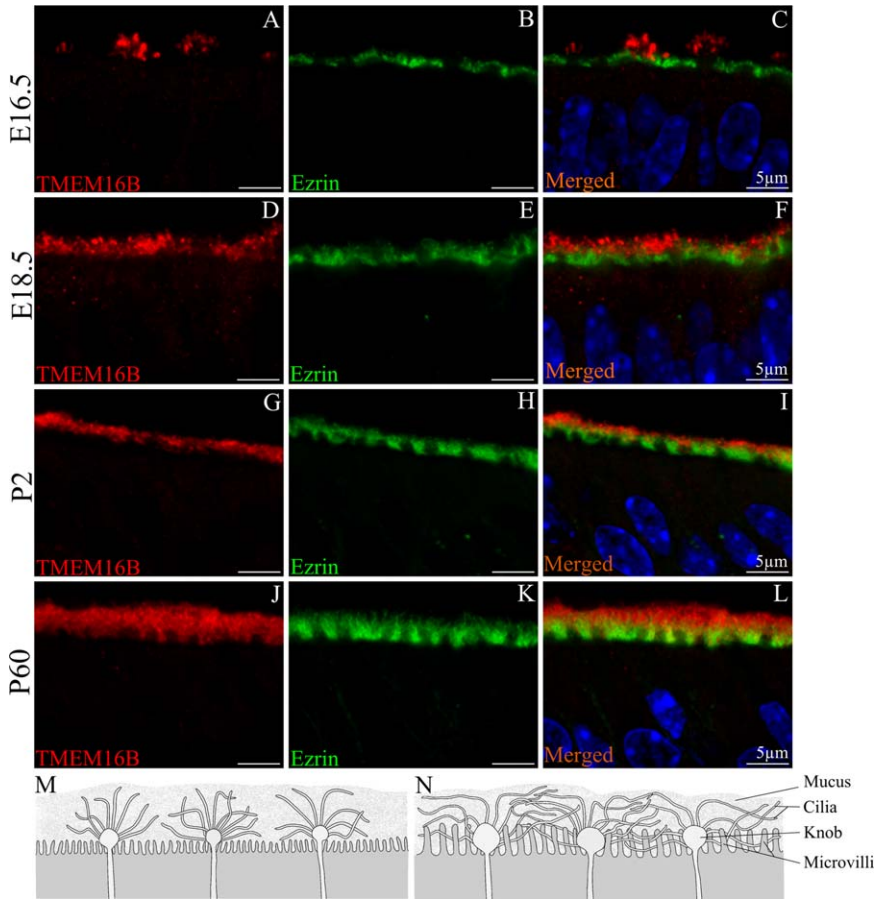

Figure 9 Expression of TMEM16B and ezrin in a region of the olfactory epithelium near the transition zone with the respiratory epithelium of wild-type mice. Confocal images of coronal sections of the olfactory epithelium at E16.5, E18.5, P2 and P60. A-L: coimmunostaining for TMEM16B and the microvilli marker ezrin. Ezrin was expressed in a layer below TMEM16B (A-L). At E16.5 and E18.5, immunoreactivity for TMEM16B and ezrin did not overlap, while at P2 and P60 some overlapping was observed (I,L). Cell nuclei were stained by DAPI. Scale bars = 5μm. M-N: schematic drawings of the apical surface of the olfactory epithelium showing that cilia of olfactory sensory neurons and microvilli of supporting cells do not superimpose in embryos (M, drawing based on Fig. 29c from Cuschieri and Bannister, 1975b), while both cilia and microvilli elongate during development and partially superimpose in postnatal mice (N, drawing based on Fig. 1 from Menco, 1995). [Color figure can be viewed in the online issue, which is available at wileyonlinelibrary.com.]

cavity of mouse embryos, the animals responded with different behaviors according to which odorant was delivered, showing that the embryos discriminated between the two odorants (Coppola and Millar, 1997). Moreover, neonatal mice preferentially suckled on the nipple of lactating female. They also suckled on the nipple of non-lactating females only when the nipple was coated with amniotic fluid (Al Aïn et al., 2012; Patris et al., 2013). Logan et al. (2012) altered the amniotic fluid by changing the diet of the pregnant mice introducing garlic oil or vanillin to the drinking water (Logan et al., 2012). The authors found that neonatal mice preferred to suckle from the nipple with the same odor they experienced as embryos. These studies indicate that embryonic mice have olfactory experiences that are important for feeding behaviors after birth.

Tmem16A: Proliferation and Secretory Processes

Gritli-Linde et al. (2009) first analyzed the expression patterns of several members of the *Tmem16* gene family (with the exception of *Tmem16b*) during murine cephalic development. At E12.5, the olfactory and the respiratory epithelia showed high *Tmem16a* expression, which greatly decreased after E18.5.

Our data show that at E12.5 the expression of TMEM16A was uniform at the apical surface of both the olfactory and the respiratory epithelium. However, at E16.5, TMEM16A immunoreactivity decreased in the dorsal area of the olfactory epithelium and was present only in areas of the olfactory epithelium near the transition zone with the respiratory epithelium. At E18.5 and in postnatal mice, TMEM16A immunoreactivity was even more restricted toward the respiratory epithelium. The decreased expression of TMEM16A during embryonic development is in agreement with previous *in situ* hybridization data (Gritli-Linde et al., 2009). In addition, we showed that, during embryonic development and in postnatal mice, TMEM16A was not expressed in olfactory sensory neurons but was expressed at the apical part of supporting cells. Indeed, TMEM16A and ezrin (a marker for microvilli) largely colocalized at the apical surface of the olfactory epithelium at E16.5. Ezrin immunoreactivity increased in the following days because microvilli elongated with development (Menco and Farbman, 1985). From E18.5 to postnatal age, we further showed that TMEM16A was mainly localized to the proximal part of microvilli of supporting cells and to the apical part of supporting cells.

The dynamic expression of TMEM16A during embryonic development raises interesting questions about its physiological role. TMEM16A has been shown to be involved in various physiological processes, including cell proliferation. The expression of TMEM16A increased in some cancerous and proliferating cells (West et al., 2004; Carles et al., 2006, Carneiro et al., 2008; Ayoub et al., 2010) and TMEM16A was shown to be involved in cell migration (Jacobsen et al., 2013). Moreover, blockers of calcium-activated chloride channels affected the mitotic process, and cell proliferation was restricted in TMEM16A knockout mice (Stanich et al., 2011). In the developing olfactory epithelium, mitotic cells are abundant at the apical surface at E12.5 (Cuschieri and Bannister, 1975a; Taniguchi and Taniguchi, 2008), and the majority of mitoses occur in the apical layer up to about E14, whereas later proliferative activity is transferred to the basal layer (Smart, 1971; Farbman, 1994). Based on these observations, we speculate that during earlier stages, until E14.5, the expression of TMEM16A at the apical surface may play a role in cell proliferation, although further studies are necessary to investigate this hypothesis.

Among other physiological roles, TMEM16A also controls fluid secretion in many epithelial cell types. Indeed, previous studies in knockout mice for TMEM16A have shown that calcium-dependent chloride secretion was eliminated in salivary acinar cells and in other epithelial cells (Ousingsawat et al., 2009; Rock et al., 2009; Ferrera et al., 2011; Huang et al. 2012a). Furthermore, in acinar cells TMEM16A regulates bicarbonate anion permeability (Jung et al., 2013), and in the airway epithelium it is strongly expressed with mucin secreting cells and modulates mucin secretion (Huang et al., 2012b). As supporting cells are known to be involved in the regulation of the extracellular ionic environment (Breipohl et al., 1974; Rafols and Getchell, 1983; Getchell, 1986; Menco and Morrison, 2003), it is likely that TMEM16A contributes to this process. The mucus layer at the surface of the olfactory epithelium is critical for olfaction, as odorant molecules dissolve in the mucus before reaching the cilia and the ion concentrations determine the electrical response. Supporting cells express the amiloride-sensitive sodium channels (Menco et al., 1998), members of the aquaporin family (Ablimit at el., 2006, 2008; Merigo et al., 2011), and the cystic fibrosis transmembrane conductance regulator (Grubb et al., 2007; Merigo et al., 2011). TMEM16A is likely to act in concert with these ion and water channels to regulate water and ionic balance in the mucus.

CONCLUSIONS

Our data provide the first immunohistochemistry study of the expression of the calcium-activated chloride channels TMEM16A and TMEM16B in the mouse olfactory epithelium during embryonic development. Both proteins begin developing in embryos and remain expressed in adult mice. The different pattern of distribution of TMEM16B in the cilia of mature olfactory sensory neurons and of TMEM16A at the apical part of supporting cells, indicate that TMEM16A is likely to play a role in the regulation of the extracellular ionic environment in the mucus, while TMEM16B is likely to be involved in olfactory transduction. What precise roles these proteins play in the developing and in the adult olfactory epithelium still need to be established, but this is certainly an exciting area for future research.

The authors thank Dr. Peter Mombaerts (Max Planck Institute of Biophysics, Frankfurt, Germany) for providing OMP-GFP mice; Dr. Sidney Simon (Duke University, Durham, USA) and Dr. Simone Pifferi for constructive discussions and comments on the manuscript; all members of the laboratory for discussions. They also acknowledge the help of Elettra Grdina, Angela Morriello and Angel Pascual Camerota for their support in mice breeding at the SISSA animal house facility.

REFERENCES

Ablimit A, Aoki T, Matsuzaki T, Suzuki T, Hagiwara H, Takami S, Takata K. 2008. Immunolocalization of water channel aquaporins in the vomeronasal organ of the rat: Expression of AQP4 in neuronal sensory cells. Chem Senses 33:481–488.

Ablimit A, Matsuzaki T, Tajika Y, Aoki T, Hagiwara H, Takata K. 2006. Immunolocalization of water channel aquaporins in the nasal olfactory mucosa. Arch Histol Cytol 69:1–12.

Al Aïn S, Belin L, Schaal B, Patris B. 2013. How does a newly born mouse get to the nipple? odor substrates eliciting first nipple grasping and sucking responses. Dev Psychobiol 55:888–901.

Ayoub C, Wasylyk C, Li Y, Thomas E, Marisa L, Robé A, Roux M, et al. 2010. ANO1 amplification and expression in HNSCC with a high propensity for future distant metastasis and its functions in HNSCC cell lines. Br J Cancer 103:715–726.

Baker H, Grillo M, Margolis FL. 1989. Biochemical and immunocytochemical characterization of olfactory marker protein in the rodent central nervous system. J Comp Neurol 285:246–261.

Billig GM, Pál B, Fidzinski P, Jentsch TJ. 2011. Ca2+-activated Cl− currents are dispensable for olfaction. Nat Neurosci 14:763–769.

Boccaccio A, Lagostena L, Hagen V, Menini A. 2006. Fast adaptation in mouse olfactory sensory neurons does not require the activity of phosphodiesterase. J Gen Physiol 128:171–184.

Boccaccio A, Menini A. 2007. Temporal development of cyclic nucleotide-gated and Ca2+ -activated Cl- currents in isolated mouse olfactory sensory neurons. J Neurophysiol 98:153–60.

Breipohl W, Laugwitz HJ, Bornfeld N. 1974. Topological relations between the dendrites of olfactory sensory cells and sustentacular cells in different vertebrates. An ultrastructural study. J Anat 117:89–94.

Caputo A, Caci E, Ferrera L, Pedemonte N, Barsanti C, Sondo E, Pfeffer U, et al. 2008. TMEM16A, a membrane protein associated with calcium-dependent chloride channel activity. Science 322:590–594.

Carles A, Millon R, Cromer A, Ganguli G, Lemaire F, Young J, Wasylyk C, et al. 2006. Head and neck squamous cell carcinoma transcriptome analysis by comprehensive validated differential display. Oncogene 25:1821–1831.

Carneiro A, Isinger A, Karlsson A, Johansson J, Jönsson G, Bendahl P-O, Falkenback D, et al. 2008. Prognostic impact of array-based genomic profiles in esophageal squamous cell cancer. BMC Cancer 8:98.

Chuang J-Z, Chou S-Y, Sung C-H. 2010. Chloride intracellular channel 4 is critical for the epithelial morphogenesis of RPE cells and retinal attachment. Mol Biol Cell 21: 3017–3028.

Col JAD, Matsuo T, Storm DR, Rodriguez I. 2007a. Adenylyl cyclase-dependent axonal targeting in the olfactory system. Development 134:2481–2489.

Coppola DM, Millar LC. 1997. Olfaction in utero: Behavioral studies of the mouse fetus. Behav Process 39:53–68.

Cuschieri A, Bannister LH. 1975a. The development of the olfactory mucosa in the mouse: Light microscopy. J Anat 119:277–286.

Cuschieri A, Bannister LH. 1975b. The development of the olfactory mucosa in the mouse: Electron Microscopy. J Anat 119:471–498.

Cygnar KD, Zhao H. 2009. Phosphodiesterase 1C is dispensable for rapid response termination of olfactory sensory neurons. Nat Neurosci 12:454–462.

Dauner K, Lissmann J, Jeridi S, Frings S, Möhrlen F. 2012. Expression patterns of anoctamin 1 and anoctamin 2 chloride channels in the mammalian nose. Cell Tissue Res 347:327–341.

Davis AJ, Shi J, Pritchard HAT, Chadha PS, Leblanc N, Vasilikostas G, Yao Z, et al. 2013. Potent vasorelaxant activity of the TMEM16A inhibitor T16A(inh) -A01. Br J Pharmacol 168:773–784.

Dibattista M, Amjad A, Maurya DK, Sagheddu C, Montani G, Tirindelli R, Menini A. 2012. Calcium-activated chloride channels in the apical region of mouse vomeronasal sensory neurons. J Gen Physiol 140:3–15.

Eckler MJ, McKenna WL, Taghvaei S, McConnell SK, Chen B. 2011. Fezf1 and Fezf2 are required for olfactory development and sensory neuron identity. J Comp Neurol 519:1829–1846.

Elsaesser R, Montani G, Tirindelli R, Paysan J. 2005. Phosphatidyl-inositide signalling proteins in a novel class of sensory cells in the mammalian olfactory epithelium. Eur J Neurosci 21:2692–2700.

Farbman AI. 1994. Developmental biology of olfactory sensory neurons. Semin Cell Biol 5:3–10.

Ferrera L, Zegarra-Moran O, Galietta LJV. 2011. Ca2+-activated Cl- channels. Compr Physiol 1:2155–2174.

Frings S. 2009. Primary processes in sensory cells: Current advances. J Comp Physiol A Neuroethol Sens Neural Behav Physiol 195:1–19.

Frings S. 2010. Chloride-Based Signal Amplification in Olfactory Sensory Neurons. In: Alvarez-Leefmans FJ, Delpire E, editors. Physiology and Pathology of Chloride Transporters and Channels in the Nervous System. San Diego: Academic Press, pp 413–424.

Furmanski O, Gajavelli S, Lee JW, Collado ME, Jergova S, Sagen J. 2009. Combined extrinsic and intrinsic manipulations exert complementary neuronal enrichment in embryonic rat neural precursor cultures: An in vitro and in vivo analysis. J Comp Neurol 515:56–71.

Getchell TV. 1986. Functional properties of vertebrate olfactory receptor neurons. Physiol Rev 66:772–818.

Gomez-Pinilla PJ, Gibbons SJ, Bardsley MR, Lorincz A, Pozo MJ, Pasricha PJ, Van de Rijn M, et al. 2009. Ano1 is a selective marker of interstitial cells of Cajal in the human and mouse gastrointestinal tract. Am J Physiol Gastrointest Liver Physiol 296:G1370–G1381.

Graziadei GA, Stanley RS, Graziadei PP. 1980. The olfactory marker protein in the olfactory system of the mouse during development. Neuroscience 5:1239–1252.

Gritli-Linde A, Vaziri Sani F, Rock JR, Hallberg K, Iribarne D, Harfe BD, Linde A. 2009. Expression patterns of the Tmem16 gene family during cephalic development in the mouse. Gene Exp Patterns 9:178–191.

Grubb BR, Rogers TD, Kulaga HM, Burns KA, Wonsetler RL, Reed RR, Ostrowski LE. 2007. Olfactory epithelia exhibit progressive functional and morphological defects in CF mice. Am J Physiol Cell Physiol 293:C574–583.

Hansen A, Finger TE. 2008. Is TrpM5 a reliable marker for chemosensory cells? Multiple types of microvillous cells in the main olfactory epithelium of mice. BMC Neurosci 9:115.

Hengl T, Kaneko H, Dauner K, Vocke K, Frings S, Möhrlen F. 2010. Molecular components of signal amplification in olfactory sensory cilia. Proc Natl Acad Sci U S A 107:6052–6057

Huang F, Wong X, Jan LY. 2012a. International Union of Basic and Clinical Pharmacology. LXXXV: Calcium-activated chloride channels. Pharmacol Rev 64:1–15.

Huang F, Zhang H, Wu M, Yang H, Kudo M, Peters CJ, Woodruff PG, et al. 2012b. Calcium-activated chloride channel TMEM16A modulates mucin secretion and airway smooth muscle contraction. Proc Natl Acad Sci U S A 109:16354–16359.

Jacobsen KS, Zeeberg K, Sauter DR, Poulsen KA, Hoffmann EK, Schwab A. 2013. The role of TMEM16A (ANO1) and TMEM16F (ANO6) in cell migration. Pflugers Arch 465;1753–1762.

Jung J, Nam JH, Park HW, Oh U, Yoon J-H, Lee MG. 2013. Dynamic modulation of ANO1/TMEM16A HCO3- permeability by Ca2+/calmodulin. Proc Natl Acad Sci U S A 110:360–365.

Keller A, Margolis FL. 1975. Immunological studies of the rat olfactory marker protein. J Neurochem 24:1101–1106.

Kleene SJ. 1993. Origin of the chloride current in olfactory transduction. Neuron 11:123–132.

Kleene SJ. 1997. High-gain, low-noise amplification in olfactory transduction. Biophys J 73:1110–1117.

Kleene SJ. 2008. The electrochemical basis of odor transduction in vertebrate olfactory cilia. Chem Senses 33: 839–59.

Kleene SJ, Gesteland RC. 1991. Calcium-activated chloride conductance in frog olfactory cilia. J Neurosci 11:3624–3629.

Kleene SJ, Pun RY. 1996. Persistence of the olfactory receptor current in a wide variety of extracellular environments. J Neurophysiol 75:1386–1391.

Kurahashi T, Yau KW. 1993. Co-existence of cationic and chloride components in odorant-induced current of vertebrate olfactory receptor cells. Nature 363:71–74.

Lam RS, Mombaerts P. 2013. Odorant responsiveness of embryonic mouse olfactory sensory neurons expressing the odorant receptors S1 or MOR23. Eur J Neurosci 38: 2210–2217.

Lee VM, Pixley SK. 1994. Age and differentiation-related differences in neuron-specific tubulin immunostaining of olfactory sensory neurons. Brain Res Dev Brain Res 83: 209–215.

Lin W, Margolskee R, Donnert G, Hell SW, Restrepo D. 2007. Olfactory neurons expressing transient receptor potential channel M5 (TRPM5) are involved in sensing semiochemicals. Proc Natl Acad Sci U S A 104:2471–2476.

Logan DW, Brunet LJ, Webb WR, Cutforth T, Ngai J, Stowers L. 2012. Learned recognition of maternal signature odors mediates the first suckling episode in mice. Curr Biol 22:1998–2007.

Lowe G, Gold GH. 1993. Nonlinear amplification by calcium-dependent chloride channels in olfactory receptor cells. Nature 366:283–286.

Ma M. 2010. Multiple olfactory subsystems convey various sensory signals. In: Menini A, editor. The Neurobiology of Olfaction. Frontiers in Neuroscience. Boca Raton (FL): CRC Press, pp 225–241.

Marcucci F, Maier-Balough E, Zou D-J, Firestein S. 2011. Exuberant growth and synapse formation of olfactory sensory neuron axonal arborizations. J Comp Neurol 519: 3713–3726.

Martín-Ibáñez R, Crespo E, Urbán N, Sergent-Tanguy S, Herranz C, Jaumot M, Valiente M, et al. 2010. Ikaros-1 couples cell cycle arrest of late striatal precursors with neurogenesis of enkephalinergic neurons. J Comp Neurol 518:329–351.

Mayer U, Küller A, Daiber PC, Neudorf I, Warnken U, Schnölzer M, Frings S, et al. 2009. The proteome of rat olfactory sensory cilia. Proteomics 9:322–334.

McEwen DP, Jenkins PM, Martens JR. 2008. Olfactory cilia: Our direct neuronal connection to the external world. Curr Top Dev Biol 85:333–370.

Menco BP, Birrell GB, Fuller CM, Ezeh PI, Keeton DA, Benos DJ. 1998. Ultrastructural localization of amiloride-sensitive sodium channels and Na+,K(+)-ATPase in the rat's olfactory epithelial surface. Chem Senses 23:137–149.

Menco BP, Farbman AI. 1985. Genesis of cilia and microvilli of rat nasal epithelia during pre-natal development. II. Olfactory epithelium, a morphometric analysis. J Cell Sci 78:311–336.

Menco BP, Farbman AI. 1992. Ultrastructural evidence for multiple mucous domains in frog olfactory epithelium. Cell Tissue Res 270:47–56.

Menco BP. 1995. Freeze-fracture, deep-etch, and freeze-substitution studies of olfactory epithelia, with special emphasis on immunocytochemical variables. Microsc Res Tech 32:337–356.

Menco BP, Morrison EE. 2003. Morphology of the Mammalian Olfactory Epithelium. In: Doty RL, editor. Handbook of Olfaction and Gustation. New York: Marcel Dekker, Inc., pp 17–49.

Mendoza AS. 1993. Morphological studies on the rodent main and accessory olfactory systems: The regio olfactoria and vomeronasal organ. Ann Anat 175:425–446.

Merigo F, Mucignat-Caretta C, Cristofoletti M, Zancanaro C. 2011. Epithelial membrane transporters expression in the developing to adult mouse vomeronasal organ and olfactory mucosa. Dev Neurobiol 71:854–869.

Michalakis S, Reisert J, Geiger H, Wetzel C, Zong X, Bradley J, Spehr M, et al. 2006. Loss of CNGB1 protein leads to olfactory dysfunction and subciliary cyclic nucleotide-gated channel trapping. J Biol Chem 281: 35156–35166.

Miller AM, Treloar HB, Greer CA. 2010. Composition of the migratory mass during development of the olfactory nerve. J Comp Neurol 518:4825–4841.

Noda M, Harada Y. 1981. Development of olfactory epithelium in the mouse: Scanning electron microscopy. Biomed Res 2(suppl.): 449–454.

Nomura T, Takahashi S, Ushiki T. 2004. Cytoarchitecture of the normal rat olfactory epithelium: Light and scanning electron microscopic studies. Arch Histol Cytol 67: 159–170.

Ousingsawat J, Martins JR, Schreiber R, Rock JR, Harfe BD, Kunzelmann K. 2009. Loss of TMEM16A causes a defect in epithelial Ca2+-dependent chloride transport. J Biol Chem 284:28698–28703.

Patris B, Al Aïn S, Schaal B. 2013. Suckling odours in rats and mice: Biological substrates that guide newborns to the nipple. In: East ML, Dehnhard M, editors. Chemical signals in vertebrates 12. New York: Springer science and Business media, pp 77–85.

Pifferi S, Boccaccio A, Menini A. 2006. Cyclic nucleotide-gated ion channels in sensory transduction. FEBS Lett 580:2853–2859.

Pifferi S, Dibattista M, Menini A. 2009a. TMEM16B induces chloride currents activated by calcium in mammalian cells. Pflugers Arch 458:1023–1038.

Pifferi, S, Dibattista M, Sagheddu C, Boccaccio A, Al Qteishat A, Ghirardi F, Tirindelli R, et al. 2009b. Calcium-activated chloride currents in olfactory sensory neurons from mice lacking bestrophin-2. J Physiol 587: 4265–4279.

Pifferi S, Menini A, Kurahashi T. 2010. Signal transduction in vertebrate olfactory cilia. In: Menini A, editor. The Neurobiology of Olfaction. Frontiers in Neuroscience. Boca Raton (FL): CRC Press, pp 203–224.

Pifferi S, Cenedese V, Menini A. 2012. Anoctamin 2/TMEM16B: A calcium-activated chloride channel in olfactory transduction. Exp Physiol 97:193–199.

Piperno G, Fuller MT. 1985. Monoclonal antibodies specific for an acetylated form of alpha-tubulin recognize the antigen in cilia and flagella from a variety of organisms. J Cell Biol 101:2085–2094.

Potter SM, Zheng C, Koos DS, Feinstein P, Fraser SE, Mombaerts P. 2001. Structure and emergence of specific olfactory glomeruli in the mouse. J Neurosci 21:9713–9723.

Rafols JA, Getchell TV. 1983. Morphological relations between the receptor neurons, sustentacular cells and Schwann cells in the olfactory mucosa of the salamander. Anat Rec 206:87–101.

Rasche S, Toetter B, Adler J, Tschapek A, Doerner JF, Kurtenbach S, Hatt H, et al. 2010. Tmem16b is specifically expressed in the cilia of olfactory sensory neurons. Chem Senses 35:239–245.

Reisert J, Lai J, Yau K-W, Bradley J. 2005. Mechanism of the excitatory Cl- response in mouse olfactory receptor neurons. Neuron 45:553–561.

Reisert J, Zhao H. 2011. Perspectives on: Information and coding in mammalian sensory physiology: Response kinetics of olfactory receptor neurons and the implications in olfactory coding. J Gen Physiol 138:303–310.

Rochelle LG, Li DC, Ye H, Lee E, Talbot CR, Boucher RC. 2000. Distribution of ion transport mRNAs throughout murine nose and lung. Am J Physiol Lung Cell Mol Physiol 279:L14–24.

Rock JR, Futtner CR, Harfe BD. 2008. The transmembrane protein TMEM16A is required for normal development of the murine trachea. Dev Biol 321:141–149.

Rock JR, O'Neal WK, Gabriel SE, Randell SH, Harfe BD, Boucher RC, Grubb BR. 2009. Transmembrane protein 16A (TMEM16A) is a Ca2+-regulated Cl- secretory channel in mouse airways. J Biol Chem 284:14875–14880.

Rodriguez-Gil DJ, Greer CA. 2008. Wnt/Frizzled family members mediate olfactory sensory neuron axon extension. J Comp Neurol 511:301–317.

Roskams AJ, Cai X, Ronnett GV. 1998. Expression of neuron-specific beta-III tubulin during olfactory neurogenesis in the embryonic and adult rat. Neuroscience 83: 191–200.

Ross AJ, May-Simera H, Eichers ER, Kai M, Hill J, Jagger DJ, Leitch CC, et al. 2005. Disruption of Bardet-Biedl syndrome ciliary proteins perturbs planar cell polarity in vertebrates. Nat Genet 37:1135–1140.

Sagheddu C, Boccaccio A, Dibattista M, Montani G, Tirindelli R, Menini A. 2010. Calcium concentration jumps reveal dynamic ion selectivity of calcium-activated chloride currents in mouse olfactory sensory neurons and TMEM16b-transfected HEK 293T cells. J Physiol 588:4189–4204.

Schild D, Restrepo D. 1998. Transduction mechanisms in vertebrate olfactory receptor cells. Physiol Rev 78: 429–66.

Schroeder BC, Cheng T, Jan YN, Jan LY. 2008. Expression cloning of TMEM16A as a calcium-activated chloride channel subunit. Cell 134:1019–1029.

Schwarzenbacher K, Fleischer J, Breer H. 2005. Formation and maturation of olfactory cilia monitored by odorant receptor-specific antibodies. Histochem Cell Biol 123: 419–428.

Scudieri P, Sondo E, Ferrera L, Galietta LJ. 2011. The anoctamin family: TMEM16A and TMEM16B as calcium-activated chloride channels. Exp Pysiol 97: 177–183.

Smart IH. 1971. Location and orientation of mitotic figures in the developing mouse olfactory epithelium. J Anat 109:243–251.

Stanich JE, Gibbons SJ, Eisenman ST, Bardsley MR, Rock JR, Harfe BD, Ordog T, et al. 2011. Ano1 as a regulator of proliferation. Am J Physiol Gastrointest Liver Physiol 301:G1044–G1051.

Stephan AB, Shum EY, Hirsh S, Cygnar KD, Reisert J, Zhao H. 2009. ANO2 is the cilial calcium-activated chloride channel that may mediate olfactory amplification. Proc Natl Acad Sci U S A 106:11776–11781.

Sullivan SL, Bohm S, Ressler KJ, Horowitz LF, Buck LB. 1995. Target-independent pattern specification in the olfactory epithelium. Neuron 15:779–789.

Sun H, Xia Y, Paudel O, Yang X-R, Sham JSK. 2012. Chronic hypoxia-induced upregulation of Ca2+-activated Cl- channel in pulmonary arterial myocytes: A mechanism contributing to enhanced vasoreactivity. J Physiol 590:3507–3521.

Taniguchi K, Taniguchi K. 2008. Embryonic and postnatal differentiation of olfactory epithelium and vomeronasal organ in the Syrian hamster. J Vet Med Sci Jpn Soc Vet Sci 70:57–64.

Treloar HB, Miller AM, Ray A, Greer CA. 2010. Development of the Olfactory System. In: Menini A, editor. The Neurobiology of Olfaction. Frontiers in Neuroscience. Boca Raton (FL): CRC Press, pp 131–156.

Treloar HB, Uboha U, Jeromin A, Greer CA. 2005. Expression of the neuronal calcium sensor protein NCS-1 in the developing mouse olfactory pathway. J Comp Neurol 482:201–216.

Wei H, Lang M-F, Jiang X. 2013. Calretinin is expressed in the intermediate cells during olfactory receptor neuron development. Neurosci Lett 542:42–46.

West RB, Corless CL, Chen X, Rubin BP, Subramanian S, Montgomery K, et al. 2004. The novel marker, DOG1, is expressed ubiquitously in gastrointestinal stromal tumors irrespective of KIT or PDGFRA mutation status. Am J Pathol 165:107–113.

Wong ST, Trinh K, Hacker B, Chan GC, Lowe G, Gaggar A, Xia Z, et al. 2000. Disruption of the type III adenylyl cyclase gene leads to peripheral and behavioral anosmia in transgenic mice. Neuron 27:487–497.

Yang YD, Cho H, Koo JY, Tak MH, Cho Y, Shim W-S, Park SP, et al. 2008. TMEM16A confers receptor-activated calcium-dependent chloride conductance. Nature 455:1210–1215.

Yu T-T, McIntyre JC, Bose SC, Hardin D, Owen MC, McClintock TS. 2005. Differentially expressed transcripts from phenotypically identified olfactory sensory neurons. J Comp Neurol 483:251–262.

Zou D-J, Chesler AT, Pichon CEL, Kuznetsov A, Pei X, Hwang EL, Firestein S. 2007. Absence of adenylyl cyclase 3 perturbs peripheral olfactory projections in mice. J Neurosci 27:6675–6683.

4.3 Development of the olfactory epithelium and nasal glands in TMEM16A$^{-/-}$ and TMEM16A$^{+/+}$ mice.

Development of the olfactory epithelium and nasal glands in TMEM16A$^{-/-}$ and TMEM16A$^{+/+}$ mice

Devendra Kumar Maurya[1], Monica Marini[2], Nicoletta Pedemonte[2], Luis J.V. Galietta[2], Jason R Rock[3], Brian D Harfe[4], Anna Menini[1]

[1]Laboratory of Olfactory Transduction, SISSA, International School for Advanced Studies, Trieste, Italy

[2]Istituto Giannina Gaslini, Genova, Italy

[3]Department of Anatomy, UCSF School of Medicine, San Francisco, CA, USA

[4]Department of Molecular Genetics and Microbiology Genetics Institute, University of Florida, College of Medicine, Gainesville, FL, USA

Corresponding author

Anna Menini

SISSA

Via Bonomea 265

34136 Trieste

Italy

Tel +39-0403787706

menini@sissa.it

Abstract

TMEM16A/ANO1 is a calcium-activated chloride channel expressed in several types of epithelia and involved in various physiological processes, including proliferation and development. During mouse embryonic development, the expression of TMEM16A in the olfactory epithelium is dynamic. TMEM16A is expressed at the apical surface of the entire olfactory epithelium at embryonic day E12.5 while from E16.5 its expression is restricted to a region near the transition zone with the respiratory epithelium. To investigate whether TMEM16A plays a role in the development of the mouse olfactory epithelium, we obtained the first immunohistochemistry study comparing the morphological properties of the olfactory epithelium and nasal glands in TMEM16A$^{-/-}$ and TMEM16A$^{+/+}$ littermate mice. A comparison between the expression of the olfactory marker protein and adenylyl cyclase III shows that genetic ablation of TMEM16A did not affect the maturation of olfactory sensory neurons and their ciliary development. As TMEM16A is expressed at the apical part of supporting cells and in their microvilli, we used ezrin and cytokeratin 8 as markers, respectively, of microvilli and cell body of supporting cells, and found that morphology and development of supporting cells were not affected by the absence of TMEM16A. Moreover, we also established that the morphology of Bowman's glands, nasal septal glands and lateral nasal glands was not influenced by the genetic ablation of TMEM16A. We conclude that TMEM16A is not involved in the development of the mouse olfactory epithelium and nasal glands.

Keywords:

Olfaction, Supporting cell, TMEM16A, OSNs, Bowman's gland.

Introduction

TMEM16A/ANO1, a member of the family of transmembrane proteins with unknown function 16 [1, 2], has been recently identified as a calcium-activated chloride channel [3-5].

TMEM16A overexpression had been reported in several malignant tumors before TMEM16A was identified as a calcium-activated chloride channel. TMEM16A was known with different names, such as DOG1 (Discovered On Gastrointestinal stromal tumor protein 1 [6-7]), TAOS2 (Tumor Amplified and Overexpressed Sequence 2 [8]) overexpressed in oral squamous cell carcinomas, and ORAOV2 (Oral Cancer Overexpressed 2 [9]) overexpressed in oral and esophageal squamous cell carcinomas.

In addition to a potential role for TMEM16A in proliferation suggested by the overexpression of this channel in some tumors, TMEM16A has also been shown to be a regulator of cell proliferation in healthy cells. Indeed, Stanich et al [10] showed that TMEM16A regulates proliferation of interstitial cells of Cajal at the G_1/S transition of the cell cycle.

TMEM16A is expressed in several types of cells of secretory epithelia, smooth muscle cells [11-13] , as well as in cells of sensory systems: cochlea [14-15], retina [16-18], nociceptive neurons [19-20], vomeronasal sensory epithelium [16, 21, 22], and olfactory epithelium [16, 21, 23].

Rock et al [24] showed that TMEM16A is expressed in the epithelium of the developing trachea and in the embryonic tracheal muscle of mice. Furthermore, the same authors produced knockout mice for TMEM16A and showed that these mice have alterations in the formation of tracheal cartilage rings and die within one month, possibly because of tracheomalacia. In addition to providing a mouse model of tracheomalacia, these results point out to the possible role of TMEM16A in epithelial and smooth muscle cell organization in development [24]. Reduced transepithelial current and accumulation of mucus in the trachea of these mice indicate that TMEM16A also play a role in secretory processes [25, 26]. Additional alterations caused by TMEM16A loss of function include block of gastrointestinal peristalsis and reduced nociception [20, 27].

Another study [15], suggested that TMEM16A plays a developmental role in the mouse postnatal developing cochlea. Indeed, these authors showed that supporting cells in the greater epithelial ridge of the cochlea exhibited spontaneous calcium-dependent volume changes that were inhibited by anion channel blockers, indicating that volume changes may be related to the activity of calcium-activated chloride channels. Moreover, volume changes were correlated with the time course and location of TMEM16A expression in the cochlea,

suggesting that TMEM16A may be the pacemaker of spontaneous activities in postnatal developing cochlea.

Based on previous studies showing that TMEM16A plays a role in cell proliferation and in development [10, 15, 24] and on our previous observation that at embryonic day E12.5 TMEM16A immunoreactivity was present at the apical surface of the entire olfactory epithelium, whereas from E16.5 was restricted to a region near the transition zone with the respiratory epithelium [23], we investigated whether TMEM16A plays a role in the development of the olfactory epithelium. For this purpose, we used immunohistochemistry to identify morphological properties of the olfactory epithelium and nasal glands during mouse embryonic development and at postnatal age in TMEM16A$^{+/+}$ and TMEM16A$^{-/-}$ mice.

Material and Methods

Ethics Statement

All animals were handled in accordance with the Italian Guidelines for the Use of Laboratory Animals (Decreto Legislativo 27/01/1992, no. 116) and European Union guidelines on animal research (No. 86/609/EEC). Experimental procedures were notified to and approved by the Italian Ministry of Health, Directorate General for Animal Health. The work has been performed on the explanted tissues from sacrificed mice and did not require ethical approval, as stated by the Italian law (decree 116/92). The entire procedure is in accordance with the regulations of the Italian Animal Welfare Act, with the relevant EU legislation and guidelines on the ethical use of animals and is approved by the local Authority Veterinary Service.

Experiments were performed on TMEM16A$^{-/-}$ and TMEM16A$^{+/+}$ littermate mice obtained by breeding TMEM16A$^{+/-}$ mice generated by Rock et al. [24]. Male and female mice were put together for mating in the evening and separated the next morning. If a vaginal plug was observed in the morning, that day was designated as embryonic day 0.5 (E0.5). Once the mouse was positive for vaginal plug, on the prerequisite embryonic day the mouse was anaesthetized by CO_2 inhalation, followed by cervical dislocation. Embryos were removed from the uterus and decapitated. The head region was further processed for immunohistochemistry. For postnatal mice, date of birth was defined as postnatal day 0 (P0). Postnatal mice were anaesthetized by CO_2 inhalation and decapitated. Nose was separated from the rest of head and further processed.

Genotyping protocol

To check the genotype of mouse for *Tmem16a* gene, genotyping for deletion of exon-12 of *Tmem16a* and insertion of PGK-neo cassette was done. Genomic DNA was isolated from the mouse tails by using 5'PRIME Kit (Eppendorf, Milano, Italy), according to manufacturer's protocol. PCR was carried out in a total volume of 25 µl under the following conditions for 40 cycles: 94°C for 5 min (for 1 cycle), 94°C for 30 sec, 60°C for 30 sec and 72°C for 30 sec. The final reaction mixture contained 100 ng of genomic DNA, using Taq Polymerase Master Mix (VWR, Milano, Italy). Two separate PCRs were required to identify homozygous knockout mouse: one for the mutant allele (PGK-neo instead of exon-12) and one for the wild type allele. Wild type allele size was 330 bp and mutant allele was 450 bp. DNA was separated by electrophoresis on 1,5% agarose gel with ethidium bromide.

Primers used:

WT (f): 5'-CCTATGACTGCCAGGGACGCCC-3'
WT(rev): 5'-TGTTCCTGTCCCTGCAATGCGG-3'
Mut (f): 5'-GACGCCCTCCATTGACCC-3'
Mut (rev): 5'-GCAGTAGAAGGTGGCGCGAAG-3'

Immunohistochemistry

For E14.5 whole head region and for E16.5, E18.5 and P4 dissected out nose was fixed in 4% paraformaldehyde prepared in 0.01 M phosphate-buffered saline (PBS) for overnight at 4°C. Tissues with olfactory epithelium were equilibrated at 4°C in 30% (wt/vol) sucrose until the tissue sank to base in solution for cryoprotection. Then the tissue was embedded in O.C.T. (Bio-optica, Milano, Italy) and stored at −80°C. Before sectioning on cryostat, O.C.T. blocks were kept at −20°C for at least 12 hours. With a cryostat, 12-14 µm coronal sections were cut and stored (−80°C) for further use. Further sections were treated with SDS 0.5% (wt/vol) in PBS for 15 min. Sections were incubated in a blocking solution (2% [vol/vol] FBS and 0.2% [vol/vol] Triton X-100 in PBS) for 90 minutes, and then with the primary antibody (diluted in the blocking solution) overnight at 4°C. Sections were then rinsed with 0.1% (vol/vol) Tween 20 in PBS (PBS-T) and incubated with the fluorophore-conjugated secondary antibody (diluted in PBS-T) for 2 h at room temperature. After washing with PBS-T, sections were treated with 0.1 µg/ml DAPI for 30 min, washed with PBS-T, and mounted with Vectashield (Vector Laboratories). Postnatal mice tissues were fixed for 6 hours and processed as described for the embryonic tissues. As far as possible, different embryonic and postnatal tissues were processed in parallel at the same time to avoid any discrepancies in results.

For each age, sections were analyzed from at least three mice obtained from at least two litters.

All chemicals, unless otherwise stated, were purchased from Sigma, Milano, Italy.

The primary antibodies used in this study are listed in Table 1.

Secondary antibodies

The following secondary antibodies obtained from Invitrogen, Eugene, OR, USA, were used: donkey anti-rabbit Alexa Fluor 488 (1:500; catalog no. A21206), donkey anti-goat Alexa Fluor 594 (1:500; catalog no. A11058), goat anti-rabbit Alexa Fluor 594 (1:500; catalog no. A11037), goat anti-mouse Alexa Fluor 488 (1:500; catalog no. A11001)

Imaging

Immunoreactivity was visualized with a confocal microscope (TCS SP2; Leica) using 40X/1.25NA or 63X/1.4NA oil immersion objectives. Images were acquired using Leica software (at 1,024 × 1,024 pixel resolution). All images were taken as average of z-stacks of 1-2 µm thickness. Images were prepared and assembled in Inkscape version 0.48.2. Images were not modified other than to level illumination. Only DAPI signals were enhanced, to show the anatomy of the olfactory epithelium. In any case, data were not altered because of the above adjustments.

Cell counting

To determine cell density, the number of nuclei in a 150 x 150 μm^2 area of the olfactory epithelium was counted with imageJ 1.48v software. As nuclei the olfactory epithelium have various shapes, we counted the cells manually using the cell counter tool of imageJ 1.48v. To discriminate the cell types we considered the position and the shape of each cell nucleus. The sox2 positive oval shaped nuclei in upper one third part of the epithelium were counted as nuclei of supporting cells. The remaining nuclei above the lamina propria were counted as neuronal nuclei, with the exception of the flat shape nuclei near the most basal layer of the epithelium corresponding to basal cells' nuclei. During counting of neuronal nuclei we tried to be consistent with shape as much as possible by applying the same criteria of counting to all sections. The number of neurons was estimated by counting all supra-basal round nuclei in the epithelium. The number of supporting cells was estimated by referring the number of oval-shaped sox2 positive nuclei in the most superficial nuclear layer. From each animal eight coronal sections of 16 µm thickness were collected for counting. For E14.5 every fourth section, for E16.5, E18.5 and P4 every seventh section was collected. Approximately 40–47 areas were selected from the septum and turbinates in each animal to count the cells. Areas were chosen randomly at different epithelial thicknesses. In each group at least three animals were used.

Number of cells are reported as average ± SEM. Statistical significance was

determined using paired or unpaired Student's *t* -tests and p values <0.05 were considered significant.

Results

The olfactory epithelium is mainly composed of olfactory sensory neurons and supporting cells. Olfactory sensory neurons are bipolar neurons with a single dendritic process that terminates in a knob from which several cilia protrude at the apical surface of the epithelium, while supporting cells have columnar cell bodies and microvilli at the apical side.

We have previously shown that TMEM16A is expressed at E12.5 at the apical surface of the entire olfactory epithelium, whereas from E16.5 it is expressed only in a region of the olfactory epithelium near the transition zone with the respiratory epithelium [23]. Moreover, Gritli-Linde et al. [28] showed a dynamic expression of *Tmem16a* during embryonic development, with the highest expression at E12.5, which greatly decreased after E18.5. TMEM16A has been shown to be involved in various physiological processes, including cell proliferation and development. In the developing olfactory epithelium, mitotic cells are abundant at the apical surface at E12.5 [29, 30], and the majority of mitoses occur in the apical layer up to about E14, whereas later proliferative activity is transferred to the basal layer [31, 32]. Based on these observations, we investigated the hypothesis that TMEM16A may play a role in cell proliferation and development of the mouse olfactory epithelium by comparing results obtained with TMEM16A$^{-/-}$ and TMEM16A$^{+/+}$ littermates.

Expression of ACIII and OMP in TMEM16A$^{-/-}$ and TMEM16A$^{+/+}$ mice

In a first set of experiments, we investigated the expression of TMEM16A and ACIII, a well known ciliary marker protein in olfactory sensory neurons [33-35]. In the olfactory epithelium of TMEM16A$^{-/-}$ mice, TMEM16A immunoreactivity was absent, thus confirming the loss of TMEM16A and the specificity of the antibody for this protein, while ACIII was expressed at the apical surface of the olfactory epithelium (Figure 1).

In TMEM16A$^{+/+}$ mice, we confirmed our previous results [23], showing that TMEM16A was expressed at E14.5 at the apical surface of the entire olfactory epithelium, whereas from E16.5 to postnatal age it was expressed only in a region of the olfactory epithelium near the transition zone with the respiratory epithelium (data not shown). Figure 1B shows that at E14.5 both ACIII and TMEM16A were expressed at the apical surface of the olfactory epithelium, with ACIII present in small clusters and TMEM16A expressed in a layer just below the ACIII clusters (Figure 1B). At subsequent days of development ACIII immunoreactivity increased and at P4 the two antibodies stained distinct layers at the apical

surface without any overlap (Figure 1H), indicating that TMEM16A was not expressed in the cilia of olfactory sensory neurons (Figure 1A-H).

As ACIII is expressed in the cilia of olfactory sensory neurons, a comparison between TMEM16A$^{-/-}$ and TMEM16A$^{+/+}$ littermates indicate that TMEM16A does not influence the development of the ciliary organization in the olfactory epithelium (Figure 1A-H).

To further evaluate whether TMEM16A has an influence on the maturation of olfactory sensory neurons during development, we used olfactory marker protein (OMP) as the typical marker for mature olfactory sensory neurons [36]. A small number of OMP immunopositive neurons was present at E14.5 both in TMEM16A$^{-/-}$ and TMEM16A$^{+/+}$ embryos (Figure 2A, B). With development, the density of mature neurons increased and firmly packed OMP positive neurons were present at postnatal stage in both types of mice (Figure 2A-H).

These results show that genetic ablation of TMEM16A does not affect the maturation of neurons and their ciliary development in the olfactory epithelium (Figure 1, 2).

Supporting cells in TMEM16A$^{-/-}$ and TMEM16A$^{+/+}$ mice

We have previously reported that TMEM16A is localized at the apical part of supporting cells and in their microvilli [23]. Here, we investigate whether TMEM16A has an influence on the development of supporting cells. We used cytokeratin 8, ezrin and sox2 as markers for supporting cells. Figure 3A shows that cytokeratin 8, a cytoskeleton protein, stained cells with the typical morphology of supporting cells, characterized by large cell bodies with the shape of an inverted flask located in the upper one third of the epithelium and processes in the lower two thirds of the epithelium, although microvilli at the apical surface were not marked by cytokeratin 8. Furthermore, we performed a double-labelling experiment using OMP (Figure 3B) showing that cytokeratin 8 and OMP immunoreactivity did not overlap (Figure 3A-C), indicating that cytokeratin 8 does not label olfactory neurons and is a good marker for supporting cells. Figure 3D further shows that cytokeratin 8 immunoreactivity was absent in microvilli, as illustrated by the absence of overlap with ezrin immunoreactivity. Figure 3E shows that sox2 is a good marker for the nuclei of supporting cells, although it also stains nuclei of basal cells of the olfactory epithelium, in agreement with previous reports [37-39].

To examine the anatomical organization of supporting cells, we first stained the olfactory epithelium with cytokeratin 8. Figure 4A-D shows that organization of supporting cells was similar in TMEM16A$^{-/-}$ and TMEM16A$^{+/+}$ littermates. Furthermore, a comparison among microvilli of supporting cells marked by ezrin (Figure 4G-H) also show a similarity in TMEM16A$^{-/-}$ and TMEM16A$^{+/+}$ littermates. Moreover, Figure 4F, H confirms our previous observation that TMEM16A was mainly localized to the proximal part of microvilli of

supporting cells and to the apical part of supporting cells [23].

To obtain a quantitative comparison among supporting cells in the olfactory epithelia of TMEM16A$^{-/-}$ and TMEM16A$^{+/+}$ mice, we counted nuclei stained by sox2 in 150 x 150 µm^2 area from several regions of the olfactory epithelium. Although sox2 is a good marker for supporting cells, it is also expressed in basal cells. However, as nuclei of supporting cells are located in the upper one third part of the epithelium and basal cells are mainly present in the lower part of the epithelium, we counted only the sox2 positive cells in the upper one third part of the olfactory epithelium.

The average number of supporting cells at E14.5 was 45 ± 2 in TMEM16A$^{+/+}$ mice, not significantly different from the value of 48 ± 2 in TMEM16A$^{-/-}$ mice (p-value > 0.05, Figure 5A). It may be of interest to note that the average number of supporting cells decreased as the age increased, reaching the value of 32 ± 2 at E18 for both TMEM16A$^{+/+}$ and TMEM16A$^{-/-}$ mice (p-value < 0.05, Figure 5A). At every age, the average number of supporting cells was not significantly different between TMEM16A$^{+/+}$ and TMEM16A$^{-/-}$ mice (Figure 5A).

The average number of olfactory sensory neurons at E14.5 was 185 ± 8 in TMEM16A$^{+/+}$ mice, that was not significantly different from the value of 170 ± 14 in TMEM16A$^{-/-}$ mice (Figure 5B). As observed for supporting cells, also the average number of neurons at every age was not significantly different between TMEM16A$^{+/+}$ and TMEM16A$^{-/-}$ mice.

Thus, genetic ablation of TMEM16A does not affect the morphology and development of supporting cells nor the number of neurons and supporting cells during mouse embryonic development and at postnatal age.

Bowman and nasal glands in TMEM16A$^{-/-}$ and TMEM16A$^{+/+}$ mice

We investigated the expression of TMEM16A in Bowman's glands, nasal septal glands, and lateral nasal glands, whose localization is schematically represented in Figure 6G, and used aquaporin 5 as a marker for these glands [40].

Figure 6A, D shows that aquaporin 5 stained the internal wall of the duct of a Bowman's gland as well as microvilli of supporting cells. Previous reports showed expression of TMEM16A in the duct of Bowman's glands and in the luminal surface of nasal septal glands and lateral nasal glands [21]. However, in TMEM16A$^{+/+}$ mice, we did not find expression of TMEM16A in Bowman's glands, whereas the luminal surface of nasal septal glands and lateral nasal glands expressed both TMEM16A and aquaporin 5 (Figure 6B, C). A comparison with results with TMEM16A$^{-/-}$ mice shows that immunostaining of aquaporin 5 remains unchanged, whereas TMEM16A immunoreactivity was absent. The morphology of

Bowman's gland, nasal septal glands and lateral nasal glands remained the same in both types of mice.

Thus, the absence of TMEM16A does not influence the development of Bowman's glands, nasal septal glands and lateral nasal glands.

Discussion

In this study, we have obtained for the first time immunohistochemistry data comparing morphological and anatomical properties of the olfactory epithelium and of Bowman's and nasal glands during mouse embryonic development and at postnatal ages in TMEM16A$^{+/+}$ and TMEM16A$^{-/-}$ mice.

Olfactory sensory neurons and supporting cells

As TMEM16A$^{-/-}$ mice die before reaching P30 and 90% of them die before P9, we restricted our study up to the age of P4. In the first part of this study, we showed that the development and the morphology of olfactory sensory neurons was similar between TMEM16A$^{+/+}$ and TMEM16A$^{-/-}$ mice. Interestingly, an *in vitro* study suggested that TMEM16A is involved in the early phase of ciliogenesis [41]. In the olfactory epithelium, we did not find expression of TMEM16A in the cilia of olfactory sensory neurons [23]. Furthermore, the unaltered morphology of cilia and knobs in TMEM16A$^{-/-}$ mice shows that TMEM16A does not mediate ciliogenesis in olfactory sensory neurons.

To investigate whether TMEM16A has an influence on the development of supporting cells we first used cytokeratin 8 as a marker for supporting cells. Cytokeratin 8 or keratin 8 is a subtype of keratin intermediate filaments. It is type II (basic) keratin and is found associated with type I (acidic) cytokeratin 18 and cytokeratin 19 in various epithelial cells [42-44]. We found that cytokeratin 8 was a selective marker for supporting cells of the olfactory epithelium, indeed cytokeratin 8 immunostaining revealed cells with the typical morphology of supporting cells and, in addition, did not overlap with the immunopositive signals of OMP that stains mature olfactory sensory neurons. As cytokeratin 8 stains the cytoskeleton, its use allows the investigation of changes in supporting cells' cytoskeleton during development. Both cytokeratin 8 and cytokeratin 18 are the abundant intermediate filament subtypes during mouse embryonic development [45]. Using cytokeratin 8 as a marker for supporting cells' cytoskeleton, we found that at E14.5 the cytoskeleton was loosely organized and individual filaments of the cytoskeleton could be observed (data not shown). In postnatal mice, cytokeratin 8 immunopositive cytoskeletons became densely packed and supporting cells' nuclei aligned in the top layer of the olfactory epithelium. In TMEM16A$^{+/+}$ mice, TMEM16A expression was observed just above the cytokeratin 8

immunopositive signals, but we did not found any overlap in their expression (Figure 4). TMEM16A$^{-/-}$ mice were devoid of TMEM16A expression, but cytokeratin 8 expression pattern remained same as in the TMEM16A$^{+/+}$ littermate mice, showing that organization and morphology of supporting cells were not affected by the absence of TMEM16A.

TMEM16A has been shown to interact with ezrin in salivary gland epithelial cells [46]. We confirmed our previous observation that TMEM16A was expressed in the apical part of supporting cells and in their apical microvilli marked by ezrin [23]. Double staining of TMEM16A with ezrin showed that at E16.5 TMEM16A and ezrin immunoreactivity largely overlapped, whereas at later ages TMEM16A was only expressed in the proximal part of microvilli. The same pattern of expression was observed in TMEM16A$^{+/+}$ mice. A comparison between ezrin expression in microvilli in TMEM16A$^{+/+}$ and TMEM16A$^{-/-}$ littermate mice showed that microvilli development was not altered by the absence of TMEM16A.

It is of interest to note that TMEM16A, ezrin and cytokeratin 8 expressed in supporting cells, but cytokeratin 8 immunoreactivity did not even partially overlap with TMEM16A or ezrin immunoreactivity (Figure 4). An explanation for the absence of overlap between cytokeratin 8 and TMEM16A may arise from the ultrastructural study of the morphology of supporting cells by Frisch [47]. Indeed, Frisch [47] reported that, at the apical part of supporting cells, the cytoplasm seems to be strongly gelated and devoid of cellular organelles. Indeed, we observed a space between ezrin and cytokeratin 8 immunoreactivity (Figure 3D), which resembles the apical organelle free area described by Frisch [47]. TMEM16A was expressed in the free apical region of supporting cells and in the proximal part of microvilli (Figure 4). A similar free space without cellular organelles just below microvilli has also been reported in intestinal brush border cells [48].

TMEM16A plays a role in cell proliferation in several systems. For example proliferation of interstitial cells of Cajal in TMEM16A$^{-/-}$ mice has been shown to be severely affected by the absence of TMEM16A [10]. In addition, TMEM16A is widely known for its role in carcinogenic tumor proliferation [6-9, 49, 50]. Several studies from cancerous cell lines showed that cell proliferation was severely affected by reducing TMEM16A expression with siRNA or inhibiting its activity by using TMEM16A blockers [10, 51, 52], although other studies showed that TMEM16A overexpression did not affect proliferation [49, 52-54] .

In the olfactory epithelium, Gritli-Linde et al. [28] showed that *Tmem16a* expression was high at E12.5, but greatly decreased after E18.5. We observed TMEM16A expression in supporting cells all over the olfactory epithelium during early stages of development (E12.5 and E14.5), whereas from E16.5 onward TMEM16A expression became restricted toward the transition zone between the olfactory and the respiratory epithelium [23]. In the early stages of development dividing cells are abundant in the apical part of the olfactory

epithelium [31, 32] and TMEM16A may play a role in cell division. Based on these observations, we counted the number of supporting cells and of olfactory sensory neurons and found that at E14.5 the average number of supporting cells was significantly higher than average values at later stages of development. However, similar values were estimated in TMEM16A$^{+/+}$ and TMEM16A$^{-/-}$ littermate mice, indicating that TMEM16A did not play a role in this process.

The average number of olfactory sensory neurons was not significantly different from E14.5 to P4 and between TMEM16A$^{+/+}$ and TMEM16A$^{-/-}$ mice, ruling out out the possibility that TMEM16A expression affects proliferation in the olfactory epithelium.

Bowman's and nasal glands

TMEM16A is expressed in various secretory epithelia and glands and regulates anion secretion [25-27, 55, 56]. The nasal cavity contains several types of secretory glands, such as Bowman's glands, nasal septal glands and lateral nasal glands. The olfactory epithelium is directly exposed to changes in environment and prone to be in contact with hazardous chemicals and stimuli. The apical part of the olfactory epithelium is always covered with the mucus, which continuously eliminates the unwanted molecules from the surface. Mucus is primarily secreted by Bowman's gland and supporting cells are involved in mucus secretion and ionic composition maintenance [47, 57].

Aquaporin 5, a water channel, is expressed in Bowman's gland and supporting cells' microvilli [40, 58]. We observed aquaporin 5 expression in the duct cells and secretory acinar cells of Bowman's gland both in TMEM16A$^{+/+}$ and TMEM16A$^{-/-}$ littermate mice (Figure 6). We could distinguish only a limited number of completely formed Bowman's gland at E16.5 (data not shown), while at E18.5 and in postnatal mice up to P4, numerous Bowman's glands were present. As the majority of TMEM16A$^{-/-}$ mice die by P9, our study was limited to P4. We did not find TMEM16A expression in Bowman's glands till P4, although one study showed expression of TMEM16A in Bowman's gland in adult mice and rats [21]. However, we found that at P4 nasal septal glands and lateral nasal glands showed a strong TMEM16A immunopositive signal. In both types of glands TMEM16A was expressed in the apical region of secretory acinar cells and in the luminal surface of the glands, where it coexpressed with aquaporin 5 (Figure 6).

In TMEM16A$^{-/-}$ mice, aquaporin 5 immunopositive signals were similar to those observed in TMEM16A$^{+/+}$ mice showing that the morphology of Bowman's glands, nasal septal glands and lateral nasal glands was not altered by the absence of TMEM16A.

Conclusions

In conclusion, our data provide the first immunohistochemistry study comparing the development of the olfactory epithelium in TMEM16A$^{+/+}$ and TMEM16A$^{-/-}$ littermate mice during embryonic development. We did not find any significant difference in the olfactory epithelium up to P4 between the two types of mice, indicating that TMEM16A is not involved in proliferation and development of the olfactory epithelium. As TMEM16A$^{-/-}$ mice die soon after birth [24], preventing functional and behavioral studies in adult mice, the development and use of conditional knockout mice for TMEM16A will allow planning of additional experiments to improve our present knowledge of the function of TMEM16A in the olfactory system.

Acknowledgments

We thank Prof. Sidney Simon (Duke University, Durham, USA) and all members of the laboratory for constructive discussions. We would also like to acknowledge the help of Elettra Grdina, Angela Morriello and Angel Pascual Camerota for their support in mice breeding at the SISSA animal house facility. This study was supported by a grant from the Italian Ministry of Education, Universities, and Research (MIUR).

References

1. Tsutsumi S, Kamata N, Vokes TJ, Maruoka Y, Nakakuki K, Enomoto S, Omura K, Amagasa T, Nagayama M, Saito-Ohara F, Inazawa J, Moritani M, Yamaoka T, Inoue H, Itakura M (2004) The novel gene encoding a putative transmembrane protein is mutated in gnathodiaphyseal dysplasia (GDD). Am J Hum Genet 74:1255–1261. doi: 10.1086/421527
2. Galindo BE, Vacquier VD (2005) Phylogeny of the TMEM16 protein family: some members are overexpressed in cancer. Int J Mol Med 16:919–924. doi: 10.3892/ijmm.16.5.919.
3. Caputo A, Caci E, Ferrera L, Pedemonte N, Barsanti C, Sondo E, Pfeffer U, Ravazzolo R, Zegarra-Moran O, Galietta LJ (2008) TMEM16A, a membrane protein associated with calcium-dependent chloride channel activity. Science 322:590–594. doi: 10.1126/science.1163518
4. Schroeder BC, Cheng T, Jan YN, Jan LY (2008) Expression cloning of TMEM16A as a calcium-activated chloride channel subunit. Cell 134:1019–1029. doi: 10.1016/j.cell.2008.09.003
5. Yang YD, Cho H, Koo JY, Tak MH, Cho Y, Shim WS, Park SP, Lee J, Lee B, Kim BM, Raouf R, Shin YK, Oh (2008) TMEM16A confers receptor-activated calcium-dependent chloride conductance. Nature 455:1210–1215. doi: 10.1038/nature07313
6. West RB, Corless CL, Chen X, Rubin BP, Subramanian S, Montgomery K, Zhu S, Ball CA, Nielsen TO, Patel R, Goldblum JR, Brown PO, Heinrich MC, van de Rijn M (2004) The novel marker, DOG1, is expressed ubiquitously in gastrointestinal stromal tumors irrespective of KIT or PDGFRA mutation status. Am J Pathol 165:107–113. doi: 10.1016/S0002-9440(10)63279-8.

7. Espinosa I, Lee C-H, Kim MK, Rouse BT, Subramanian S, Montgomery K, Varma S, Corless CL, Heinrich MC, Smith KS, Wang Z, Rubin B, Nielsen TO, Seitz RS, Ross DT, West RB, Cleary ML, van de Rijn M (2008) A novel monoclonal antibody against DOG1 is a sensitive and specific marker for gastrointestinal stromal tumors. Am J Surg Pathol 32:210–218. doi: 10.1097/PAS.0b013e3181238cec.

8. Huang X, Godfrey TE, Gooding WE, McCarty KS Jr, Gollin S. (2006) Comprehensive genome and transcriptome analysis of the 11q13 amplicon in human oral cancer and synteny to the 7F5 amplicon in murine oral carcinoma. Genes Chromosomes Cancer 45:1058–1069. doi: 10.1002/gcc.20371.

9. Kashyap MK, Marimuthu A, Kishore CJH, Peri S, Keerthikumar S, Prasad TS, Mahmood R, Rao S, Ranganathan P, Sanjeeviah RC, Vijayakumar M, Kumar KV, Montgomery EA, Kumar RV, Pandey A (2009) Genome wide mRNA profiling of esophageal squamous cell carcinoma for identification of cancer biomarkers. Cancer Biol Ther 8:36–46. doi: 10.4161/cbt.8.1.7090

10. Stanich JE, Gibbons SJ, Eisenman ST, Bardsley MR, Rock JR, Harfe BD, Ordog T, Farrugia G (2011) Ano1 as a regulator of proliferation. Am J Physiol Gastrointest Liver Physiol 301:G1044–1051. doi: 10.1152/ajpgi.00196.2011

11. Huang F, Wong X, Jan LY (2012) International Union of Basic and Clinical Pharmacology. LXXXV: calcium-activated chloride channels. Pharmacol Rev 64:1–15. doi: 10.1124/pr.111.005009.

12. Pedemonte N, Galietta LJV (2014) Structure and function of TMEM16 proteins (anoctamins). Physiol Rev 94:419–459. doi: 10.1152/physrev.00039.2011.

13. Jang Y, Oh U (2014) Anoctamin 1 in secretory epithelia. Cell Calcium 55:355–361. doi: 10.1016/j.ceca.2014.02.006

14. Jeon JH, Park JW, Lee JW, Jeong SW, Yeo SW, Kim IB (2011) Expression and immunohistochemical localization of TMEM16A/anoctamin 1, a calcium-activated chloride channel in the mouse cochlea. Cell Tissue Res 345:223–230. doi: 10.1007/s00441-011-1206-6

15. Yi E, Lee J, Lee CJ (2013) Developmental Role of Anoctamin-1/TMEM16A in Ca(2+)-Dependent Volume Change in Supporting Cells of the Mouse Cochlea. Exp Neurobiol 22:322–329. doi: 10.5607/en.2013.22.4.322

16. Billig GM, Pál B, Fidzinski P, Jentsch TJ (2011) Ca2+-activated Cl− currents are dispensable for olfaction. Nat Neurosci 14:763–769. doi: 10.1038/nn.2821

17. Mercer AJ, Rabl K, Riccardi GE, Brecha NC, Stella SL Jr, Thoreson WB (2011) Location of release sites and calcium-activated chloride channels relative to calcium channels at the photoreceptor ribbon synapse. J Neurophysiol 105:321-335. doi: 10.1152/jn.00332.2010.

18. Jeon JH, Paik SS, Chun MH, Oh U, Kim IB (2013) Presynaptic Localization and Possible Function of Calcium-Activated Chloride Channel Anoctamin 1 in the Mammalian Retina. PLoS One 8:e67989. doi: 10.1371/journal.pone.006798.

19. Liu B, Linley JE, Du X, Zhang X, Ooi L, Zhang H, Gamper N. 2010. The acute nociceptive signals induced by bradykinin in rat sensory neurons are mediated by inhibition of M-type K+ channels and activation of Ca2+-activated Cl- channels. J Clin Invest 120:1240–1252.

20. Cho H, Yang YD, Lee J, Lee B, Kim T, Jang Y, Back SK, Na HS, Harfe BD, Wang F, Raouf R, Wood JN, Oh U (2012) The calcium-activated chloride channel anoctamin 1 acts as a heat sensor in nociceptive neurons. Nat Neurosci 15:1015-1021. doi: 10.1038/nn.3111

21. Dauner K, Lissmann J, Jeridi S, Frings S, Möhrlen F (2012) Expression patterns of anoctamin 1 and anoctamin 2 chloride channels in the mammalian nose. Cell Tissue Res 347:327–341. doi: 10.1007/s00441-012-1324-9

22. Dibattista M, Amjad A, Maurya DK, Sagheddu C, Montani G, Tirindelli R, Menini A (2012) Calcium-activated chloride channels in the apical region of mouse vomeronasal sensory neurons. J Gen Physiol 140:3–15. doi: 10.1085/jgp.201210780

23. Maurya DK, Menini A (2014) Developmental expression of the calcium-activated chloride channels TMEM16A and TMEM16B in the mouse olfactory epithelium. Dev Neurobiol 74:657–675. doi: 10.1002/dneu.22159

24. Rock JR, Futtner CR, Harfe BD (2008) The transmembrane protein TMEM16A is required for normal development of the murine trachea. Dev Biol 321:141–149. doi: 10.1016/j.ydbio.2008.06.009.

25. Rock JR, O'Neal WK, Gabriel SE, Randell SH, Harfe BD, Boucher RC, Grubb BR (2009) Transmembrane protein 16A (TMEM16A) is a Ca2+-regulated Cl- secretory channel in mouse airways. J Biol Chem 284:14875–14880. doi: 10.1074/jbc.C109.000869

26. Ousingsawat J, Martins JR, Schreiber R, Rock JR, Harfe BD, Kunzelmann K (2009) Loss of TMEM16A causes a defect in epithelial Ca2+-dependent chloride transport. J Biol Chem 284:28698–28703. doi: 10.1074/jbc.M109.012120

27. Huang F, Rock JR, Harfe BD, Cheng T, Huang X, Jan YN, Jan LY (2009) Studies on expression and function of the TMEM16A calcium-activated chloride channel. Proc Natl Acad Sci U S A 106:21413–21418. doi: 10.1073/pnas.0911935106

28. Gritli-Linde A, Vaziri Sani F, Rock JR, Hallberg K, Iribarne D, Harfe BD, Linde A (2009) Expression patterns of the Tmem16 gene family during cephalic development in the mouse. Gene Expr Patterns 9:178–191. doi: 10.1016/j.gep.2008.11.002

29. Cuschieri A, Bannister LH (1975) The development of the olfactory mucosa in the mouse: light microscopy. J Anat 119:277–286.

30. Taniguchi K, Taniguchi K (2008) Embryonic and postnatal differentiation of olfactory epithelium and vomeronasal organ in the Syrian hamster. J Vet Med Sci Jpn Soc Vet Sci 70:57–64. doi: 10.1292/jvms.70.57

31. Smart IH (1971) Location and orientation of mitotic figures in the developing mouse olfactory epithelium. J Anat 109:243–251.

32. Farbman AI (1994) Developmental biology of olfactory sensory neurons. Semin Cell Biol 5:3–10.

33. Wong ST, Trinh K, Hacker B, Chan GC, Lowe G, Gaggar A, Xia Z, Gold GH, Storm DR (2000) Disruption of the type III adenylyl cyclase gene leads to peripheral and behavioral anosmia in transgenic mice. Neuron 27:487–497. doi: 10.1016/S0896-6273(00)00060-X

34. Col JAD, Matsuo T, Storm DR, Rodriguez I (2007) Adenylyl cyclase-dependent axonal targeting in the olfactory system. Development 134:2481–2489. doi: 10.1242/dev.006346

35. Zou D-J, Chesler AT, Pichon CEL, Kuznetsov A, Pei X, Hwang EL, Firestein S (2007) Absence of Adenylyl Cyclase 3 Perturbs Peripheral Olfactory Projections in Mice. J Neurosci 27:6675–6683. doi: 10.1523/JNEUROSCI.0699-07.2007

36. Keller A, Margolis FL (1975) Immunological studies of the rat olfactory marker protein. J Neurochem 24(6):1101-1106.

37. Guo Z, Packard A, Krolewski RC, Harris MT, Manglapus GL, Schwob JE (2010) Expression of pax6 and sox2 in adult olfactory epithelium. J Comp Neurol 518:4395–4418. doi: 10.1002/cne.22463

38. Gokoffski KK, Wu H-H, Beites CL, Kim J, Kim EJ, Matzuk MM, Johnson JE, Lander AD, Calof AL (2011) Activin and GDF11 collaborate in feedback control of neuroepithelial stem cell proliferation and fate. Development 138:4131–4142. doi: 10.1242/dev.065870

39. Krolewski RC, Packard A, Jang W, Wildner H, Schwob JE (2012) Ascl1 (Mash1) Knockout Perturbs Differentiation of Nonneuronal Cells in Olfactory Epithelium. PLoS ONE 7:e51737. doi: 10.1371/journal.pone.0051737

40. Solbu TT, Holen T (2012) Aquaporin pathways and mucin secretion of Bowman's glands might protect the olfactory mucosa. Chem Senses 37:35–46. doi: 10.1093/chemse/bjr063

41. Ruppersburg CC, Hartzell HC (2014) The Ca2+-activated Cl- channel ANO1/TMEM16A regulates primary ciliogenesis. Mol Biol Cell 25:1793–1807. doi: 10.1091/mbc.E13-10-0599

42. Moll R, Franke WW, Schiller DL, Geiger B, Krepler R (1982) The catalog of human cytokeratins: patterns of expression in normal epithelia, tumors and cultured cells. Cell 31:11–24. doi: 10.1016/0092-8674(82)90400-7

43. Coulombe PA (1993) The cellular and molecular biology of keratins: beginning a new era. Curr Opin Cell Biol 5:17–29. doi: 10.1016/S0955-0674(05)80004-3

44. Casanova L, Bravo A, Were F, Ramírez A, Jorcano JJ, Vidal M (1995) Tissue-specific and efficient expression of the human simple epithelial keratin 8 gene in transgenic mice. J Cell Sci 108:811–820.

45. Franke WW, Grund C, Kuhn C, Jackson BW, Illmensee K (1982) Formation of cytoskeletal elements during mouse embryogenesis. III. Primary mesenchymal cells and the first appearance of vimentin filaments. Differ Res Biol Divers 23:43–59. doi: 10.1111/j.1432-0436.1982.tb01266.x

46. Perez-Cornejo P, Gokhale A, Duran C, Cui Y, Xiao Q, Hartzell HC, Faundez V (2012) Anoctamin 1 (Tmem16A) Ca2+-activated chloride channel stoichiometrically interacts with an ezrin-radixin-moesin network. Proc Natl Acad Sci U S A 109:10376–10381. doi: 10.1073/pnas.1200174109

47. Frisch D (1967) Ultrastructure of mouse olfactory mucosa. Am J Anat 121:87–120.

48. Drenckhahn D, Dermietzel R (1988) Organization of the actin filament cytoskeleton in the intestinal brush border: a quantitative and qualitative immunoelectron microscope study. J Cell Biol 107:1037–1048. doi: 10.1083/jcb.107.3.1037

49. Wanitchakool P, Wolf L, Koehl GE, Sirianant L, Schreiber R, Kulkarni S, Duvvuri U, Kunzelmann K (2014) Role of anoctamins in cancer and apoptosis. Philos Trans R Soc Lond B Biol Sci 369:20130096. doi: 10.1098/rstb.2013.0096

50. Qu Z, Yao W, Yao R, Liu X, Yu K, Hartzell C (2014) The Ca(2+) -activated Cl(-) channel, ANO1 (TMEM16A), is a double-edged sword in cell proliferation and tumorigenesis. Cancer Med 3:453–461. doi: 10.1002/cam4.232

51. Mazzone A, Bernard CE, Strege PR, Beyder A, Galietta LJ, Pasricha PJ, Rae JL, Parkman HP, Linden DR, Szurszewski JH, Ördög T, Gibbons SJ, Farrugia G (2011) Altered expression of Ano1 variants in human diabetic gastroparesis. J Biol Chem 286:13393–13403. doi: 10.1074/jbc.M110.196089

52. Britschgi A, Bill A, Brinkhaus H, Rothwell C, Clay I, Duss S, Rebhan M, Raman P, Guy CT, Wetzel K, George E, Popa MO, Lilley S, Choudhury H, Gosling M, Wang L, Fitzgerald S, Borawski J, Baffoe J, Labow M, Gaither LA, Bentires-Alj M (2013) Calcium-activated chloride channel ANO1 promotes breast cancer progression by activating EGFR and CAMK signaling. Proc Natl Acad Sci U S A 110:E1026–1034. doi: 10.1073/pnas.1217072110

53. Ayoub C, Wasylyk C, Li Y, Thomas E, Marisa L, Robé A, Roux M, Abecassis J, de Reyniès A, Wasylyk B (2010) ANO1 amplification and expression in HNSCC with a high propensity for future distant metastasis and its functions in HNSCC cell lines. Br J Cancer 103:715–726. doi: 10.1038/sj.bjc.6605823

54. Ruiz C, Martins JR, Rudin F, Schneider S, Dietsche T, Fischer CA, Tornillo L, Terracciano LM, Schreiber R, Bubendorf L, Kunzelmann K (2012) Enhanced expression of ANO1 in head and neck squamous cell carcinoma causes cell migration and correlates with poor prognosis. PloS One 7:e43265. doi: 10.1371/journal.pone.0043265

55. Romanenko VG, Catalán MA, Brown DA, Putzier I, Hartzell HC, Marmorstein AD, Gonzalez-Begne M, Rock JR, Harfe BD, Melvin JE (2010) Tmem16A encodes the Ca2+-activated Cl- channel in mouse submandibular salivary gland acinar cells. J Biol Chem 285:12990–13001. doi: 10.1074/jbc.M109.068544

56. Duran C, Hartzell HC (2011) Physiological roles and diseases of Tmem16/Anoctamin proteins: are they all chloride channels? Acta Pharmacol Sin 32:685–692. doi: 10.1038/aps.2011.48

57. Getchell TV, Margolis FL, Getchell ML (1984) Perireceptor and receptor events in vertebrate olfaction. Prog Neurobiol 23:317–345. doi: 10.1016/0301-0082(84)90008-X

58. Ablimit A, Matsuzaki T, Tajika Y, Aoki T, Hagiwara H, Takata K (2006) Immunolocalization of water channel aquaporins in the nasal olfactory mucosa. Arch Histol Cytol 69:1–12. doi: 10.1679/aohc.69.1

Figure Legends

Figure 1: Expression of TMEM16A and ACIII in the olfactory epithelium of TMEM16A$^{-/-}$ and TMEM16A$^{+/+}$ littermate mice. Confocal images of coronal sections of the olfactory epithelium from a region near to the transition zone with the respiratory epithelium at E14.5, E16.5, E18.5 and P4. **A, C, E, G:** No immunoreactivity to TMEM16A was detectable in TMEM16A$^{-/-}$ mice (goat anti-TMEM16A). **B, D, F, H:** TMEM16A expression in TMEM16A$^{+/+}$ mice was below adenylyl cyclase III (ACIII) expression and did not overlap with ACIII. TMEM16A immunostaining is disccontinuous because of interruption by dendritic knobs of olfactory sensory neurons. Expression of ACIII was similar in both types of mice. Images are averages of z-stacks of ~1.0 µm thickness. Cell nuclei were stained by DAPI. Scale bars = 5 µm

Figure 2: Olfactory sensory neurons in the developing olfactory epithelium of TMEM16A$^{-/-}$ and TMEM16A$^{+/+}$ mice. Mature olfactory sensory neurons express the olfactory marker protein (OMP). Confocal images of coronal sections of the olfactory epithelium at E14.5, E16.5, E18.5 and P4 from TMEM16A$^{-/-}$ (**A, C, E, G**) or TMEM16A$^{+/+}$ (**B, D, F, H)** mice. In both mice, at E14.5 a limited number of mature neurons was present (**A, B**), but the number progressively increased from E16.5 to P4 (**C-H**). ACIII signals were seen in the cilia protruding from the dendritic knob of mature olfactory sensory neurons (**A-H**). Mature neurons expressing OMP and cilia marked by ACIII were similar in TMEM16A$^{-/-}$ and TMEM16A$^{+/+}$ littermates. Images are averages of z-stacks of ~1.5 µm thickness. Cell nuclei were stained by DAPI. Scale bars = 5 µm.

Figure: 3: Markers for supporting cells. A-C: Cytokeratin 8 marked cells with the typical morphology of supporting cells. Double staining of cytokeratin 8 with OMP showed no co-localization. **D:** Microvilli of supporting cells stained by ezrin were not stained by cytokeratin 8. **E:** Double staining of cytokeratin 8 with sox2 shows that sox2 is a nuclear marker for supporting cells. Coronal sections of the olfactory epithelium of wild type mice at P60 (**A-C**), or P4 (**D, E**). Images are averages of z-stacks of ~1.5 µm thickness. Cell nuclei were stained by DAPI. Scale bars: A-C, D = 5 µm; E = 10 µm.

Figure 4: Expression of TMEM16A, cytokeratin8 and ezrin in olfactory epithelium of TMEM16A$^{-/-}$ and TMEM16A$^{+/+}$ littermate mice. Confocal images of coronal sections of the olfactory epithelium from a region near to the transition zone with the respiratory epithelium at E16.5 and P4 from TMEM16A$^{-/-}$ (**A, C, E, G**) or TMEM16A$^{+/+}$ (**B, D, F, H)**. No immunoreactivity to TMEM16A was detectable in TMEM16A$^{-/-}$ mice. **A-D:** Supporting cells marked by cytokeratin 8 were similar in both types of mice. In TMEM16A$^{+/+}$ mice, TMEM16A (goat anti-TMEM16A) and

cytokeratin 8 immunoreactivity did not overlap (**B, D**), whereas TMEM16A expression (rabbit anti-TMEM16A). partially overlapped with ezrin immunopositive signals (**F, H**). Supporting cells marked by cytokeratin 8 and microvilli marked by ezrin were similar in both types of mice. Images are averages of z-stacks of ~1.5 µm thickness. Cell nuclei were stained by DAPI. Scale bars = 5 µm.

Figure 5: Cell densities in the olfactory epithelium of TMEM16A$^{-/-}$ and TMEM16A$^{+/+}$ littermate mice. Comparison among the average number of supporting cells and olfactory sensory neurons in the olfactory epithelium of TMEM16A$^{-/-}$ and TMEM16A$^{+/+}$ littermate mice. Average number of supporting cells (**A**) or olfactory sensory neurons (**B**) was calculated by counting nuclei in 150 x 150 µm^2 areas from several regions of the olfactory epithelium. Counting was done in three different animals for each group and presented as average ± SEM.

Figure 6: Expression of TMEM16A in various nasal glands of TMEM16A$^{-/-}$ and TMEM16A$^{+/+}$ littermate mice. Expression of TMEM16A and aquaporin5 in the Bowman's gland (BG), nasal septal gland (NSG) and lateral nasal gland (LNG) of TMEM16A$^{-/-}$ and TMEM16A$^{+/+}$ littermate mice. **A, D:** aquaporin 5 immuno-positive signals were seen in Bowman's gland in P4 mice. Aquaporin 5 expression in gland and ducts is clearly visible. TMEM16A immunoreactivity (goat anti-TMEM16A) was not present in Bowman's glands of TMEM16A$^{-/-}$ nor of TMEM16A$^{+/+}$ littermate mice (**A, D)**. However, aquaporin 5 and TMEM16A were co-expressed in nasal septal glands (**B**) and lateral nasal glands (**C**) of TMEM16A$^{+/+}$ mice. No immunoreactivity to TMEM16A was detectable in TMEM16A$^{-/-}$ mice (**E, F**). Glands marked by aquaporin 5 were similar in both types of mice. (**g**) The location of the different glands is shown in the schematic diagram of a nose coronal section. Images are averages of z-stacks of thickness of ~2.0 µm for **A, D**, or ~1 µm for **B, C, E, F**. Cell nuclei were stained by DAPI. Scale bars: **A-F** = 10 µm.

Tables

TABLE 1: Primary antibodies used in this study.

Primary antibody	Immunogen	Dilution	Manufacturer/catalog number/lot number or clone
Rabbit polyclonal TMEM16A	Synthetic peptides corresponding to amino acid residues 424-519, 628-731 and 904-986 of human TMEM16A	1:50	Abcam/ab53212/ GR71118-3
Goat polyclonal TMEM16A	Synthetic peptide corresponding to amino acid residues 825-875 of human TMEM16A	1:50	Santa Cruz Biotech/ sc-69343/ H0713
Rabbit polyclonal adenylyl cyclase III (ACIII)	Synthetic peptide corresponding to amino acid residues 1125-1144 of human ACIII	1:100	Santa Cruz Biotech/ sc-588/ K0608
Goat polyclonal olfactory marker protein (OMP)	Purified natural rat OMP	1:1000	Wako Chemicals/ 544-10001/ IUP1001
Mouse monoclonal ezrin	Synthetic peptide corresponding to amino acid residues 362-585 of human ezrin	1:100	Abcam/ab4069/3C12
Rabbit monoclonal cytokeratin 8	Synthetic peptide corresponding to amino acid residues 300-350 of human cytokeratin 8	1:150	Novus Biologicals/ NB110-56919/ EP1628Y
Rabbit polyclonal aquaporin 5	Synthetic peptide corresponding to 17 amino acid sequence in the cytoplasmic region of rat aquaporin 5	1:150	Calbiochem/178615/ D00140208
Goat polyclonal Sox2	Synthetic peptide corresponding to amino acid residues 277-293 of human sox2	1:50	Santa Cruz Biotech/ sc-17320/ A1314

Figure 1:

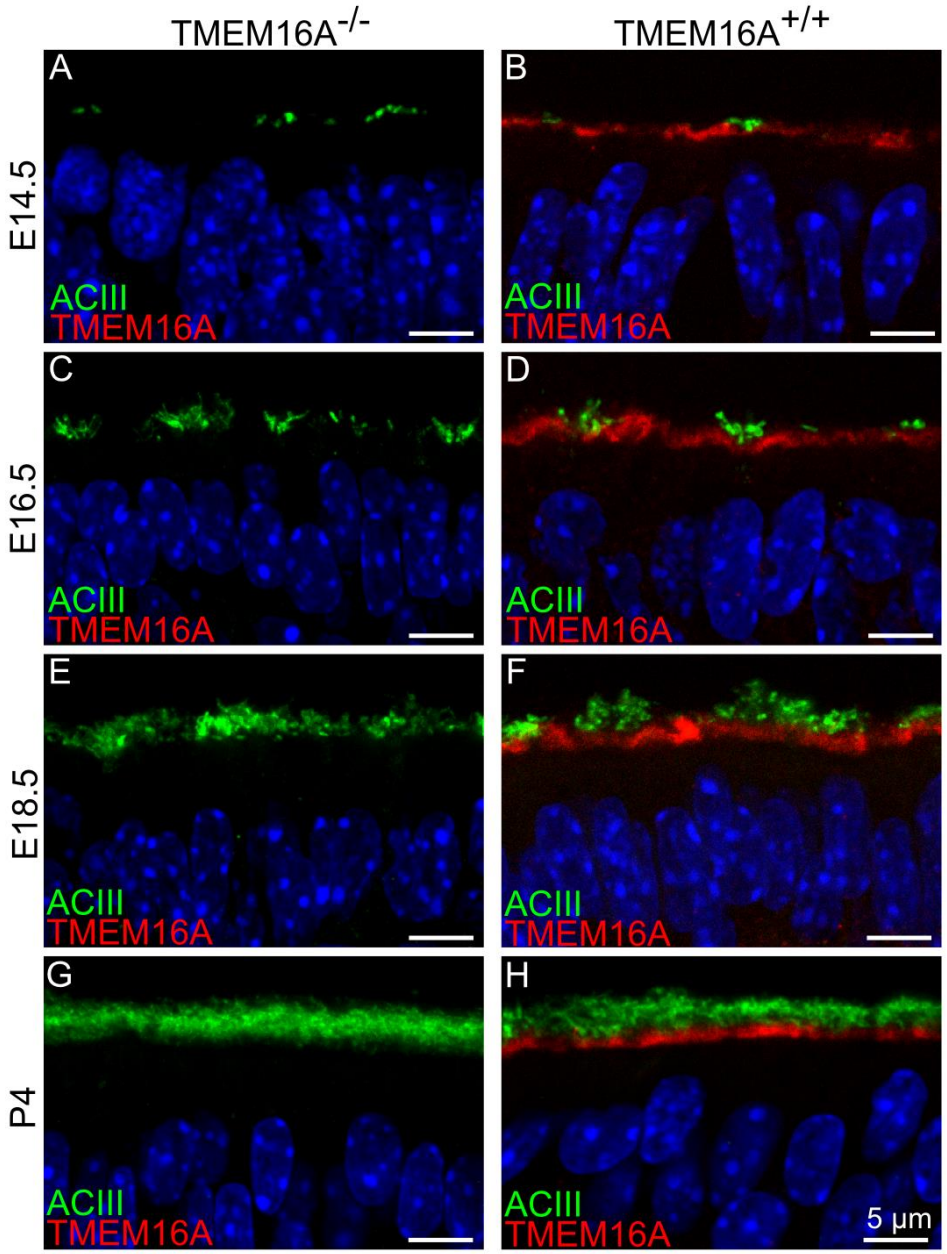
TMEM16A-/-
TMEM16A+/+
A
B
C
D
E
F
G
H
E14.5
E16.5
E18.5
P4
ACIII
TMEM16A
5 µm

Figure 2:

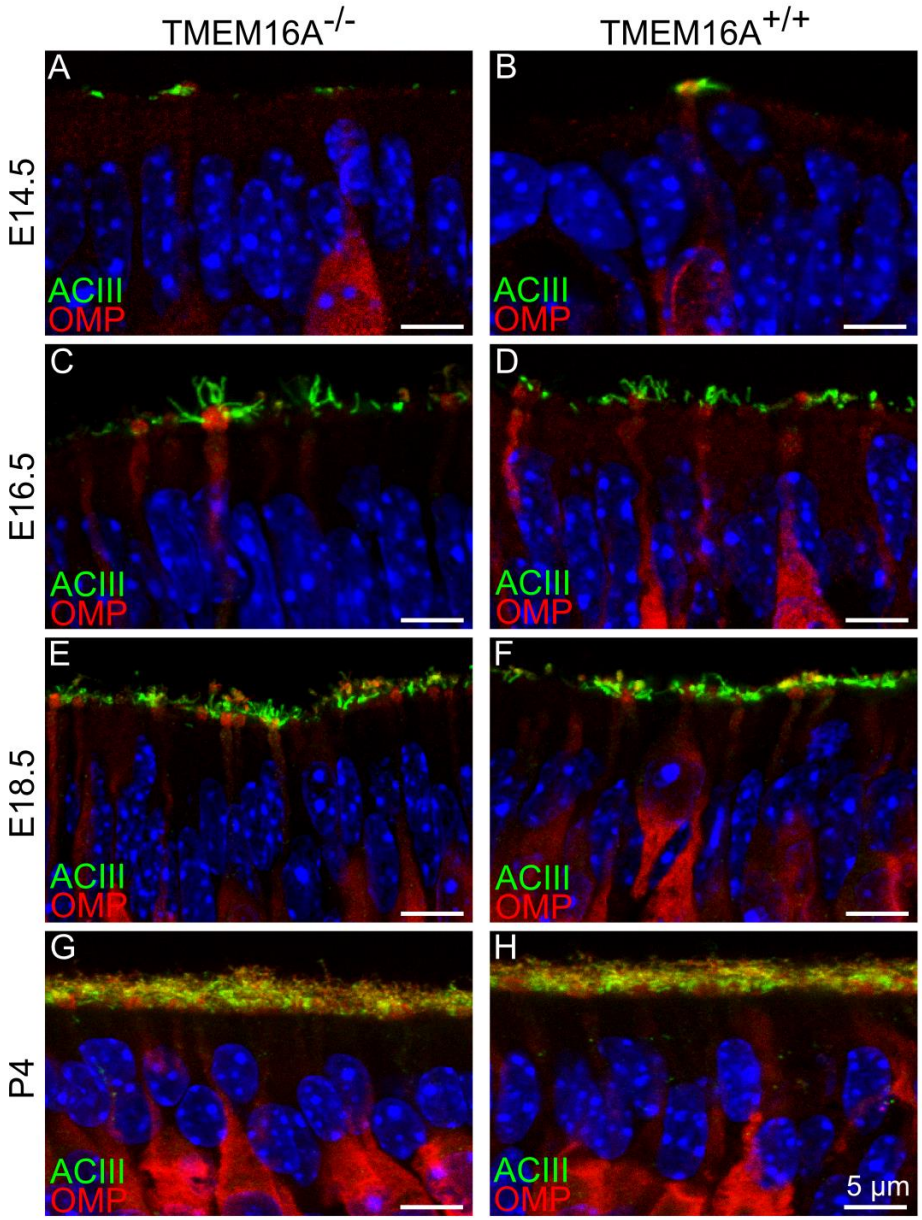

Figure 3:

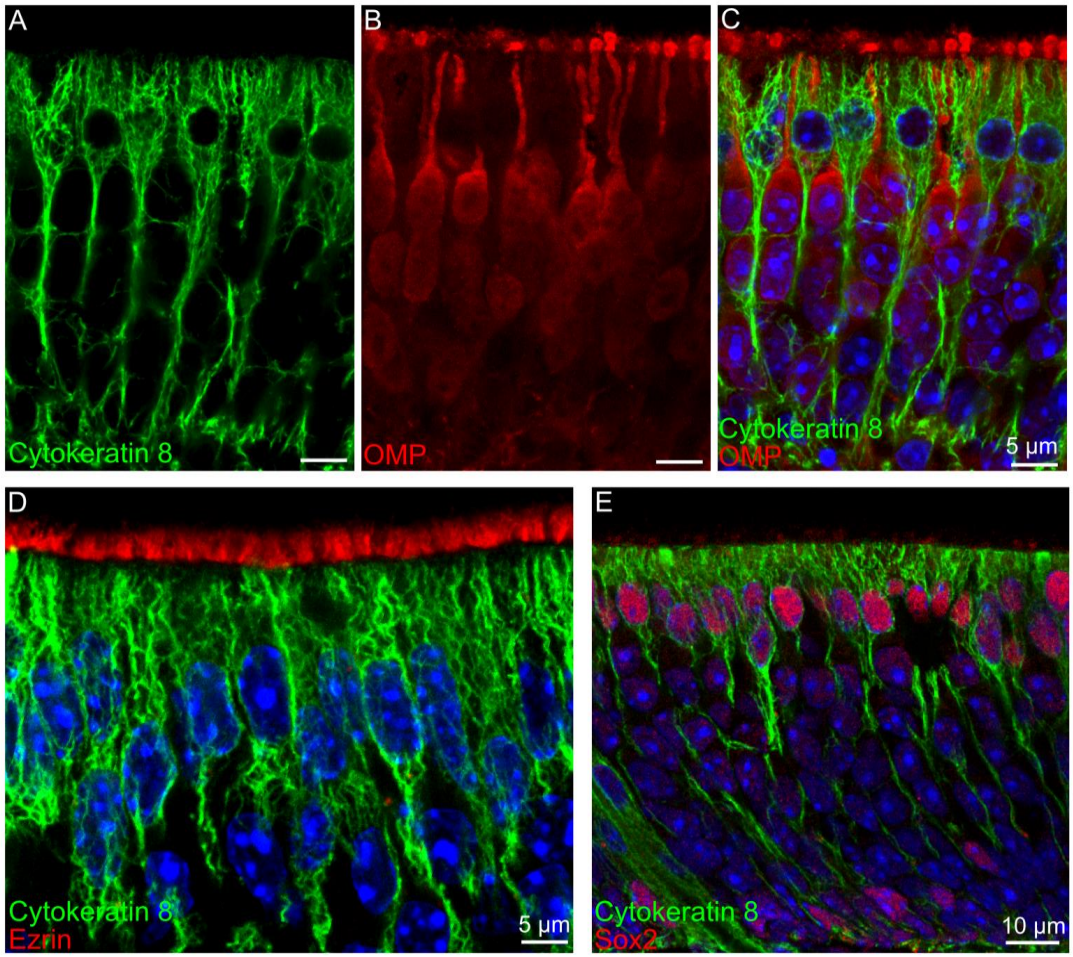
A
Cytokeratin 8
B
OMP
C
Cytokeratin 8
OMP
5 µm
D
Cytokeratin 8
Ezrin
5 µm
E
Cytokeratin 8
Sox2
10 µm

Figure 4:

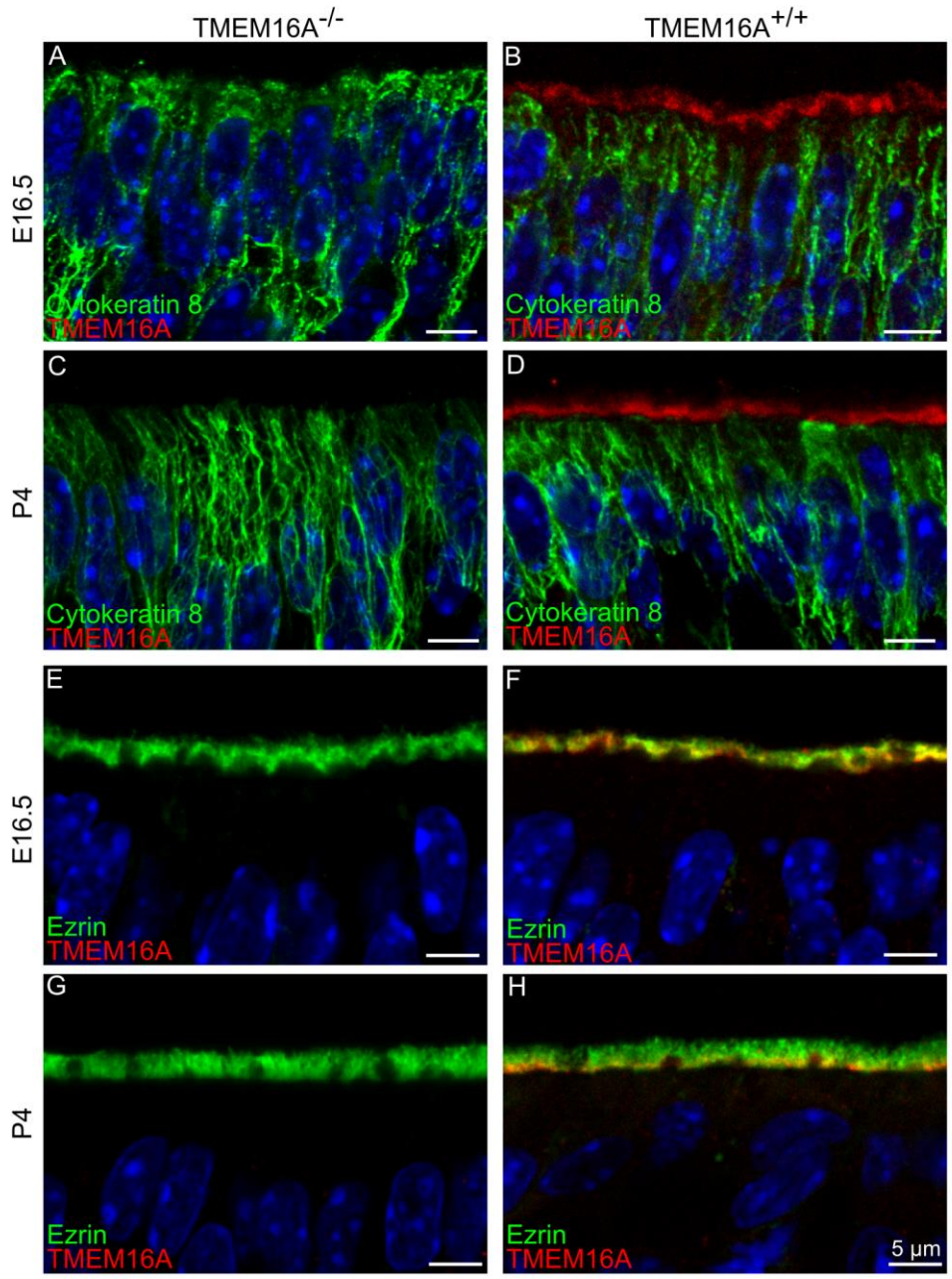
TMEM16A-/-
TMEM16A+/+
A
B
C
D
E
F
G
H
E16.5
P4
E16.5
P4
Cytokeratin 8
TMEM16A
Ezrin
TMEM16A
5 µm

Figure 5:

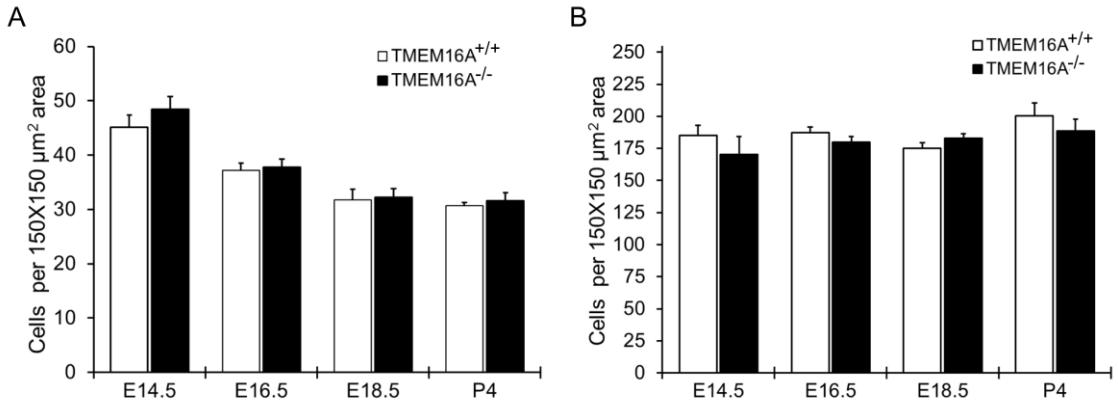
A
B
TMEM16A+/+
TMEM16A-/-
Cells per 150X150 µm² area
E14.5
E16.5
E18.5
P4

Figure 6:

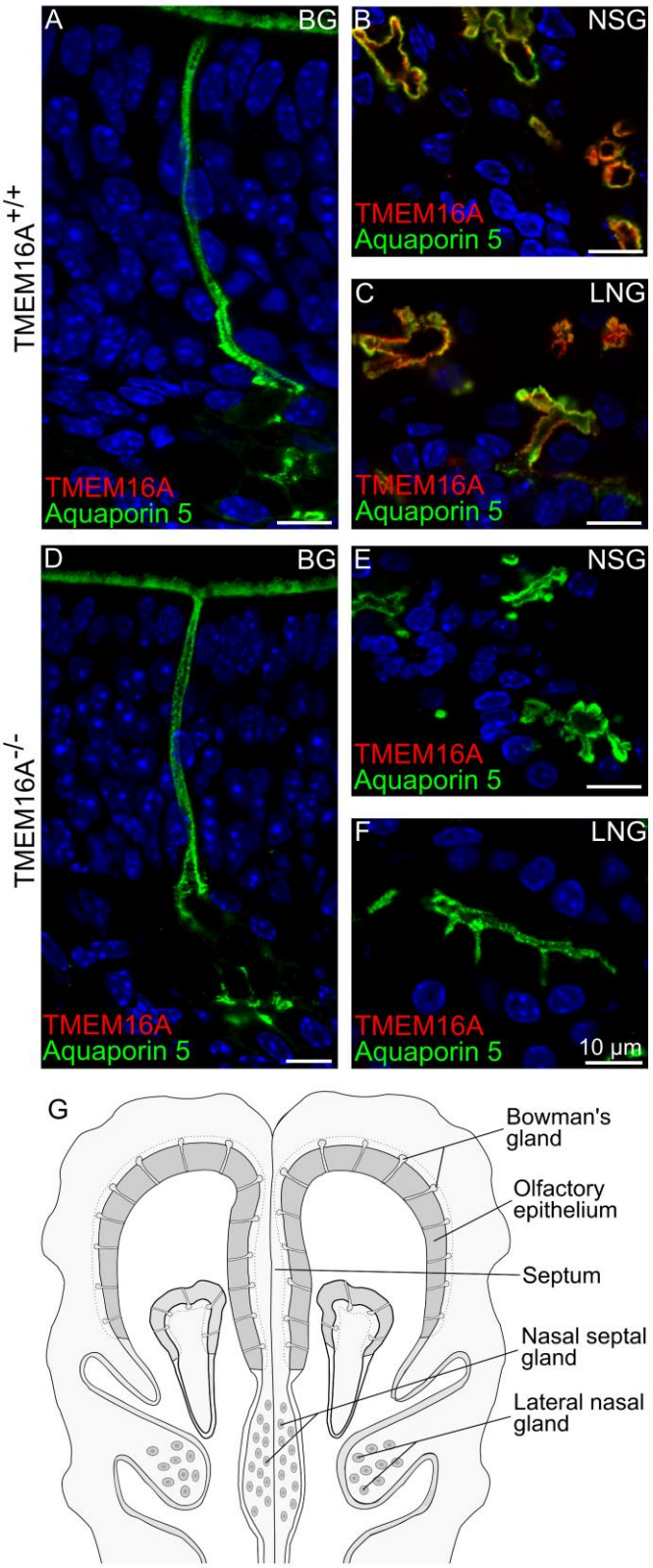
A
BG
B
NSG
TMEM16A
Aquaporin 5
C
LNG
TMEM16A
Aquaporin 5
TMEM16A+/+
D
BG
E
NSG
TMEM16A
Aquaporin 5
F
LNG
TMEM16A
Aquaporin 5
10 µm
TMEM16A-/-
G
Bowman's gland
Olfactory epithelium
Septum
Nasal septal gland
Lateral nasal gland

5. Discussion

The physiological importance of calcium-activated chloride channels is well known in olfactory systems. However their molecular identity has only been characterized in recent years. The TMEM16 protein family members TMEM16A and TMEM16B were found to have biophysical properties similar to putative calcium-activated chloride channels. During my thesis, I have investigated the expression of TMEM16A and TMEM16B along with other neuronal and non-neuronal proteins in the main olfactory epithelium and the vomeronasal organ. The findings of my thesis are additional contributions towards our understanding of the physiological role of calcium-activated chloride channels in olfactory systems.

To study TMEM16A and TMEM16B expression, I first tested the specificity of commercially available antibodies against them. Anti-TMEM16A and TMEM16B antibodies were tested for their specificity in transiently transfected HEK 293T cells with TMEM16A or TMEM16B plasmids. Anti-TMEM16A and TMEM16B antibodies showed specific immuno-positive signals respectively with TMEM16A and TMEM16B expressing cells. Further, I found specificity of antibodies used in this study also in the respective knockout mouse models.

In the vomeronasal organ, I found expression of TMEM16A and TMEM16B in the luminal surface of the sensory epithelium, where both co-express with the TRPC2 cation channel. For unambiguous confirmation of TMEM16A and TMEM16B co-expression in neurons I studied expression of both proteins in isolated neurons. I found co-expression of TMEM16A and TMEM16B in microvilli of isolated vomeronasal sensory neurons. Further, using anti-PDE4A and Gαo antibodies as markers for apical and basal neurons, respectively, I found expression of TMEM16A and TMEM16B in both types of neurons. Thus TMEM16A and TMEM16B are co-expressed in microvilli of almost all types of vomeronasal sensory neurons. On the contrary, in the olfactory epithelium I found expression of only TMEM16B in olfactory sensory neurons, in agreement with previous studies (Stephan et al. 2009; Hengl et al. 2010; Sagheddu et al. 2010).

Olfactory epithelium and vomeronasal sensory epithelium have a common origin, the olfactory placode. It is interesting to note that, despite the common origin, olfactory sensory neurons express only TMEM16B while vomeronasal sensory neurons express TMEM16B along with TMEM16A. To have an in depth understanding of TMEM16A and TMEM16B expression in the olfactory epithelium, I studied their expression pattern during embryonic development of the olfactory epithelium. At embryonic day 12.5 (E12.5), the olfactory epithelium is almost formed and anatomically recognizable so that we can study the expression of various proteins in neurons. I studied temporal and spatial expression of TMEM16A and TMEM16B along with ACIII, CNGA2, acetylated-tubulin, OMP, ezrin, β-tubulin-III, cytokeratin-8 and aquaporin-5 during embryonic development of olfactory epithelium from E12.5 to postnatal day 60 (P60).

In situ hybridization analysis showed *Tmem16a* gene expression in the olfactory and the respiratory epithelia at E12.5, which greatly decreased after E18.5 (Gritli-Linde et al. 2009). At E12.5, I found uniform expression of TMEM16A protein at the apical surface of both the olfactory and the respiratory epithelium. Interestingly, at E16.5 TMEM16A immuno-reactivity decreased in the dorsal area of the olfactory epithelium and was present only in areas of the olfactory epithelium near the transition zone with the respiratory epithelium. At E18.5 and in postnatal mice, TMEM16A immunoreactivity was even more restricted toward the respiratory epithelium. The decreased expression of TMEM16A during embryonic development is in agreement with previous *in situ* hybridization data (Gritli-Linde et al., 2009). TMEM16A immuno-positive signal did not overlap either with β-tubulin-III or OMP expressing olfactory sensory neurons. In neonates and adult mice, cilia form a prominent apical layer in the olfactory epithelium. ACIII is expressed in this ciliary layer, TMEM16A did not co-express with ACIII and TMEM16A expression was seen just below this layer. These results confirm that during embryonic development and in postnatal mice, TMEM16A was not expressed in olfactory sensory neurons but was expressed at the apical part of supporting cells. Indeed, TMEM16A and ezrin (a marker for microvilli) largely co-localized at the apical surface of the olfactory epithelium at E16.5. Ezrin immuno-reactivity increased in the following days because microvilli elongated with development (Menco and Farbman, 1985). From E18.5 to postnatal age, TMEM16A was mainly localized to the proximal part of microvilli of supporting cells and to the apical part of supporting cells.

Cytokeratin-8 or keratin-8 is type II (basic) keratin and is a component of intermediate filaments in various epithelial cells (Moll et al. 1982; Coulombe 1993; Casanova et al. 1995). I found its expression in supporting cells of olfactory epithelium, whereas neurons were devoid of it. It is interesting that TMEM16A, ezrin and cytokeratin-8 express in supporting cells but cytokeratin-8 does not co-express with either of them. The apical part of supporting cells is gelated and devoid of cellular organelles (Frisch 1967). Cytokeratin-8 immunostained intermediate filaments were not continuous in the apical organelle free region of supporting

cells. Furthermore, ezrin expresses only in microvilli, an outgrowth of apical surface of supporting cells (Hengl et al. 2010, Dauner et al. 2012, Maurya and Menini 2014). This could be the reason why cytokeratin-8 and ezrin immuno-positive signals did not overlap though both are expressed in supporting cells. Space between ezrin and cytokeratin-8 resembles to the apical organelle free area of supporting cells. In my observations TMEM16A is expressed in organelle free apical region of supporting cells and proximal part of microvilli.

During mouse embryonic development, TMEM16B did not express at E12.5. In mature olfactory sensory neurons at E14.5, TMEM16B expression was seen in the apical part of neurons. TMEM16B immunoreactivity increased in the following days because the number of mature neurons increased and the cilia elongated with development. Indeed, it has been reported that at E14.5 cilia are short (~1-2 µm) and with development elongate reaching a length of up to 60 µm before birth (Noda and Harda 1981; Schwarzenbacher et al. 2005; McEwen et al. 2008). From E16.5 onwards, acetylated tubulin immunoreactivity clearly indicated that several cilia protruded from dendritic knobs and that their length increased with development. TMEM16B immunoreactivity largely overlapped with acetylated tubulin immunoreactivity, indicating that TMEM16B expression was correlated with ciliary growth. Moreover, TMEM16B was also seen in the dendritic knobs of some mature olfactory sensory neurons. During development and in postnatal mice, TMEM16B immunoreactivity was not found in the respiratory epithelium, thus TMEM16B expression was restricted to the olfactory epithelium. In neonate and adult mouse TMEM16A expressed in a prominent layer just below TMEM16B expressing ciliary layer. Thus these two proteins never co-localized in olfactory epithelium.

5.1 TMEM16A: proliferation and secretory processes

The dynamic expression of TMEM16A during embryonic development raises interesting questions about its physiological role. TMEM16A has been shown to be involved in various physiological processes, including cell proliferation. TMEM16A is also widely known for its role in carcinogenic tumours proliferation (West et al. 2004; Espinosa et al. 2008; Huang et al. 2006; Kashyap et al. 2009; Qu et al 2014; Wanitchakool et al 2014).

Several studies from cancerous cell lines had shown that after reducing TMEM16A function by either siRNA or by using TMEM16A blockers, proliferation of cells is severely affected (Mazzone et al. 2011; Stanich et al. 2011; Britschgi et al. 2013). Moreover, *in vitro* proliferation of interstitial cells of Cajal is down-regulated in the TMEM16A knockout mice (Stanich et al. 2011). In the developing olfactory epithelium, mitotic cells are abundant at the apical surface at E12.5 (Smart 1971; Cuschieri and Bannister 1975a; Taniguchi and Taniguchi 2008) and the majority of mitoses occurs in the apical layer up to about E14.5, whereas later proliferative activity is limited only to the basal layer (Smart 1971; Farbman

1994). These observations further suggest that until E14.5, the expression of TMEM16A at the apical surface may play a role in cell proliferation.

In order to comprehend the correlation between TMEM16A and proliferation, I compared the distributions of cells in the olfactory epithelium in TMEM16A$^{-/-}$ and littermate TMEM16A$^{+/+}$ mice. Genetic ablation of TMEM16A is lethal in mice and 90% homozygous knockout pups die within postnatal day nine (P9) (Rock et al. 2008). I was able to get many P4 pups, so the studies of TMEM16A$^{-/-}$ mice were limited to four days old pups. Sox2 is expressed in the supporting cell nuclei throughout life and can be used to identify supporting cells. However, sox2 is also expressed in the basal cells (Guo et al. 2010; Gokoffski et al. 2011; Krolewski et al. 2012). I found sox2 expression in nuclei of cytokeratin-8 immuno positive supporting cells. To evaluate the effect of TMEM16A on supporting cells density, I counted the sox2 positive supporting cell nuclei specifically in the upper one third of olfactory epithelium, i.e. the site of supporting cells in the olfactory epithelium. On average at E14.5 the sox2 positive supporting cells per 150X150 μm^2 area were 45±02 and 48±02 respectively in TMEM16A$^{+/+}$ and in littermate TMEM16A$^{-/-}$ mice. In postnatal mice, the density was reduced to 31±01 and 32±02 respectively in TMEM16A$^{+/+}$ and in TMEM16A$^{-/-}$ mice. Though the density of supporting cells decreased from embryonic to postnatal life, it remained almost similar in TMEM16A$^{-/-}$ mice compared to equivalent embryonic or postnatal littermate TMEM16A$^{+/+}$ mice. In advanced phases of development and in postnatal mice dividing cells are not present in the apical part of olfactory epithelium, however till E14.5 they are also in the apical part of olfactory epithelium (Smart 1971; Farbman 1994). This could be the reason why I saw a decline in sox-2 positive supporting cells density after E14.5.

Neuronal cell density in the olfactory epithelium also remained the same in both types of mice. At E14.5 it was 185±08 in TMEM16A$^{+/+}$ and 170±14 in TMEM16A$^{-/-}$ mice, while in postnatal it was 201±10 in TMEM16A$^{+/+}$ mice and 188±09 in TMEM16A$^{-/-}$ mice. Cell density analysis suggests that either TMEM16A does not play any role in proliferation or knock-down of TMEM16A does not affect the proliferation in the olfactory epithelium. Interestingly, it has been found that in some cancerous cell lines TMEM16A overexpression did not affect proliferation (Ayoub et al. 2010; Ruiz et al. 2012; Wanitchakool et al. 2014, Qu et al. 2014). During the writing of this thesis an article was published showing that the overexpression of TMEM16A in gastrointestinal stromal tumour (GIST) cells has a very minor influence over viability and proliferation of cells *in vitro*, which is in contrast to earlier findings (Berglund et al. 2014). So, it could be possible that TMEM16A is involved in various physiological pathways and can act differently in different tissues depending on the extracellular and intracellular factors.

Among other physiological roles, TMEM16A also controls fluid secretion and primarily regulates secretion of anions in many epithelial cell types. Indeed, previous studies in knockout mice for TMEM16A have shown that calcium-dependent chloride secretion was

eliminated in salivary acinar cells and in other epithelial cells (Ousingsawat et al. 2009; Rock et al. 2009; Ferrera et al. 2011; Huang et al. 2012a). Furthermore, in acinar cells TMEM16A regulates bicarbonate anion permeability (Jung et al. 2013), and in the airway epithelium it is strongly expressed in mucin secreting cells and modulates mucin secretion (Huang et al., 2012b). As supporting cells are known to be involved in the regulation of the extracellular ionic environment (Breipohl et al. 1974; Rafols and Getchell 1983; Getchell 1986; Menco and Morrison 2003), it is likely that TMEM16A contributes to this process. The mucus layer at the surface of the olfactory epithelium is critical for olfaction, as odorant molecules dissolve in the mucus before reaching the cilia and the ion concentrations determine the electrical response. Supporting cells express amiloride-sensitive sodium channels (Menco et al. 1998), members of the aquaporin family (Ablimit at el. 2006, 2008; Merigo et al. 2011), and the cystic fibrosis transmembrane conductance regulator (Grubb et al. 2007; Merigo et al. 2011), and TMEM16A is likely to act in concert with these ion and water channels to regulate water and ionic balance in the mucus.

TMEM16A is expressed in supporting cells but I did not find any changes in supporting cells population and morphology in TMEM16A$^{-/-}$ mouse. Further to assess the effect of TMEM16A on other secretory glands in the nasal cavity, I studied TMEM16A and aquaporin-5 expression in Bowman's gland (BG), nasal septal gland (NSG) and lateral nasal gland (LNG). Aquaporin-5, a water channel, is expressed in Bowman's gland and supporting cells microvilli (Ablimit et al. 2006; Solbu and Holen 2012). Expression of aquaporin-5 was observed in the duct cells and secretory acinar cells of Bowman's gland in TMEM16A$^{+/+}$ mice. I did not found TMEM16A expression in Bowman's gland till P4 but in the same preparations I found robust TMEM16A immuno-positive signals in nasal septal glands and lateral nasal glands. In both types of glands TMEM16A was expressed in the apical surface of secretory acinar cells and formed luminal surface of glands. In the lumen of glands TMEM16A co-expressed with the aquaporin-5. In littermate TMEM16A$^{-/-}$ mice, though nasal septal glands and lateral nasal glands were devoid of TMEM16A, aquaporin-5 immuno-positive signals were the same as in TMEM16A$^{+/+}$ mice in both glands. I did not notice any change in morphology of Bowman's glands, nasal septal glands and lateral nasal glands. Thus genetic ablation of TMEM16A does not alter the anatomical organization of supporting cells and secretory glands in olfactory epithelium and nasal cavity. However it is possible that the composition of mucus is changed, although this study could not be carried out in this thesis.

5.2 TMEM16B: olfactory signal transduction

TMEM16B expression is mainly found in neurons. TMEM16B transcripts are expressed in adult mouse olfactory epithelium (Yu et al. 2005; Stephan et al. 2009; Rasche et al. 2010; Sagheddu et al. 2010). Proteomic and immunohistochemistry analysis have found TMEM16B expression in olfactory cilia (Mayer et al. 2009; Stephan et al. 2009; Hengl

et al. 2010; Sagheddu et al. 2010). However it was not known at which stage TMEM16B is expressed during embryonic development and if it has any role in prenatal olfaction.

Olfaction related behaviours and preferences have been found in neonatal mice. Neonates preferentially suckled on the nipple of lactating female. They also suckled on the nipple of non-lactating females only when the nipple was coated with amniotic fluid (Al Aïn et al. 2012; Patris et al. 2013). Logan et al. (2012) altered the amniotic fluid by changing the diet of the pregnant mice introducing garlic oil or vanillin to the drinking water (Logan et al. 2012). The authors found that neonatal mice preferred to suckle from the nipple with the same odor they experienced as embryos. These studies indicate that embryonic mice have olfactory experiences that are important for feeding behaviours after birth. There is also evidence from behavioral studies for prenatal olfaction and learning. Embryos receive odorant information from the amniotic fluid, which fills their nasal cavity. When one of two odorants, iso-amyl acetate or iso-valeric acid, was introduced into the nasal cavity of mouse embryos at E18, the animals responded with different behaviours according to which odorant was delivered, showing that the embryos discriminated between the two odorants (Coppola and Millar 1997). Lam and Mombaerts (2013) showed that at E16.5, (but not at E15.5 or E14.5) olfactory sensory neurons expressing the odorant receptor genes S1 or MOR23 responded to the corresponding odor ligands. Also in rats Gesteland et al. (1982) were able to record electro-olfactogram and single unit recordings at E16, but only after E19 olfactory sensory neurons responded specifically to different odorants (Gesteland et al. 1982). Thus before birth mouse or rat have a functional olfactory epithelium that is necessary for their survival.

In my observations TMEM16B first expressed at E14.5 in the apical part of mature olfactory sensory neurons. Other important proteins involved in olfactory signal transduction expressed at the apical surface of the olfactory epithelium at different days during embryonic development, ACIII at E12.5 and CNGA2 at E16.5. Similar spatial and temporal expression pattern of ACIII and CNGA2 were reported also in other studies (Sullivan et al. 1995; Treloar et al. 2005; Col et al. 2007). Along with the elongation of cilia and increase in number of mature olfactory sensory neurons TMEM16B, ACIII and CNGA2 expression increased. In parallel to previous evidence for embryonic and neonate olfactory behaviour and in view of the role of calcium-activated chloride channels in signal to noise ration amplification; my findings about TMEM16B expression during embryonic development along with ACIII and CNGA2 in the cilia of olfactory sensory neurons suggest the involvement of calcium-activated chloride channel TMEM16B in prenatal and neonates olfaction.

In conclusion, my work about the calcium-activated chloride channels TMEM16A and TMEM16B expression in olfactory systems provide an insightful understanding of their dynamic expression during embryonic development of mouse. It is interesting that olfactory and vomeronasal sensory neurons have the same origin (olfactory placode), but different proteins are involved in the respective signal transduction mechanism. However, when it

comes to calcium-activated chloride channels, olfactory sensory neurons express only TMEM16B, while vomeronasal sensory neurons also express TMEM16B along with TMEM16A. Expression of TMEM16B in cilia and microvilli of olfactory and vomeronasal sensory neurons respectively, along with other proteins involved in signal transduction suggests a important role in sensory transduction. Prenatal expression of TMEM16B in cilia indicates its role in embryonic and neonate olfaction too. TMEM16A expression is quite diverse. It is expressed in vomeronasal sensory neurons but olfactory sensory neurons are devoid of it. At E12.5, it is found all over the nasal cavity in non-neuronal cells but from E16.5 it is seen only in specific areas of the nasal cavity including supporting cells of the olfactory epithelium. Bowman's glands are devoid of TMEM16A but nasal septal glands and lateral nasal glands express it. Furthermore, genetic ablation of TMEM16A is lethal for mice; in this scenario it seems that TMEM16A has a central role in various physiological processes. But I did not found any significant difference in TMEM16A$^{-/-}$ and littermate TMEM16A$^{+/+}$ mice in olfactory epithelium and various nasal glands. Thus, in contrast to other tissues (like trachea and intestine) TMEM16A does not affect developmental and proliferation processes in the olfactory epithelium and nasal glands.

5. References

Ablimit A, Aoki T, Matsuzaki T, Suzuki T, Hagiwara H, Takami S, Takata K. 2008. Immunolocalization of water channel aquaporins in the vomeronasal organ of the rat: expression of AQP4 in neuronal sensory cells. Chem Senses 33:481–488.

Ablimit A, Matsuzaki T, Tajika Y, Aoki T, Hagiwara H, Takata K. 2006. Immunolocalization of water channel aquaporins in the nasal olfactory mucosa. Arch Histol Cytol 69:1–12.

Al Aïn S, Belin L, Schaal B, Patris B. 2013. How does a newly born mouse get to the nipple? Odor substrates eliciting first nipple grasping and sucking responses. Dev Psychobiol 55:888–901.

Antolin S, Reisert J, Matthews HR. 2010. Olfactory response termination involves Ca2+-ATPase in vertebrate olfactory receptor neuron cilia. J Gen Physiol 135:367–378.

Asan E, Drenckhahn D. 2005. Immunocytochemical characterization of two types of microvillar cells in rodent olfactory epithelium. Histochem Cell Biol 123:157–168.

Ayoub C, Wasylyk C, Li Y, Thomas E, Marisa L, Robé A, Roux M, Abecassis J, de Reyniès A, Wasylyk B. 2010. ANO1 amplification and expression in HNSCC with a high propensity for future distant metastasis and its functions in HNSCC cell lines. Br J Cancer 103:715–726.

Bakalyar HA, Reed RR. 1990. Identification of a specialized adenylyl cyclase that may mediate odorant detection. Science 250:1403–1406.

Balasubramanian S, Lynch JW, Barry PH. 1996. Calcium-dependent modulation of the agonist affinity of the mammalian olfactory cyclic nucleotide-gated channel by calmodulin and a novel endogenous factor. J Membr Biol 152:13–23.

Beites CL, Kawauchi S, Crocker CE, Calof AL. 2005. Identification and molecular regulation of neural stem cells in the olfactory epithelium. Exp Cell Res 306:309–316.

Belluscio L, Gold GH, Nemes A, Axel R. 1998. Mice deficient in G(olf) are anosmic. Neuron 20:69–81.

Berghard A, Buck LB. 1996. Sensory transduction in vomeronasal neurons: evidence for G alpha o, G alpha i2, and adenylyl cyclase II as major components of a pheromone signaling cascade. J Neurosci 16:909–918.

Berglund E, Akcakaya P, Berglund D, Karlsson F, Vukojević V, Lee L, Bogdanović D, Lui W-O, Larsson C, Zedenius J, Fröbom R, Bränström R. 2014. Functional role of the Ca(2+)-activated Cl(-) channel DOG1/TMEM16A in gastrointestinal stromal tumor cells. Exp Cell Res 326:315–325.

Bhandawat V, Reisert J, Yau K-W. 2005. Elementary response of olfactory receptor neurons to odorants. Science 308:1931–1934.

Billig GM, Pál B, Fidzinski P, Jentsch TJ. 2011. Ca2+-activated Cl− currents are dispensable for olfaction. Nat Neurosci 14:763–769.

Boccaccio A, Menini A. 2007. Temporal development of cyclic nucleotide-gated and Ca2+ -activated Cl- currents in isolated mouse olfactory sensory neurons. J Neurophysiol 98:153–160.

Boehm U, Zou Z, Buck LB. 2005. Feedback loops link odor and pheromone signaling with reproduction. Cell 123:683–695.

Bradley J, Bönigk W, Yau K-W, Frings S. 2004. Calmodulin permanently associates with rat olfactory CNG channels under native conditions. Nat Neurosci 7:705–710.

Bradley J, Reuter D, Frings S. 2001. Facilitation of calmodulin-mediated odor adaptation by cAMP-gated channel subunits. Science 294:2176–2178.

Brechbühl J, Klaey M, Broillet M-C. 2008. Grueneberg ganglion cells mediate alarm pheromone detection in mice. Science 321:1092–1095.

Breipohl W, Laugwitz HJ, Bornfeld N. 1974. Topological relations between the dendrites of olfactory sensory cells and sustentacular cells in different vertebrates. An ultrastructural study. J Anat 117:89–94.

Britschgi A, Bill A, Brinkhaus H, Rothwell C, Clay I, Duss S, Rebhan M, Raman P, Guy CT, Wetzel K, George E, Popa MO, Lilley S, Choudhury H, Gosling M, Wang L, Fitzgerald S, Borawski J, Baffoe J, Labow M, Gaither LA, Bentires-Alj M. 2013. Calcium-activated chloride channel ANO1 promotes breast cancer progression by activating EGFR and CAMK signaling. Proc Natl Acad Sci U S A 110:E1026–1034.

Britton FC, Leblanc N, Kenyon JL. 2010. Calcium-Activated Chloride Channels. In: Alvarez-Leefmans FJ, Delpire E, editors. Physiology and Pathology of Chloride Transporters and Channels in the Nervous System. San Diego: Academic Press. pp 233–256.

Brunet LJ, Gold GH, Ngai J. 1996. General anosmia caused by a targeted disruption of the mouse olfactory cyclic nucleotide-gated cation channel. Neuron 17:681–693.

Buck L, Axel R. 1991. A novel multigene family may encode odorant receptors: a molecular basis for odor recognition. Cell 65:175–187.

Caggiano M, Kauer JS, Hunter DD. 1994. Globose basal cells are neuronal progenitors in the olfactory epithelium: a lineage analysis using a replication-incompetent retrovirus. Neuron 13:339–352.

Caputo A, Caci E, Ferrera L, Pedemonte N, Barsanti C, Sondo E, Pfeffer U, Ravazzolo R, Zegarra-Moran O, Galietta LJV. 2008. TMEM16A, a membrane protein associated with calcium-dependent chloride channel activity. Science 322:590–594.

Carr VM, Farbman AI, Colletti LM, Morgan JI. 1991. Identification of a new non-neuronal cell type in rat olfactory epithelium. Neuroscience 45:433–449.

Carson C, Murdoch B, Roskams AJ. 2006. Notch 2 and Notch 1/3 segregate to neuronal and glial lineages of the developing olfactory epithelium. Dev Dyn 235:1678–1688.

Carter LA, MacDonald JL, Roskams AJ. 2004. Olfactory horizontal basal cells demonstrate a conserved multipotent progenitor phenotype. J Neurosci 24:5670–5683.

Casanova L, Bravo A, Were F, Ramirez A, Jorcano JJ, Vidal M. 1995. Tissue-specific and efficient expression of the human simple epithelial keratin 8 gene in transgenic mice. J Cell Sci 108:811–820.

Chamero P, Katsoulidou V, Hendrix P, Bufe B, Roberts R, Matsunami H, Abramowitz J, Birnbaumer L, Zufall F, Leinders-Zufall T. 2011. G protein G(alpha)o is essential for vomeronasal function and aggressive behavior in mice. Proc Natl Acad Sci U S A 108:12898–12903.

Chess A, Simon I, Cedar H, Axel R. 1994. Allelic inactivation regulates olfactory receptor gene expression. Cell 78:823–834.

Cho H, Yang YD, Lee J, Lee B, Kim T, Jang Y, Back SK, Na HS, Harfe BD, Wang F, Raouf R, Wood JN, Oh U. 2012. The calcium-activated chloride channel anoctamin 1 acts as a heat sensor in nociceptive neurons. Nat Neurosci 15:1015–1021.

Clowney EJ, LeGros MA, Mosley CP, Clowney FG, Markenskoff-Papadimitriou EC, Myllys M, Barnea G, Larabell CA, Lomvardas S. 2012. Nuclear aggregation of olfactory receptor genes governs their monogenic expression. Cell 151:724–737.

Col JAD, Matsuo T, Storm DR, Rodriguez I. 2007. Adenylyl cyclase-dependent axonal targeting in the olfactory system. Development 134:2481–2489.

Coppola DM, Budde J, Millar L. 1993. The vomeronasal duct has a protracted postnatal development in the mouse. J Morphol 218:59–64.

Coppola DM, Millar LC. 1997. Olfaction in utero: Behavioral studies of the mouse fetus. Behav Processes 39:53–68.

Coppola DM, O'Connell RJ. 1989. Stimulus access to olfactory and vomeronasal receptors in utero. Neurosci Lett 106:241–248.

Coulombe PA. 1993. The cellular and molecular biology of keratins: beginning a new era. Curr Opin Cell Biol 5:17–29.

Cuschieri A, Bannister LH. 1975a. The development of the olfactory mucosa in the mouse: light microscopy. J Anat 119:277–286.

Cuschieri A, Bannister LH. 1975b. The development of the olfactory mucosa in the mouse: electron microscopy. J Anat 119:471–498.

Cygnar KD, Zhao H. 2009. Phosphodiesterase 1C is dispensable for rapid response termination of olfactory sensory neurons. Nat Neurosci 12:454–462.

Dahl AR, Hadley WM. 1991. Nasal Cavity Enzymes Involved in Xenobiotic Metabolism: Effects on the Toxicity of Inhalants. Crit Rev Toxicol 21:345–372.

Dalton RP, Lyons DB, Lomvardas S. 2013. Co-opting the unfolded protein response to elicit olfactory receptor feedback. Cell 155:321–332.

Dauner K, Lissmann J, Jeridi S, Frings S, Möhrlen F. 2012. Expression patterns of anoctamin 1 and anoctamin 2 chloride channels in the mammalian nose. Cell Tissue Res 347:327–341.

Dauner K, Möbus C, Frings S, Möhrlen F. 2013. Targeted expression of anoctamin calcium-activated chloride channels in rod photoreceptor terminals of the rodent retina. Invest Ophthalmol Vis Sci 54:3126–3136.

Dhallan RS, Yau KW, Schrader KA, Reed RR. 1990. Primary structure and functional expression of a cyclic nucleotide-activated channel from olfactory neurons. Nature 347:184–187.

Dibattista M, Amjad A, Maurya DK, Sagheddu C, Montani G, Tirindelli R, Menini A. 2012. Calcium-activated chloride channels in the apical region of mouse vomeronasal sensory neurons. J Gen Physiol 140:3–15.

Donner AL, Episkopou V, Maas RL. 2007. Sox2 and Pou2f1 interact to control lens and olfactory placode development. Dev Biol 303:784–799.

Døving KB, Trotier D. 1998. Structure and function of the vomeronasal organ. J Exp Biol 201:2913–2925.

Dulac C, Torello AT. 2003. Molecular detection of pheromone signals in mammals: from genes to behaviour. Nat Rev Neurosci 4:551–562.

Duran C, Hartzell HC. 2011. Physiological roles and diseases of Tmem16/Anoctamin proteins: are they all chloride channels? Acta Pharmacol Sin 32:685–692.

Duvvuri U, Shiwarski DJ, Xiao D, Bertrand C, Huang X, Edinger RS, Rock JR, Harfe BD, Henson BJ, Kunzelmann K, Schreiber R, Seethala RS, Egloff AM, Chen X, Lui VW, Grandis JR, Gollin SM. 2012. TMEM16A induces MAPK and contributes directly to tumorigenesis and cancer progression. Cancer Res 72:3270–3281.

Espinosa I, Lee C-H, Kim MK, Rouse B-T, Subramanian S, Montgomery K, Varma S, Corless CL, Heinrich MC, Smith KS, Wang Z, Rubin B, Nielsen TO, Seitz RS, Ross DT, West RB, Cleary ML, van de Rijn M. 2008. A novel monoclonal antibody against DOG1 is a sensitive and specific marker for gastrointestinal stromal tumors. Am J Surg Pathol 32:210–218.

Farbman AI. 1994. Developmental biology of olfactory sensory neurons. Semin Cell Biol 5:3–10.

Feinstein PG, Schrader KA, Bakalyar HA, Tang WJ, Krupinski J, Gilman AG, Reed RR. 1991. Molecular cloning and characterization of a Ca2+/calmodulin-insensitive adenylyl cyclase from rat brain. Proc Natl Acad Sci U S A 88:10173–10177.

Ferrera L, Caputo A, Ubby I, Bussani E, Zegarra-Moran O, Ravazzolo R, Pagani F, Galietta LJV. 2009. Regulation of TMEM16A chloride channel properties by alternative splicing. J Biol Chem 284:33360–33368.

Fischer H, Illek B, Sachs L, Finkbeiner WE, Widdicombe JH. 2010. CFTR and calcium-activated chloride channels in primary cultures of human airway gland cells of serous or mucous phenotype. Am J Physiol Lung Cell Mol Physiol 299:L585–L594.

Francia S, Pifferi S, Menini A, Tirindelli R. 2014. Vomeronasal Receptors and Signal Transduction in the Vomeronasal Organ of Mammals. In: Mucignat-Caretta C, editor. Neurobiology of Chemical Communication. Frontiers in Neuroscience. Boca Raton (FL): CRC Press pp 297-324.

French DA, Badamdorj D, Kleene SJ. 2010. Spatial distribution of calcium-gated chloride channels in olfactory cilia. PloS One 5:e15676.

Frings S. 2001. Chemoelectrical signal transduction in olfactory sensory neurons of air-breathing vertebrates. Cell Mol Life Sci 58:510–9.

Frings S. 2009. Primary processes in sensory cells: current advances. J Comp Physiol A Neuroethol Sens Neural Behav Physiol 195:1–19.

Frisch D. 1967. Ultrastructure of mouse olfactory mucosa. Am J Anat 121:87–120.

Fuss SH, Omura M, Mombaerts P. 2005. The Grueneberg ganglion of the mouse projects axons to glomeruli in the olfactory bulb. Eur J Neurosci 22:2649–2654.

Garrosa M, Gayoso MJ, Esteban FJ. 1998. Prenatal development of the mammalian vomeronasal organ. Microsc Res Tech 41:456–470.

Garrosa M, Iñiguez C, Fernandez JM, Gayoso MJ. 1992. Developmental stages of the vomeronasal organ in the rat: a light and electron microscopic study. J Für Hirnforsch 33:123–132.

Gesteland RC, Yancey RA, Farbman AI. 1982. Development of olfactory receptor neuron selectivity in the rat fetus. Neuroscience 7:3127–3136.

Getchell TV. 1986. Functional properties of vertebrate olfactory receptor neurons. Physiol Rev 66:772–818.

Ghiaroni V, Fieni F, Tirindelli R, Pietra P, Bigiani A. 2003. Ion conductances in supporting cells isolated from the mouse vomeronasal organ. J Neurophysiol 89:118–127.

Gokoffski KK, Wu H-H, Beites CL, Kim J, Kim EJ, Matzuk MM, Johnson JE, Lander AD, Calof AL. 2011. Activin and GDF11 collaborate in feedback control of neuroepithelial stem cell proliferation and fate. Development 138:4131–4142.

Graziadei GA, Stanley RS, Graziadei PP. 1980. The olfactory marker protein in the olfactory system of the mouse during development. Neuroscience 5:1239–1252.

Graziadei PPC, Graziadei GAM. 1978. Continuous Nerve Cell Renewal in the Olfactory System. In: Jacobson M, editor. Development of Sensory Systems. Handbook of Sensory Physiology. Springer Berlin Heidelberg. p 55–83.

Graziadei PP, Graziadei GA. 1979. Neurogenesis and neuron regeneration in the olfactory system of mammals. I. Morphological aspects of differentiation and structural organization of the olfactory sensory neurons. J Neurocytol 8:1–18.

Gritli-Linde A, Vaziri Sani F, Rock JR, Hallberg K, Iribarne D, Harfe BD, Linde A. 2009. Expression patterns of the Tmem16 gene family during cephalic development in the mouse. Gene Expr Patterns 9:178–191.

Grosmaitre X, Santarelli LC, Tan J, Luo M, Ma M. 2007. Dual functions of mammalian olfactory sensory neurons as odor detectors and mechanical sensors. Nat Neurosci 10:348–354.

Grubb BR, Rogers TD, Kulaga HM, Burns KA, Wonsetler RL, Reed RR, Ostrowski LE. 2007. Olfactory epithelia exhibit progressive functional and morphological defects in CF mice. Am J Physiol Cell Physiol 293:C574–583.

Grubb S, Poulsen KA, Juul CA, Kyed T, Klausen TK, Larsen EH, Hoffmann EK. 2013. TMEM16F (Anoctamin 6), an anion channel of delayed Ca(2+) activation. J Gen Physiol 141:585–600.

Guo Z, Packard A, Krolewski RC, Harris MT, Manglapus GL, Schwob JE. 2010. Expression of pax6 and sox2 in adult olfactory epithelium. J Comp Neurol 518:4395–4418.

Hagino-Yamagishi K. 2008. Diverse systems for pheromone perception: multiple receptor families in two olfactory systems. Zoolog Sci 25:1179–1189.

Hahn Y, Kim DS, Pastan IH, Lee B. 2009. Anoctamin and transmembrane channel-like proteins are evolutionarily related. Int J Mol Med 24:51–55.

Hartzell C, Putzier I, Arreola J. 2005. Calcium-activated chloride channels. Annu Rev Physiol 67:719–758.

Hengl T, Kaneko H, Dauner K, Vocke K, Frings S, Möhrlen F. 2010. Molecular components of signal amplification in olfactory sensory cilia. Proc Natl Acad Sci U S A 107:6052–6057.

Holy TE, Dulac C, Meister M. 2000. Responses of vomeronasal neurons to natural stimuli. Science 289:1569–1572.

Huang F, Wong X, Jan LY. 2012a. International Union of Basic and Clinical Pharmacology. LXXXV: calcium-activated chloride channels. Pharmacol Rev 64:1–15.

Huang F, Zhang H, Wu M, Yang H, Kudo M, Peters CJ, Woodruff PG, Solberg OD, Donne ML, Huang X, Sheppard D, Fahy JV, Wolters PJ, Hogan BLM, Finkbeiner WE, Li M, Jan Y-N, Jan LY, Rock JR. 2012b. Calcium-activated chloride channel TMEM16A modulates mucin secretion and airway smooth muscle contraction. Proc Natl Acad Sci U S A 109:16354–16359.

Huang WC, Xiao S, Huang F, Harfe BD, Jan YN, Jan LY. 2012c. Calcium-activated chloride channels (CaCCs) regulate action potential and synaptic response in hippocampal neurons. Neuron 74:179–192.

Huang X, Godfrey TE, Gooding WE, McCarty KS, Gollin SM. 2006. Comprehensive genome and transcriptome analysis of the 11q13 amplicon in human oral cancer and synteny to the 7F5 amplicon in murine oral carcinoma. Genes Chromosomes Cancer 45:1058–1069.

Huard JM, Youngentob SL, Goldstein BJ, Luskin MB, Schwob JE. 1998. Adult olfactory epithelium contains multipotent progenitors that give rise to neurons and non-neural cells. J Comp Neurol 400:469–486.

Hwang SJ, Blair PJA, Britton FC, O'Driscoll KE, Hennig G, Bayguinov YR, Rock JR, Harfe BD, Sanders KM, Ward SM. 2009. Expression of anoctamin 1/TMEM16A by interstitial cells of Cajal is fundamental for slow wave activity in gastrointestinal muscles. J Physiol 587:4887–904.

Jacobsen KS, Zeeberg K, Sauter DRP, Poulsen KA, Hoffmann EK, Schwab A. 2013. The role of TMEM16A (ANO1) and TMEM16F (ANO6) in cell migration. Pflugers Arch 465:1753-1762.

Jang Y, Oh U. 2014. Anoctamin 1 in secretory epithelia. Cell Calcium 55:355–361.

Jia C, Halpern M. 1996. Subclasses of vomeronasal receptor neurons: differential expression of G proteins (Gi alpha 2 and G(o alpha)) and segregated projections to the accessory olfactory bulb. Brain Res 719:117–128.

Jones DT, Reed RR. 1989. Golf: an olfactory neuron specific-G protein involved in odorant signal transduction. Science 244:790–795.

Juilfs DM, Fülle HJ, Zhao AZ, Houslay MD, Garbers DL, Beavo JA. 1997. A subset of olfactory neurons that selectively express cGMP-stimulated phosphodiesterase (PDE2) and guanylyl cyclase-D define a unique olfactory signal transduction pathway. Proc Natl Acad Sci U S A 94:3388–3395.

Jung J, Nam JH, Park HW, Oh U, Yoon J-H, Lee MG. 2013. Dynamic modulation of ANO1/TMEM16A HCO3(-) permeability by Ca2+/calmodulin. Proc Natl Acad Sci U S A 110:360–365.

Kaneko H, Nakamura T, Lindemann B. 2001. Noninvasive measurement of chloride concentration in rat olfactory receptor cells with use of a fluorescent dye. Am J Physiol Cell Physiol 280:C1387–1393.

Kaneko H, Putzier I, Frings S, Kaupp UB, Gensch T. 2004. Chloride accumulation in mammalian olfactory sensory neurons. J Neurosci 24:7931–7938.

Kashyap MK, Marimuthu A, Kishore CJH, Peri S, Keerthikumar S, Prasad TSK, Mahmood R, Rao S, Ranganathan P, Sanjeeviah RC, Vijayakumar M, Kumar KVV, Montgomery EA, Kumar RV, Pandey A. 2009. Genomewide mRNA profiling of esophageal squamous cell carcinoma for identification of cancer biomarkers. Cancer Biol Ther 8:36–46.

Kelliher KR, Spehr M, Li X-H, Zufall F, Leinders-Zufall T. 2006. Pheromonal recognition memory induced by TRPC2-independent vomeronasal sensing. Eur J Neurosci 23:3385–3390.

Kerjaschki D, Hörander H. 1976. The development of mouse olfactory vesicles and their cell contacts: a freeze-etching study. J Ultrastruct Res 54:420–444.

Kidd JF, Thorn P. 2000. Intracellular Ca2+ and Cl- channel activation in secretory cells. Annu Rev Physiol 62:493–513.

Kim S, Ma L, Yu CR. 2011. Requirement of calcium-activated chloride channels in the activation of mouse vomeronasal neurons. Nat Commun 2:365.

Kleene SJ. 1993. Origin of the chloride current in olfactory transduction. Neuron 11:123–132.

Kleene SJ. 1997. High-gain, low-noise amplification in olfactory transduction. Biophys J 73:1110–1117.

Kleene SJ. 1999. Both external and internal calcium reduce the sensitivity of the olfactory cyclic-nucleotide-gated channel to cAMP. J Neurophysiol 81:2675–2682.

Kleene SJ. 2008. The electrochemical basis of odor transduction in vertebrate olfactory cilia. Chem Senses 33:839–859.

Kleene SJ, Gesteland RC. 1991. Calcium-activated chloride conductance in frog olfactory cilia. J Neurosci 11:3624–3629.

Kleene SJ, Pun RY. 1996. Persistence of the olfactory receptor current in a wide variety of extracellular environments. J Neurophysiol 75:1386–1391.

Kramer RH, Siegelbaum SA. 1992. Intracellular Ca2+ regulates the sensitivity of cyclic nucleotide-gated channels in olfactory receptor neurons. Neuron 9:897–906.

Krolewski RC, Packard A, Jang W, Wildner H, Schwob JE. 2012. Ascl1 (Mash1) Knockout Perturbs Differentiation of Nonneuronal Cells in Olfactory Epithelium. PLoS ONE 7:e51737.

Kurahashi T, Yau KW. 1993. Co-existence of cationic and chloride components in odorant-induced current of vertebrate olfactory receptor cells. Nature 363:71–74.

Lam RS, Mombaerts P. 2013. Odorant responsiveness of embryonic mouse olfactory sensory neurons expressing the odorant receptors S1 or MOR23. Eur J Neurosci 38:2210–2217.

Lau YE, Cherry JA. 2000. Distribution of PDE4A and G(o) alpha immunoreactivity in the accessory olfactory system of the mouse. Neuroreport 11:27–32.

Lee RJ, Foskett JK. 2010. Mechanisms of Ca2+-stimulated fluid secretion by porcine bronchial submucosal gland serous acinar cells. Am J Physiol Lung Cell Mol Physiol 298:L210–L231.

Lee VM, Pixley SK. 1994. Age and differentiation-related differences in neuron-specific tubulin immunostaining of olfactory sensory neurons. Brain Res Dev Brain Res 83:209–215.

Leinders-Zufall T, Brennan P, Widmayer P, S PC, Maul-Pavicic A, Jäger M, Li X-H, Breer H, Zufall F, Boehm T. 2004. MHC class I peptides as chemosensory signals in the vomeronasal organ. Science 306:1033–1037.

Leypold BG, Yu CR, Leinders-Zufall T, Kim MM, Zufall F, Axel R. 2002. Altered sexual and social behaviors in trp2 mutant mice. Proc Natl Acad Sci U S A 99:6376–6381.

Liberles SD, Horowitz LF, Kuang D, Contos JJ, Wilson KL, Siltberg-Liberles J, Liberles DA, Buck LB. 2009. Formyl peptide receptors are candidate chemosensory receptors in the vomeronasal organ. Proc Natl Acad Sci U S A 106:9842–9847.

Ling G, Gu J, Genter MB, Zhuo X, Ding X. 2004. Regulation of cytochrome P450 gene expression in the olfactory mucosa. Chem Biol Interact 147:247–258.

Lin W, Arellano J, Slotnick B, Restrepo D. 2004. Odors detected by mice deficient in cyclic nucleotide-gated channel subunit A2 stimulate the main olfactory system. J Neurosci 24:3703–3710.

Liu B, Linley JE, Du X, Zhang X, Ooi L, Zhang H, Gamper N. 2010. The acute nociceptive signals induced by bradykinin in rat sensory neurons are mediated by inhibition of M-type K+ channels and activation of Ca2+-activated Cl- channels. J Clin Invest 120:1240–1252.

Liu W, Lu M, Liu B, Huang Y, Wang K. 2012. Inhibition of Ca(2+)-activated Cl(-) channel ANO1/TMEM16A expression suppresses tumor growth and invasiveness in human prostate carcinoma. Cancer Lett 326:41–51.

Logan DW, Brunet LJ, Webb WR, Cutforth T, Ngai J, Stowers L. 2012. Learned recognition of maternal signature odors mediates the first suckling episode in mice. Curr Biol CB 22:1998–2007.

Lowe G, Gold GH. 1993. Nonlinear amplification by calcium-dependent chloride channels in olfactory receptor cells. Nature 366:283–286.

Lowe G, Nakamura T, Gold GH. 1989. Adenylate cyclase mediates olfactory transduction for a wide variety of odorants. Proc Natl Acad Sci U S A 86:5641–5645.

Lucas P, Ukhanov K, Leinders-Zufall T, Zufall F. 2003. A diacylglycerol-gated cation channel in vomeronasal neuron dendrites is impaired in TRPC2 mutant mice: mechanism of pheromone transduction. Neuron 40:551–561.

Lynch JW, Lindemann B. 1994. Cyclic nucleotide-gated channels of rat olfactory receptor cells: divalent cations control the sensitivity to cAMP. J Gen Physiol 103:87–106.

Lyons DB, Allen WE, Goh T, Tsai L, Barnea G, Lomvardas S. 2013. An epigenetic trap stabilizes singular olfactory receptor expression. Cell 154:325–336.

Malnic B, Hirono J, Sato T, Buck LB. 1999. Combinatorial receptor codes for odors. Cell 96:713–723.

Ma M. 2010. Multiple Olfactory Subsystems Convey Various Sensory Signals. In: Menini A, editor. The Neurobiology of Olfaction. Frontiers in Neuroscience. Boca Raton (FL): CRC Press, pp225–241.

Mamasuew K, Breer H, Fleischer J. 2008. Grueneberg ganglion neurons respond to cool ambient temperatures. Eur J Neurosci 28:1775–1785.

Martins JR, Faria D, Kongsuphol P, Reisch B, Schreiber R, Kunzelmann K. 2011. Anoctamin 6 is an essential component of the outwardly rectifying chloride channel. Proc Natl Acad Sci U S A 108:18168–18172.

Matsuzaki O, Bakin RE, Cai X, Menco BP, Ronnett GV. 1999. Localization of the olfactory cyclic nucleotide-gated channel subunit 1 in normal, embryonic and regenerating olfactory epithelium. Neuroscience 94:131–140.

Matthews HR, Reisert J. 2003. Calcium, the two-faced messenger of olfactory transduction and adaptation. Curr Opin Neurobiol 13:469–475.

Maurya DK, Menini A. 2014. Developmental expression of the calcium-activated chloride channels TMEM16A and TMEM16B in the mouse olfactory epithelium. Dev Neurobiol 74:657–675.

Mayer U, Küller A, Daiber PC, Neudorf I, Warnken U, Schnölzer M, Frings S, Möhrlen F. 2009. The proteome of rat olfactory sensory cilia. Proteomics 9:322–334.

Mazzone A, Eisenman ST, Strege PR, Yao Z, Ordog T, Gibbons SJ, Farrugia G. 2012. Inhibition of cell proliferation by a selective inhibitor of the Ca(2+)-activated Cl(-) channel, Ano1. Biochem Biophys Res Commun 427:248–253.

McEwen DP, Jenkins PM, Martens JR. 2008. Olfactory cilia: our direct neuronal connection to the external world. Curr Top Dev Biol 85:333–370.

Melvin JE, Yule D, Shuttleworth T, Begenisich T. 2005. Regulation of fluid and electrolyte secretion in salivary gland acinar cells. Annu Rev Physiol 67:445–469.

Menco B, Morrison E. 2003. Morphology of the Mammalian Olfactory Epithelium. In: Doty RL, editor. Handbook of Olfaction and Gustation. Informa Healthcare. New York: Marcel Dekker Inc., pp-17-49.

Menco BP. 1984. Ciliated and microvillous structures of rat olfactory and nasal respiratory epithelia. A study using ultra-rapid cryo-fixation followed by freeze-substitution or freeze-etching. Cell Tissue Res 235:225–241.

Menco BP, Birrell GB, Fuller CM, Ezeh PI, Keeton DA, Benos DJ. 1998. Ultrastructural localization of amiloride-sensitive sodium channels and Na+,K(+)-ATPase in the rat's olfactory epithelial surface. Chem Senses 23:137–149.

Menco BP, Farbman AI. 1985. Genesis of cilia and microvilli of rat nasal epithelia during pre-natal development. II. Olfactory epithelium, a morphometric analysis. J Cell Sci 78:311–336.

Menco BP, Farbman AI. 1992. Ultrastructural evidence for multiple mucous domains in frog olfactory epithelium. Cell Tissue Res 270:47–56.

Menco BP, Tekula FD, Farbman AI, Danho W. 1994. Developmental expression of G-proteins and adenylyl cyclase in peripheral olfactory systems. Light microscopic and freeze-substitution electron microscopic immunocytochemistry. J Neurocytol 23:708–727.

Mendoza AS. 1993. Morphological studies on the rodent main and accessory olfactory systems: the regio olfactoria and vomeronasal organ. Ann Anat 175:425–446.

Menini A. 1999. Calcium signalling and regulation in olfactory neurons. Curr Opin Neurobiol 9:419–426.

Meredith M. 1998. Vomeronasal function. Chem Senses 23:463–466.

Merigo F, Mucignat-Caretta C, Cristofoletti M, Zancanaro C. 2011. Epithelial membrane transporters expression in the developing to adult mouse vomeronasal organ and olfactory mucosa. Dev Neurobiol 71:854–869.

Michalakis S, Reisert J, Geiger H, Wetzel C, Zong X, Bradley J, Spehr M, Hüttl S, Gerstner A, Pfeifer A, Hatt H, Yau K-W, Biel M. 2006. Loss of CNGB1 protein leads to olfactory dysfunction and subciliary cyclic nucleotide-gated channel trapping. J Biol Chem 281:35156–35166.

Milenkovic VM, Brockmann M, Stöhr H, Weber BH, Strauss O. 2010. Evolution and functional divergence of the anoctamin family of membrane proteins. BMC Evol Biol 10:319.

Moll R, Franke WW, Schiller DL, Geiger B, Krepler R. 1982. The catalog of human cytokeratins: patterns of expression in normal epithelia, tumors and cultured cells. Cell 31:11–24.

Munger SD, Lane AP, Zhong H, Leinders-Zufall T, Yau KW, Zufall F, Reed RR. 2001. Central role of the CNGA4 channel subunit in Ca2+-calmodulin-dependent odor adaptation. Science 294:2172–2175.

Munger SD, Leinders-Zufall T, Zufall F. 2009. Subsystem organization of the mammalian sense of smell. Annu Rev Physiol 71:115–140.

Nagahara T, Matsuda H, Kadota T, Kishida R. 1995. Development of substance P immunoreactivity in the mouse vomeronasal organ. Anat Embryol (Berl) 192:107–115.

Naguro T, Breipohl W. 1982. The vomeronasal epithelia of NMRI mouse. A scanning electron-microscopic study. Cell Tissue Res 227:519–534.

Nakamura T, Gold GH. 1987. A cyclic nucleotide-gated conductance in olfactory receptor cilia. Nature 325:442–444.

Nakamura T, Kaneko H, Nishida N. 1997. Direct measurement of the chloride concentration in newt olfactory receptors with the fluorescent probe. Neurosci Lett 237:5–8.

Nickell WT, Kleene NK, Gesteland RC, Kleene SJ. 2006. Neuronal chloride accumulation in olfactory epithelium of mice lacking NKCC1. J Neurophysiol 95:2003–2006.

Nickell WT, Kleene NK, Kleene SJ. 2007. Mechanisms of neuronal chloride accumulation in intact mouse olfactory epithelium. J Physiol 583:1005–1020.

Noda M, Harada Y. 1981. Development of Olfactory Epithelium in the Mouse - Scanning Electron-Microscopy. Biomed Res 2:449–454.

Noé J, Tareilus E, Boekhoff I, Breer H. 1997. Sodium/calcium exchanger in rat olfactory neurons. Neurochem Int 30:523–531.

Nomura T, Takahashi S, Ushiki T. 2004. Cytoarchitecture of the normal rat olfactory epithelium: light and scanning electron microscopic studies. Arch Histol Cytol 67:159–170.

Norlin EM, Gussing F, Berghard A. 2003. Vomeronasal phenotype and behavioral alterations in G alpha i2 mutant mice. Curr Biol CB 13:1214–1219.

Ousingsawat J, Martins JR, Schreiber R, Rock JR, Harfe BD, Kunzelmann K. 2009. Loss of TMEM16A causes a defect in epithelial Ca2+-dependent chloride transport. J Biol Chem 284:28698–28703.

Ousingsawat J, Mirza M, Tian Y, Roussa E, Schreiber R, Cook DI, Kunzelmann K. 2011. Rotavirus toxin NSP4 induces diarrhea by activation of TMEM16A and inhibition of Na+ absorption. Pflüg Arch 461:579–589.

Pace U, Hanski E, Salomon Y, Lancet D. 1985. Odorant-sensitive adenylate cyclase may mediate olfactory reception. Nature 316:255–258.

Patris B, Aïn SA, Schaal B. 2013. Suckling Odours in Rats and Mice: Biological Substrates that Guide Newborns to the Nipple. In: East ML, Dehnhard M, editors. Chemical Signals in Vertebrates 12. Springer New York. pp 77–85.

Pedemonte N, Galietta LJV. 2014. Structure and function of TMEM16 proteins (anoctamins). Physiol Rev 94:419–459.

Pfeuffer E, Mollner S, Lancet D, Pfeuffer T. 1989. Olfactory adenylyl cyclase. Identification and purification of a novel enzyme form. J Biol Chem 264:18803–18807.

Pifferi S, Boccaccio A, Menini A. 2006. Cyclic nucleotide-gated ion channels in sensory transduction. FEBS Lett 580:2853–2859.

Pifferi S, Dibattista M, Menini A. 2009. TMEM16B induces chloride currents activated by calcium in mammalian cells. Pflugers Arch 458:1023–1038.

Ponissery Saidu S, Stephan AB, Talaga AK, Zhao H, Reisert J. 2013. Channel properties of the splicing isoforms of the olfactory calcium-activated chloride channel Anoctamin 2. J Gen Physiol 141:691–703.

Purcell P, Oliver G, Mardon G, Donner AL, Maas RL. 2005. Pax6-dependence of Six3, Eya1 and Dach1 expression during lens and nasal placode induction. Gene Expr Patterns GEP 6:110–118.

Qu Z, Yao W, Yao R, Liu X, Yu K, Hartzell C. 2014. The Ca(2+) -activated Cl(-) channel, ANO1 (TMEM16A), is a double-edged sword in cell proliferation and tumorigenesis. Cancer Med 3:453–461.

Rafols JA, Getchell TV. 1983. Morphological relations between the receptor neurons, sustentacular cells and Schwann cells in the olfactory mucosa of the salamander. Anat Rec 206:87–101.

Rasche S, Toetter B, Adler J, Tschapek A, Doerner JF, Kurtenbach S, Hatt H, Meyer H, Warscheid B, Neuhaus EM. 2010. Tmem16b is specifically expressed in the cilia of olfactory sensory neurons. Chem Senses 35:239–245.

Reisert J, Bauer PJ, Yau K-W, Frings S. 2003. The Ca-activated Cl channel and its control in rat olfactory receptor neurons. J Gen Physiol 122:349–363.

Reisert J, Lai J, Yau K-W, Bradley J. 2005. Mechanism of the excitatory Cl- response in mouse olfactory receptor neurons. Neuron 45:553–561.

Reisert J, Matthews HR. 1998. Na+-dependent Ca2+ extrusion governs response recovery in frog olfactory receptor cells. J Gen Physiol 112:529–535.

Reuter D, Zierold K, Schröder WH, Frings S. 1998. A depolarizing chloride current contributes to chemoelectrical transduction in olfactory sensory neurons in situ. J Neurosci 18:6623–6630.

Rochelle LG, Li DC, Ye H, Lee E, Talbot CR, Boucher RC. 2000. Distribution of ion transport mRNAs throughout murine nose and lung. Am J Physiol Lung Cell Mol Physiol 279:L14–L24.

Rock JR, Futtner CR, Harfe BD. 2008. The transmembrane protein TMEM16A is required for normal development of the murine trachea. Dev Biol 321:141–149.

Rock JR, Harfe BD. 2008. Expression of TMEM16 paralogs during murine embryogenesis. Dev Dyn 237:2566–2574.

Rock JR, O'Neal WK, Gabriel SE, Randell SH, Harfe BD, Boucher RC, Grubb BR. 2009. Transmembrane protein 16A (TMEM16A) is a Ca2+-regulated Cl- secretory channel in mouse airways. J Biol Chem 284:14875–14880.

Rodriguez I. 2003. Nosing into pheromone detectors. Nat Neurosci 6:438–440.

Rodriguez I, Boehm U. 2009. Pheromone sensing in mice. Results Probl Cell Differ 47:77–96.

Rowley JC, Moran DT, Jafek BW. 1989. Peroxidase backfills suggest the mammalian olfactory epithelium contains a second morphologically distinct class of bipolar sensory neuron: the microvillar cell. Brain Res 502:387–400.

Ruiz C, Martins JR, Rudin F, Schneider S, Dietsche T, Fischer CA, Tornillo L, Terracciano LM, Schreiber R, Bubendorf L, Kunzelmann K. 2012. Enhanced expression of ANO1 in head and neck squamous cell carcinoma causes cell migration and correlates with poor prognosis. PloS One 7:e43265.

Ruppersburg CC, Hartzell HC. 2014. The Ca2+-activated Cl- channel ANO1/TMEM16A regulates primary ciliogenesis. Mol Biol Cell 25:1793–1807.

Ryba NJ, Tirindelli R. 1997. A new multigene family of putative pheromone receptors. Neuron 19:371–379.

Sagheddu C, Boccaccio A, Dibattista M, Montani G, Tirindelli R, Menini A. 2010. Calcium concentration jumps reveal dynamic ion selectivity of calcium-activated chloride currents in mouse olfactory sensory neurons and TMEM16b-transfected HEK 293T cells. J Physiol 588:4189–4204.

Schild D, Restrepo D. 1998. Transduction mechanisms in vertebrate olfactory receptor cells. Physiol Rev 78:429–466.

Schroeder BC, Cheng T, Jan YN, Jan LY. 2008. Expression cloning of TMEM16A as a calcium-activated chloride channel subunit. Cell 134:1019–1029.

Schwarzenbacher K, Fleischer J, Breer H. 2005. Formation and maturation of olfactory cilia monitored by odorant receptor-specific antibodies. Histochem Cell Biol 123:419–428.

Schwob JE, Huard JM, Luskin MB, Youngentob SL. 1994. Retroviral lineage studies of the rat olfactory epithelium. Chem Senses 19:671–682.

Serizawa S, Miyamichi K, Nakatani H, Suzuki M, Saito M, Yoshihara Y, Sakano H. 2003. Negative feedback regulation ensures the one receptor-one olfactory neuron rule in mouse. Science 302:2088–2094.

Serizawa S, Miyamichi K, Sakano H. 2004. One neuron-one receptor rule in the mouse olfactory system. Trends Genet 20:648–653.

Shimizu T, Iehara T, Sato K, Fujii T, Sakai H, Okada Y. 2013. TMEM16F is a component of a Ca2+-activated Cl- channel but not a volume-sensitive outwardly rectifying Cl- channel. Am J Physiol Cell Physiol 304:C748–759.

Shykind BM. 2005. Regulation of odorant receptors: one allele at a time. Hum Mol Genet 14: spec no 1, R33–39.

Smart IH. 1971. Location and orientation of mitotic figures in the developing mouse olfactory epithelium. J Anat 109:243–251.

Solbu TT, Holen T. 2012. Aquaporin pathways and mucin secretion of Bowman's glands might protect the olfactory mucosa. Chem Senses 37:35–46.

Song Y, Cygnar KD, Sagdullaev B, Valley M, Hirsh S, Stephan A, Reisert J, Zhao H. 2008. Olfactory CNG channel desensitization by Ca2+/CaM via the B1b subunit affects response termination but not sensitivity to recurring stimulation. Neuron 58:374-386.

Spehr J, Hagendorf S, Weiss J, Spehr M, Leinders-Zufall T, Zufall F. 2009. Ca2+ -calmodulin feedback mediates sensory adaptation and inhibits pheromone-sensitive ion channels in the vomeronasal organ. J Neurosci 29:2125–2135.

Spehr M, Hatt H, Wetzel CH. 2002. Arachidonic acid plays a role in rat vomeronasal signal transduction. J Neurosci Off J Soc Neurosci 22:8429–8437.

Stanich JE, Gibbons SJ, Eisenman ST, Bardsley MR, Rock JR, Harfe BD, Ordog T, Farrugia G. 2011. Ano1 as a regulator of proliferation. Am J Physiol Gastrointest Liver Physiol 301:G1044–1051.

Stephan AB, Shum EY, Hirsh S, Cygnar KD, Reisert J, Zhao H. 2009. ANO2 is the cilial calcium-activated chloride channel that may mediate olfactory amplification. Proc Natl Acad Sci U S A 106:11776–11781.

Stephan AB, Tobochnik S, Dibattista M, Wall CM, Reisert J, Zhao H. 2012. The Na(+)/Ca(2+) exchanger NCKX4 governs termination and adaptation of the mammalian olfactory response. Nat Neurosci 15:131–137.

Stöhr H, Heisig JB, Benz PM, Schöberl S, Milenkovic VM, Strauss O, Aartsen WM, Wijnholds J, Weber BHF, Schulz HL. 2009. TMEM16B, a novel protein with calcium-dependent chloride channel activity, associates with a presynaptic protein complex in photoreceptor terminals. J Neurosci 29:6809–6818.

Storan MJ, Key B. 2006. Septal organ of Grüneberg is part of the olfactory system. J Comp Neurol 494:834–844.

Stowers L, Holy TE, Meister M, Dulac C, Koentges G. 2002. Loss of sex discrimination and male-male aggression in mice deficient for TRP2. Science 295:1493–1500.

Strader CD, Fong TM, Graziano MP, Tota MR. 1995. The family of G-protein-coupled receptors. FASEB J 9:745–754.

Suárez R, García-González D, de Castro F. 2012. Mutual influences between the main olfactory and vomeronasal systems in development and evolution. Front Neuroanat 6:50.

Sullivan SL, Bohm S, Ressler KJ, Horowitz LF, Buck LB. 1995. Target-independent pattern specification in the olfactory epithelium. Neuron 15:779–789.

Sunahara RK, Dessauer CW, Gilman AG. 1996. Complexity and diversity of mammalian adenylyl cyclases. Annu Rev Pharmacol Toxicol 36:461–480.

Suzuki J, Umeda M, Sims PJ, Nagata S. 2010. Calcium-dependent phospholipid scrambling by TMEM16F. Nature 468:834–838.

Suzuki Y, Takeda M, Obara N, Suzuki N, Takeichi N. 2000. Olfactory epithelium consisting of supporting cells and horizontal basal cells in the posterior nasal cavity of mice. Cell Tissue Res 299:313–325.

Takeuchi H, Kurahashi T. 2003. Identification of second messenger mediating signal transduction in the olfactory receptor cell. J Gen Physiol 122:557–567.

Taniguchi K, Taniguchi K. 2008. Embryonic and postnatal differentiation of olfactory epithelium and vomeronasal organ in the Syrian hamster. J Vet Med Sci 70:57–64.

Tarozzo G, Cappello P, De Andrea M, Walters E, Margolis FL, Oestreicher B, Fasolo A. 1998. Prenatal differentiation of mouse vomeronasal neurones. Eur J Neurosci 10:392–396.

Tirindelli R, Dibattista M, Pifferi S, Menini A. 2009. From pheromones to behavior. Physiol Rev 89:921–956.

Touhara K. 2009. Olfactory Receptors. In: Squire LR, editor. Encyclopedia of Neuroscience. Oxford: Academic Press. pp 163–169.

Touhara K, Vosshall LB. 2009. Sensing odorants and pheromones with chemosensory receptors. Annu Rev Physiol 71:307–332.

Treloar HB, Miller AM, Ray A, Greer CA. 2010. Development of the Olfactory System. In: Menini A, editor. The Neurobiology of Olfaction. Frontiers in Neuroscience. Boca Raton (FL): CRC Press pp 131-156.

Treloar HB, Uboha U, Jeromin A, Greer CA. 2005. Expression of the neuronal calcium sensor protein NCS-1 in the developing mouse olfactory pathway. J Comp Neurol 482:201–216.

Vaccarezza OL, Sepich LN, Tramezzani JH. 1981. The vomeronasal organ of the rat. J Anat 132:167–185.

Vocke K, Dauner K, Hahn A, Ulbrich A, Broecker J, Keller S, Frings S, Möhrlen F. 2013. Calmodulin-dependent activation and inactivation of anoctamin calcium-gated chloride channels. J Gen Physiol 142:381–404.

Wanitchakool P, Wolf L, Koehl GE, Sirianant L, Schreiber R, Kulkarni S, Duvvuri U, Kunzelmann K. 2014. Role of anoctamins in cancer and apoptosis. Philos Trans R Soc Lond B Biol Sci 369:20130096.

West RB, Corless CL, Chen X, Rubin BP, Subramanian S, Montgomery K, Zhu S, Ball CA, Nielsen TO, Patel R, Goldblum JR, Brown PO, Heinrich MC, van de Rijn M. 2004. The novel marker, DOG1, is expressed ubiquitously in gastrointestinal stromal tumors irrespective of KIT or PDGFRA mutation status. Am J Pathol 165:107–113.

Wong ST, Trinh K, Hacker B, Chan GC, Lowe G, Gaggar A, Xia Z, Gold GH, Storm DR. 2000. Disruption of the type III adenylyl cyclase gene leads to peripheral and behavioral anosmia in transgenic mice. Neuron 27:487–497.

Xiao Q, Yu K, Perez-Cornejo P, Cui Y, Arreola J, Hartzell HC. 2011. Voltage- and calcium-dependent gating of TMEM16A/Ano1 chloride channels are physically coupled by the first intracellular loop. Proc Natl Acad Sci U S A 108:8891–8896.

Yang C, Delay RJ. 2010. Calcium-activated chloride current amplifies the response to urine in mouse vomeronasal sensory neurons. J Gen Physiol 135:3–13.

Yang H, Kim A, David T, Palmer D, Jin T, Tien J, Huang F, Cheng T, Coughlin SR, Jan YN, Jan LY. 2012. TMEM16F forms a Ca2+-activated cation channel required for lipid scrambling in platelets during blood coagulation. Cell 151:111–122.

Yang YD, Cho H, Koo JY, Tak MH, Cho Y, Shim W-S, Park SP, Lee J, Lee B, Kim B-M, Raouf R, Shin YK, Oh U. 2008. TMEM16A confers receptor-activated calcium-dependent chloride conductance. Nature 455:1210–1215.

Yu K, Duran C, Qu Z, Cui Y-Y, Hartzell HC. 2012. Explaining calcium-dependent gating of anoctamin-1 chloride channels requires a revised topology. Circ Res 110:990–999.

Yu T-T, McIntyre JC, Bose SC, Hardin D, Owen MC, McClintock TS. 2005b. Differentially expressed transcripts from phenotypically identified olfactory sensory neurons. J Comp Neurol 483:251–262.

Zancanaro C, Merigo F, Mucignat-Caretta C, Cavaggioni A. 2002. Neuronal nitric oxide synthase expression in the mouse vomeronasal organ during prenatal development. Eur J Neurosci 16:659–664.

Zhao H, Reed RR. 2001. X inactivation of the OCNC1 channel gene reveals a role for activity-dependent competition in the olfactory system. Cell 104:651–660.

Zheng J, Zagotta WN. 2004. Stoichiometry and assembly of olfactory cyclic nucleotide-gated channels. Neuron 42:411–421.

Zou D-J, Chesler AT, Pichon CEL, Kuznetsov A, Pei X, Hwang EL, Firestein S. 2007. Absence of Adenylyl Cyclase 3 Perturbs Peripheral Olfactory Projections in Mice. J Neurosci 27:6675–6683.